A New Approach to CNC Programming for

Accurate Multi-axis Face-Milling of Hypoid Gears

Muhammad Wasif

A Thesis

in the Department

of

Mechanical and Industrial Engineering

Presented in Partial Fulfillment of the Requirements

For the Degree of Doctor of Philosophy at

Concordia University

Montreal (Quebec) Canada

December 2012

CONCORDIA UNIVERSITY

School of Graduate Studies

This is to certify that the thesis prepared

By: Muhammad Wasif

Entitled: A new approach to CNC programming for accurate multi-axis face-milling of hypoid gears

and submitted in partial fulfillment of the requirements for the degree of

Doctor of Philosophy (Mechanical Engineering)

complies with the regulations of the University and meets the accepted standards with respect to originality and quality.

Signed by the final examining committee:

_____	Chair
Dr. Deyi Xue	External Examiner
Dr. Zhigang Tian	External to Program
Dr. Yong Zeng	Examiner
Dr. Sivakumar Narayanswamy	Examiner
Dr. Zezhong C. Chen	Thesis Supervisor

Approved by:

_____

Chair of Department or Graduate Program Director

_____   _____

Dean of Faculty

Abstract

A new approach to CNC programming for accurate multi-axis face-milling of hypoid Gears

A pair of hypoid gears refers to a pinion and a gear with skew axes. Hypoid gears are crucial to some power transmission systems, such as those of helicopters, power generation machines and automobiles. However, the design and manufacturing of hypoid gears are quite difficult. Currently, the major parameters of hypoid gears are calculated, but the geometries of the gears are not fully defined. To machine a hypoid gear, parameters of cutting systems are determined according to the gear design, whereas, settings of CNC machine tools with the machining parameters are also computed. The existing hypoid gears machining methods use the simplified blade model of the cutting systems, resulting in large errors in the machined gears. This new work proposes an accurate approach, to determine the parameters of the cutting system blades, for the face-milling of hypoid gears. In this work, a parametric model of the blades is established; and according to the hypoid gear parameters, the pressure angle and the cutting system radius are precisely calculated.

Currently, hypoid gear engineers can use special CAD/CAM software to design the gears and to calculate machine settings. Unfortunately, these software are developed only for particular machine tools; it cannot be used for hypoid gear machine tools of different configurations. Moreover, few technical articles has been published to clearly address challenges in the CNC programming and post-processing for the multi-axis face-milling of

hypoid gears, such as the parameters determination of a cutter system, its location and orientation calculation and CNC programs generation. To solve the current problems, another part of this research proposes a generic approach to CNC programming and post-processing for gear face-milling. The main contributions of this part includes (1) a new mathematical model to calculate the cutter system location and orientation and (2) a generic post-processing method to establish the machine kinematics chain and to compute the coordinates of the machine axes in face-milling. This approach provides a general and accurate methodology for the face-milling of hypoid gears on any machine tools and can be directly applied to the hypoid gear manufacturing for better quality.

Muhammad Wasif, Ph.D.

Concordia University, 2012.

Dedication

To my parents, my wife and my two kids.

Acknowledgments

I would like to express my great thanks and appreciations to my supervisor Dr. Chevy Chen for his guidance and support during the period of my PhD. work. His way of guidance developed my research experience and significantly improved my research and technical skills.

I also would like to show my sincere appreciation to my former and present fellows in the CAD/CAM laboratory (Maqsood Ahmed Khan, Shuangxui Xie, Mahmoud Rababah, Aqeel Ahmad, Sherif Abd Elkhalek, Du Chun, Liming Wang, Jiang Zhu, Yangtau Li and Ruibiao Song). The research and friendly environment in the laboratory, and the support I achived from them, encouraged me to pursue and improve my ideas for the research. Amongst them all, special thanks to Maqsood Ahmed Khan, for his endless supports and creative advices. Finally, I sincerely thank my parents and my wife for their support and patience.

Content

List of Figures

List of Tables

Chapter 1

Introduction

Gears are known to be the most fundamental and the efficient components for the power transmission. Various types of gear are invented for the different transmission needs, such as helical gear, worm gear, spurs gear and bevel gear. Amongst all types of gears, the spiral bevel gears are distinguished, due to its higher power transmission between intersecting and non-intersecting shafts, which are mostly perpendicular to each other. For the efficient and life involving applications of these gears, critical design and manufacturing concerns are needed, especially in the automobile and the aerospace vehicles. A special type of spiral bevel gear, hypoid gear, is discussed in the following section.
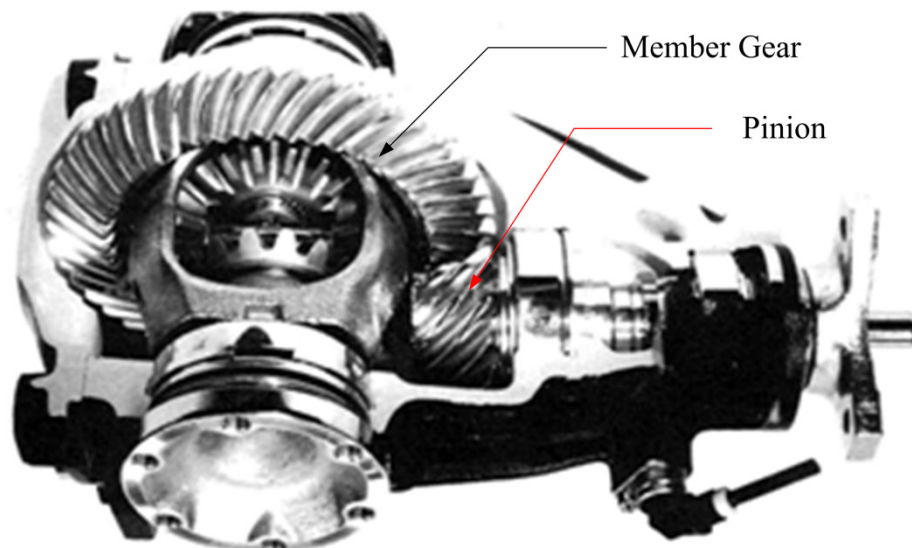
Figure 1.1. An automotive transmission system [1].

1.1. Hypoid gears

In a pair of spiral bevel gears, the gear having larger pitch cone is called member gear, whereas, the gear with smaller pitch cone is called pinion. Pair of spiral bevel gears assembled in an automotive transmission is shown in the Fig. 1.1. A special pair of spiral bevel gears with non-intersecting axes or skew axes, due to an offset between the rotation axes is called hypoid gears, which is shown in the Fig. 1.2(b).

(a)

(b)

offset
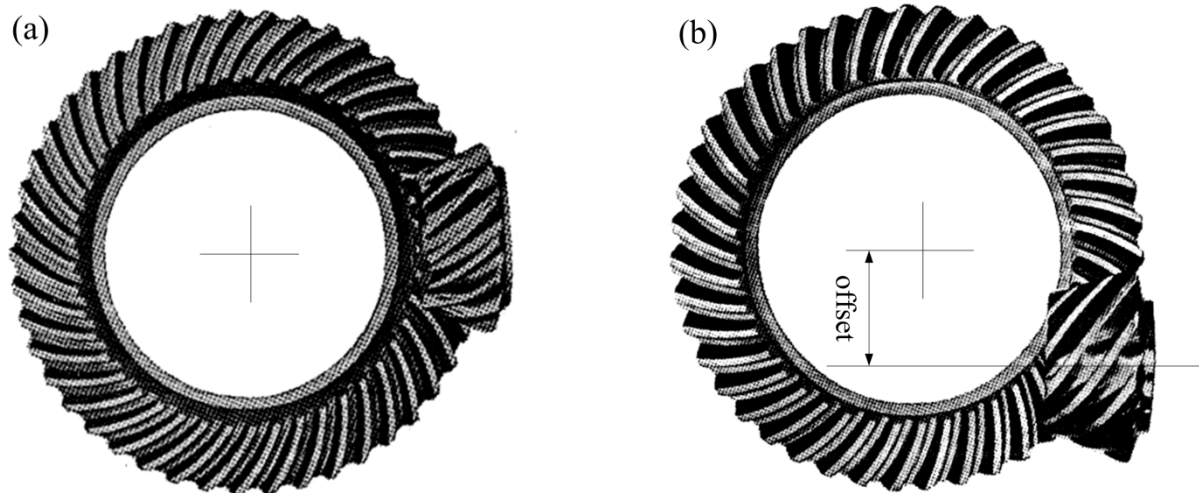
Figure 1.2. Gear with perpendicular axes, (a) Spiral bevel gears, (b) hypoid gears [1].

Hypoid gears are used almost in every kind of automobiles and high power transmission applications, following are the advantages of hypoid gears over the spiral bevel gears,

1. Pinion offset results in the larger pinion size, so it can be operated on high contact ratio and high contact fatigue with less tooth count and quiet operation.

2. Less number of teeth provides the high reduction ratio.

2

3. For the same magnitude of torque transmission, overall size of the hypoid-gear transmission is less, as compared to the bulky size of bevel gear transmission.

Due to the large sliding actions, power losses are more in the hypoid gears then the spiral bevel gears, but the use of appropriate hypoid oil supress it.

In a transmission assembly, relative positions of a hypoid gear and a pinion, are shown in the Fig. 1.3. Coordinate systems O_g and O_{pn} are rigidly connected with the gear and the pinion respectively, where, the axes X_g and X_{pn} are the rotation axes of the gear and the pinion respectively. Angular displacements of the gear and the pinion are denoted by φ_g and φ_{pn}. There is an offset of E exists between the axes X_g and X_{pn}, in case of a hypoid gear pair.
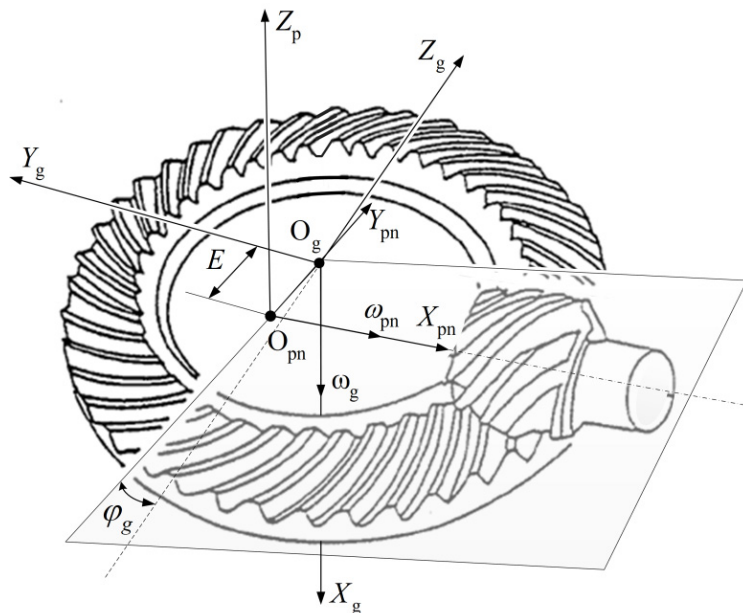
Figure 1.3. Hypoid gear and pinion assembly.

1.2. Machining processes of hypoid gears

Three machining processes are used for the machining of hypoid and spiral bevel gears;

1. Hobbing,

2. Face hobbing, and

3. Face milling.

Most of the spiral bevel and hypoid gears are produced by the face hobbing and milling processes, due the higher efficiencies of these processes. In a hobbing process, a hob cutter is used for the planetary machining of the gear, whereas, in face milling and hobbing processes, face cutter is used, which is equipped with the inside and outside blades to machine the convex and concave sides of the gear teeth. The cutter head for the face milling is shown in the Fig. 1.4.
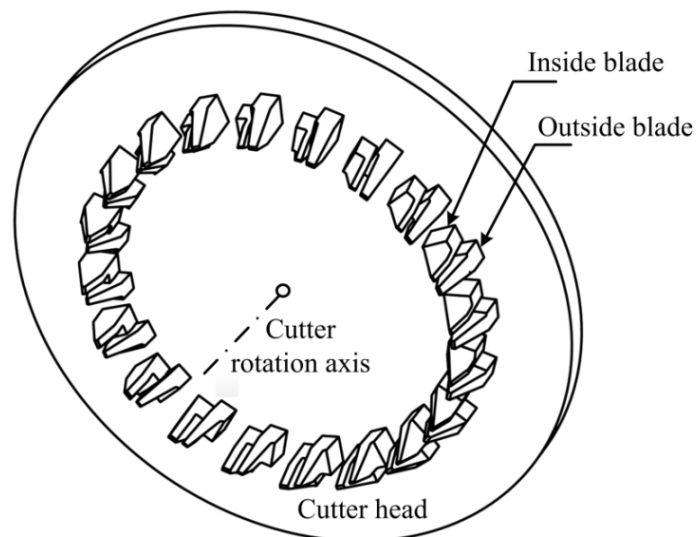
Figure 1.4. Cutter head for the face milling of hypoid gears.

1.2.1   Face hobbing

In this process, cutter blades are divided into several groups of inner and outer blades. During the machining, one group of the blades, machine the first tooth and the following group ascend to cut the next tooth as shown in Fig. 1.5(a). Rotation of the cutter, rotation of the gear blank, number of blades and number of teeth are proportional, to perform continuous indexing of blades. Teeth curvature machined by this operation is epicycloid, and the depth of the teeth is constant throughout the curvature as shown in the Fig. 1.5(b). These types of gears cannot be finished using grinding process, due to epicyclical tooth shape, therefore, the lapping process is used to finish the gear pair simultaneously.
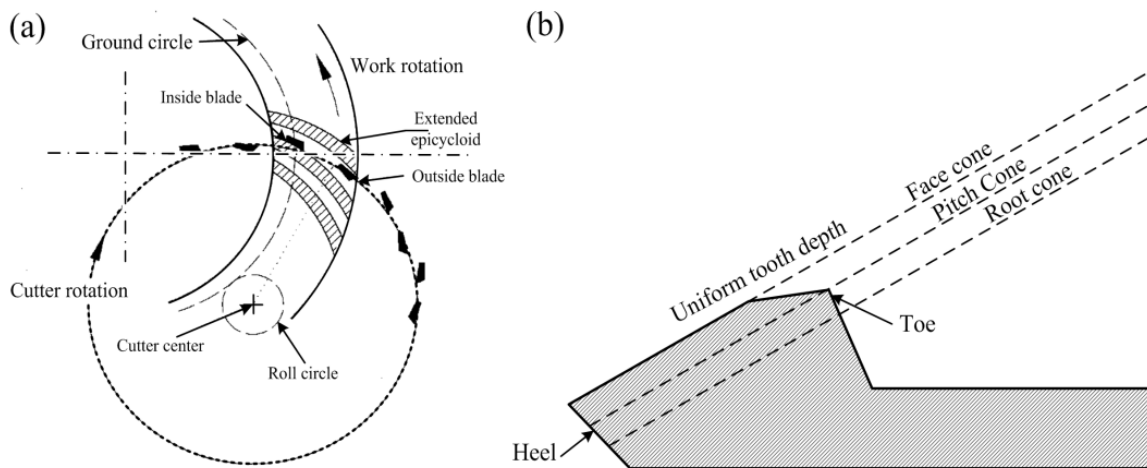
Figure 1.5. Face hobbing, (a) tooth curvature [1], (b) uniform tooth depth.

1.2.2   Face milling

In this process, a cutter head with the inner and outer blades, performs the face milling of a hypoid gear tooth completely, the gear blank is rotated with an indexing angle for the machining of the next tooth. Since the gear tooth surface is the copy of the cutter sweep envelope, therefore, the tooth curvature is same as that of the circular cutter, the process illustration is shown in the Fig. 1.6(a), whereas, the tooth depth produced by this process is tapered as shown in the Fig. 1.6(b).
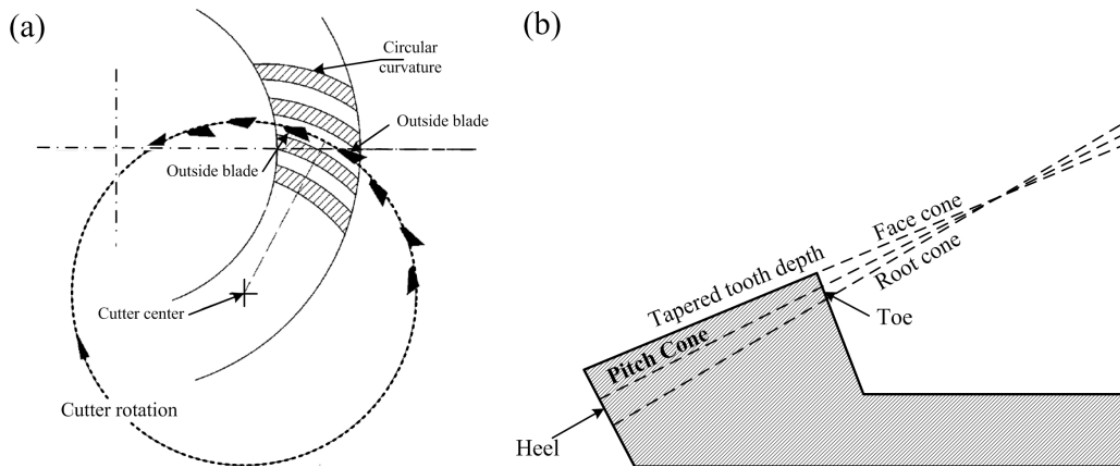
Figure 1.6. Face milling, (a) tooth curvature [1], (b) non-uniform tooth depth.

Due to the circular curvature of the teeth, these gears can be finished by a cup shaped grinder, using the same machining setup. In contrast to the face hobbing process, these types of the gears have advantage that a gear or a pinion of one pair can be used with other member of the other pair. Two basic types of the face milling processes are used for the machining of gears and pinions, due to the geometric differences in the teeth.

Non-generated method

This method is designed for the machining of a member gear. In this method, the cutter face is aligned parallel to the tangent plane of the root cone, and rotated with the cutting velocity; it is gradually fed into the gear blank, which remains stationary during the machining of the gear teeth (see Fig. 1.7).
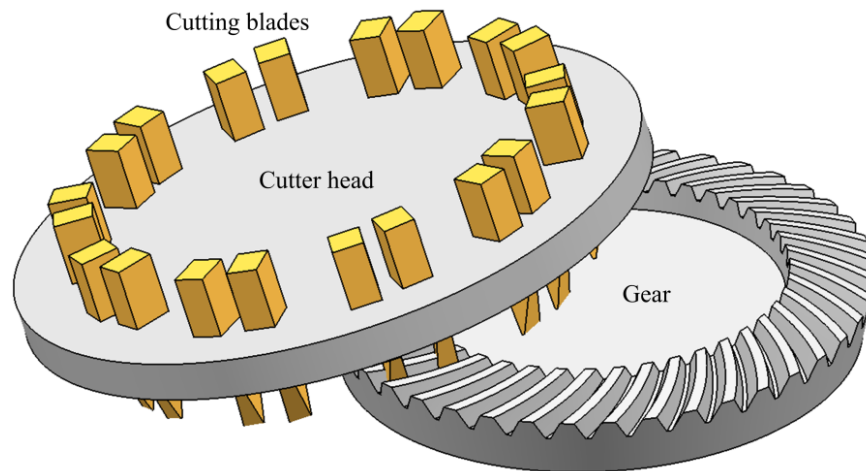
Figure 1.7. Cutter and the gear blank engagement in the non-generated machining process.

Multi-axis face-milling machine are used for the machining of the hypoid gears. In this machine, the gear blank can be moved along the X, Y and Z directions, which are calculated using the machine kinematics model.

Gear blank can be rotated about the shaft rotation axis to attain the teeth indexing. The blank can be adjusted about the B-axis to align the cutter face with the root cone tangent plane of the gear. Cutter head is rotated about the C-axis of the cradle to align the position of the cutter with respect to the gear blank. The machine configuration is shown in the Fig. 1.8. In the non-generated machining process, the Y, B and C axes are the indexing axes, whereas,

X or *Z* axis is used for the feed directions. Detailed transformations and calculations of the machining parameters are addressed in Chapter 5.
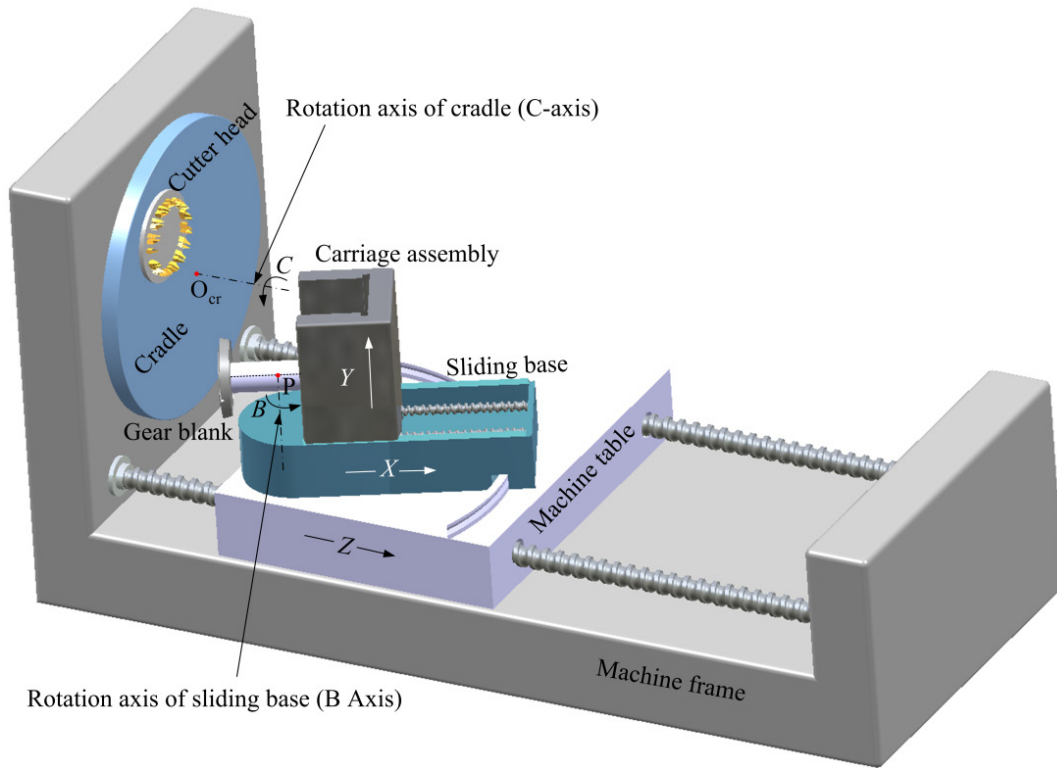
Figure 1.8. Structure of the multi-axis face-milling machine for the hypoid gears.

Generated method

In this process, the cutter head rotates with the cutting velocity and performs the machining of an imaginary crown gear; whereas, a pinion blank rolls over the imaginary gear. Therefore, as the cutter head sweeps the metal from the imaginary gear teeth, it actually removes the metal from the pinion blank as shown in the Fig. 1.9.

Axis of rotation of the gear and the cradle are same, where the cradle is rotated to perform the pairing rotation between the crown gear and the pinion. A ratio between angular velocities of the cradle and the pinion is called the roll ratio.
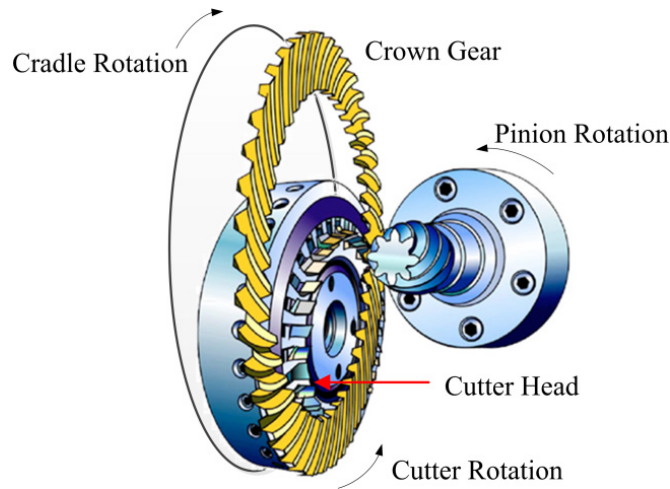
Figure 1.9. Generated method for the face milling of hypoid pinions [58].

Face-milling using the generated method is performed using multi-axis pinion generation machines. In this machine, a cradle is mounted on the frame, with a tilt mechanism, which contains the eccentric plate, swivel, and the cutter head. A pinion blank is mounted on a carriage assembly, which moves along the X, Y, and Z axes. The machine model is shown in the Fig. 1.10. The blank is rotated about the A-axis with the angular velocity of ω_p, whereas, the tilt mechanism is rotated about the C-axis with a velocity of ω_{cp}, to perform the generated machining. Cutter head is indexed with the machine settings about the B, D and E axes.
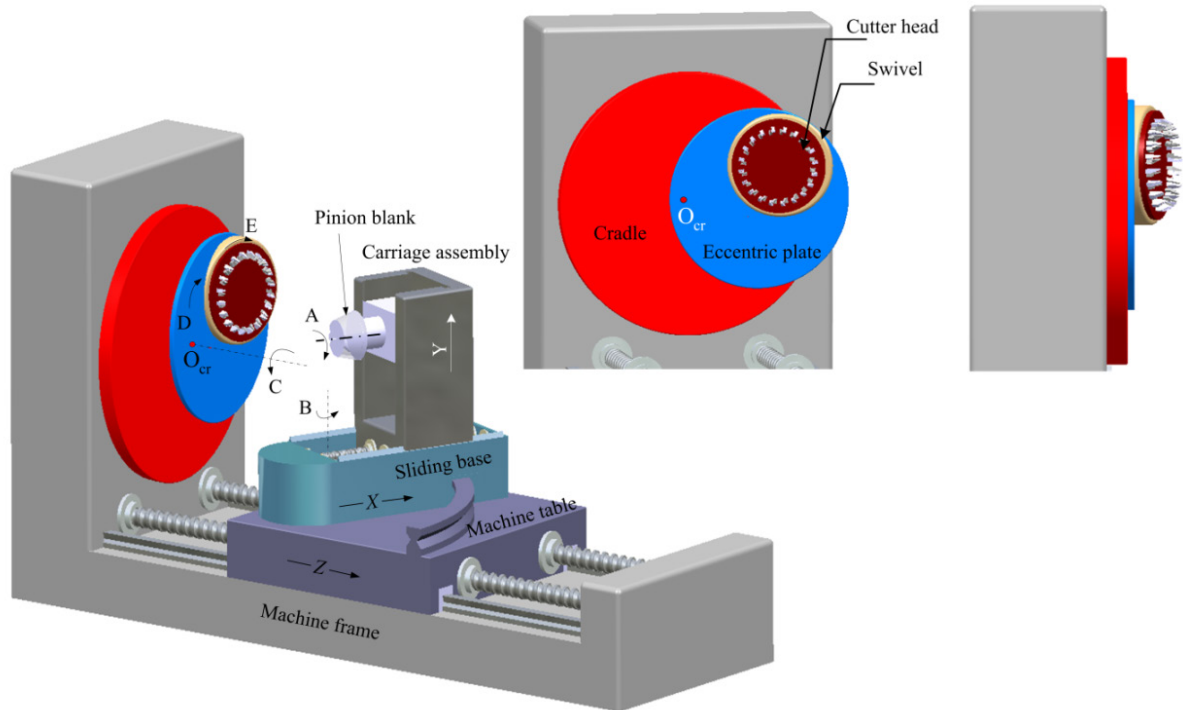
Figure 1.10. Structure of the multi-axis pinion generation machine

Chapter 2

Literature Review and Research Objectives

A comprehensive literature is studied on the machining, designing and analysis processes of spiral bevel and hypoid gears. Based on the literature review, research problems are highlighted, which are addressed to set the research objectives. This chapter consists of two main sections, in the first section; the detailed literature review is discussed, the second section contains the extracted research and industrial problems. The research objectives are evaluated to overcome the current problems and are presented in this chapter.

2.1   Literature review

Bevel gears were invented in 1820 A.D. by James White. Generation method for the manufacturing of spiral bevel was first proposed by a Frenchman named 'Monneret', A German scientist 'Paul Böttcher' published several research papers in 1910 and presented the advancements in generation method. Based on Böttcher techniques, the Gleason's Works (USA), Oerlikon-Bührle (Switzerland) and Klingelnberg Sons (Germany) designed the new methods and machine tools for the manufacturing of spiral bevel and hypoid gears.

The basic theories about the spiral bevel and hypoid gears are well described in the publications written by H. J. Stadtfeld [1] and F. L. Litvin [3, 4, 5, 6], who contributed their research for the Gleasons Works and the NASA Lewis Research Centre respectively. The

literature review about the design, manufacturing and analysis of the spiral bevel and hypoid gears are divided into three major areas, which are discussed below;

2.1.1   Mathematical models of spiral bevel and hypoid gears

Several mathematical models for the tooth surfaces of the spiral bevel and hypoid gears are presented, which vary due to the blade design and machining processes. Litvin et al. proposed the machine settings and local synthesis method using the straight profile cutters. In local synthesis method, the gear cutter, gear, pinion, and pinion cutter surfaces are taken tangent at a specified mean point. Based on the surface curvatures and the tangency conditions at that point, relationship between the four surfaces are built [7, 8, 9]. Later on, author applied the computerized method to relate the principal curvatures and the directions [10]. Litvin also designed the algorithm of tooth contact analysis (TCA) to validate the contact path in the neighbourhood of the mean point [11]. Litvin et al. developed the computerized design of face milled uniform tooth height bevel gear with the low noise and transmission errors by localizing the bearing contact (set of contact points, which are actually the set of ellipses centres under the load) and avoiding the undercuts [12, 13, 14, 15, 16, 17]. Author introduced a pre-designed parabolic function instead of linear function to avoid the vibration during the tooth shift; stress and finite element analysis (FEA) are also applied to validate the results. Litvin developed the computerized generation and simulation model, for machining of the gear surface without tilting the cutter head [18]. A method to find the existence of tooth surfaces and removal of singularities during machining processes is also presented [19].

Huston and Coy worked on the tooth geometry of the spiral bevel gear formed by circular cutter with the involute, straight, and hyperbolic profiles [20]. Authors presented the mathematical model of the tooth drive and coast sides and their curvature showing that the surfaces are simpler than the logarithmic surfaces. Fong and Tsay presented the blade profile by decomposing it intro several segments; effects of the blade profile on the gear teeth surface are observed using the different machining processes [21]. Kawasaki et al. proposed the modified tooth surface machined by the duplex spread blade method and generated the gear and pinion surfaces using a straight lined profile cutter [22]. Fong proposed mathematical model for the machining of a gear and a pinion for the better contact and the reduced noise, by applying the flank modification method, which results in localized point contact [23]. A group of Italian researcher introduced a new mathematical technique in the theory of gearing, which represents the vectors of enveloping surfaces without mentioning the localized reference system, this method reduced the mathematical models [24, 25, 26]. Fan presented the model and simulation method of spiral bevel and hypoid gears using the face-hobbing process, describing the blade model with hook, rake, and offset angles, he analysed the model using the TCA algorithm [2]. Vimercatti modified the face hobbing blade with a TOPREM to avoid the undercut [27]. Shih et al. developed the model of the universal face hobbing and the equivalency of this model with the traditional cradle type machine [28]. Fan evaluated a modified face cone element using the optimization technique, based on actual gear machining process [29]. Some researchers presented the mathematical models of the gear teeth formed by the sculptured surface machining using the end mill cutters [30, 31]. Brecher et Al. performed the analysis and simulation of several machining processes for the manufacturing of bevel gears [32]. Tsai and Hsu proposed a new approach for the machining

of the spiral bevel gear surface using a cup shape grander, approximating the contact path with a circular curve, and forming a torus shaped tooth profile [33]. Jing performed the modification in the tooth surface of the straight bevel gear by different type of cutter and observed the changes in geometrical parameters [34].

2.1.2   Determination of machine settings and the corrections

Basic machine settings are calculated using the gear cutter and the gear tooth geometry, pilot gears are produced, and then corrected machine settings are calculated based on the surface deviation between the theoretical and the machined gear surfaces. Litvin presented the machine setting settings for the FORMATE® and the Helixform® Methods using the tilted cutter head and the local syntheses method [7, 8]; Litvin also proposed the cutter tilt mechanism and the machine-setting model [35]. Krezner proposed the computer aided corrections in the machine-setting, based on the first order surface deviations, and claimed that the second order surface deviations are minor [36]. Gosselin et al. proposed the correction methods in machine setting based on the TCA and performed the numerical regression method until satisfactory machine setting achieved [37, 38, 39]. Simon proposed an algorithm to calculate the machine setting corrections to reduce the sensitivity of the gear pair misalignments; moreover, equivalent machine settings for the universal hypoid generator are also calculated [40, 41, 42, 43]. Wang and Fong generated the flank modification in the gear and the pinion for favourable point contacts using the modified radial motion, i.e. the motion of the cutter on a radial direction, which causes the deviation in the generated gear surface and hence mismatch between the gear and the pinion occurs [44, 45, 46]. Perez et al. presented the analytical method for the determination of machine settings of the bevel gears

based on three different geometry of the gear [47]. Artoni et al. developed an optimization method to calculate the machine settings with the least error using 17 different machine-setting parameters [48]. Lin et al. applied the optimization method to find the corrective machine settings for the hypoid and the spiral bevel gears, to minimize the deviation between the ideal and the real gear tooth surfaces [49]. Medvedev presented an algorithm for the determination of machine settings of spiral bevel gear with small shaft angles; this algorithm reduces the machine envelope, which is usually large for the gears with small shafts [50].

2.1.3 Tooth contact analysis (TCA) and flank modification

Tooth contact analysis is performed to validate the contact between the gear and the pinion in the neighbourhood of the defined mean point; it provides the contact curve as well as elastic deformation of the teeth models. Computer-aided TCA model is used to analyse the contact pattern of the gears before the machining process.

Litvin in 1981 proposed an algorithm, to perform the tooth contact analysis which track the contact points on a pitch plane (passing through the mean point and apices of the pitch cones) [11]. It requires huge mathematical calculations to find a single point. Gosselin et al. provided a solution to find the on-running transmission errors in a hypoid transmission by measuring it under the load, using an experimental setup; author showed that the algorithm for the loaded tooth contact analysis (LTCA) and the experimental data are matched [51]. Stadtfeld enhance the online measurement of transmission error with the tooth correction, by coupling the flank correction module with the running transmission, which suppresses the transmission errors [52]. Achtmann et al. performed an optimization on the

contact ellipse, which guarantees the reduced contact area; author also calculated the geometrical conditions suitable for that optimized ellipse [53]. Simon changed the cutter profile parameter to reduce the contact pressure between the gears; it reduces the errors and minimizes the losses for the face milling and the hobbing processes [54, 55]. Shih et al. applied the flank modifications on the tooth of a face hobbed gear, to get the favourable conditions. Machine settings and the cutter geometry are also modified and a pinion shape cutter is arranged to simulate the exact surface and flank form. It was repeated for the new 6-axis CNC hypoid generator [56, 57]. Fan provided an advanced algorithm of the contact simulations, with less iterations and mathematical efforts using a complex blade shape [58, 59]. Gabiccini claimed a robust optimization solution of the LTCA with uncertain misalignment, which often occurs during the assembly of the gear pair [60]. Artoni et al. presented their work based on an ease off topology to reduce the transmission errors by optimizing the flank shape, the machine settings and the LTCA [61, 62]. Kolviand et al. used a graphical way to present the LTCA by meshing the gear and pinion surfaces into grid and get rid of the calculations for the principal curvatures and directions [63, 64]. Sheveleva et Al. worked on the meshing and contact algorithms to observe the transmission error, the bearing contact and the pressure distribution, using the classical Hertz and non- Hertz solutions [65].

2.2   Research problems and objectives

Design, analysis, and machining of hypoid gears are quite complicated processes. For favourable geometry of the gear teeth, several experimental iterations are performed, to

evaluate the machining and design parameters. Literature reveals the designing and machining cycle, which is shown in the Fig. 2.1. For the given transmission system, parameters of the gear and the pinion blanks are calculated using the AGMA standards. The teeth surfaces are designed and analysed using the FEA module to calculate the contact and bending stresses. These surfaces are sent to the computer-based TCA algorithm, to analyse the contact conditions [1]. Machine setting parameters are calculated for these surfaces, and the pilot gear pair is machined. A physical TCA test is performed in a special machine called Universal Tester. The pilot gear and pinion surfaces are digitized using the CMM and surface deviations between the pilot gears and the designed surfaces are measured. If the surface deviations are more than the specified tolerances, the surfaces are modified in the CAD-models and the whole procedure is repeated until the measurement of surface deviations researches the specified tolerances. The corrections in the machine setting are also calculated to supress the deviations. Later on, the production of the gear pair starts.
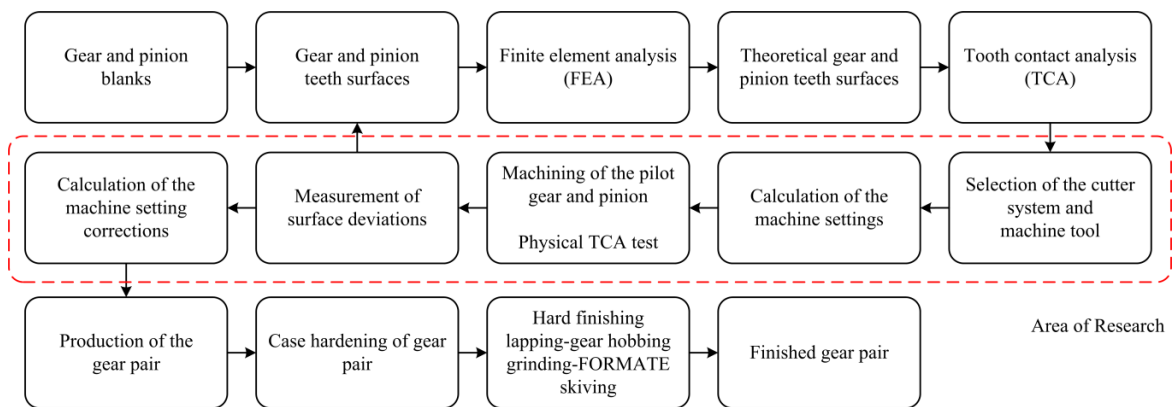
Figure 2.1. Analysis and machining cycle of spiral bevel and hypoid gears.

Deviations between the designed and the machined surfaces exist, due to the modelling approximation of the gear teeth, which is currently based on the simplified blade model; this deviation cumulates with more error due to the calculation of the machine settings by neglecting the cutter design as shown in the Fig. 2.2. This is a potential research problem, which is addressed in the current research.
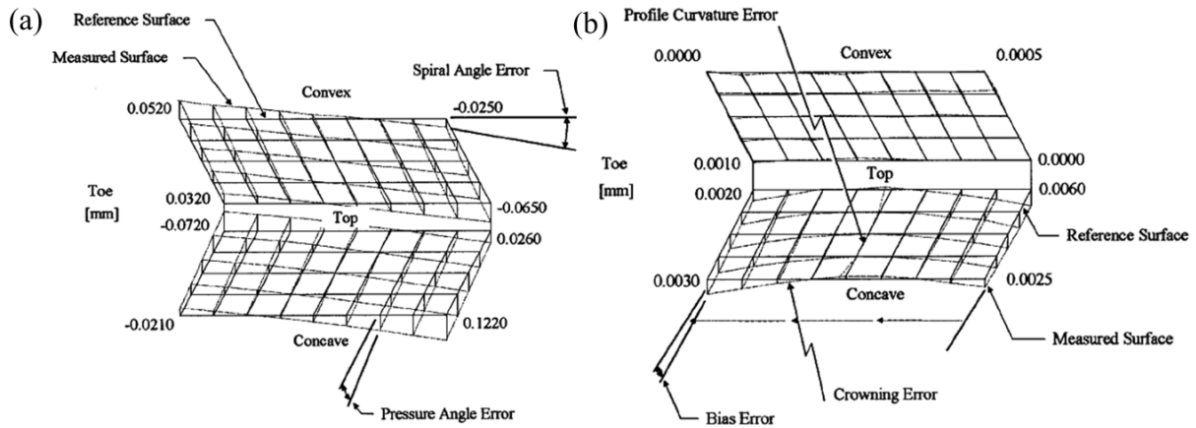
Figure 2.2. Errors between the designed and machined surfaces, (a) 1st Order errors, (b) 2nd order errors [38].

2.2.1 Identification of research problem

As discussed in the section 1.2.2, the gear tooth surface machined by the non-generated process, is the copy of cutting surface, which is formed by revolving the tooth cutting edge of the blade about the cutter rotation axis as shown in the Fig. 2.3.

In the previous research, cutting surface is formed by revolving a tooth cutting edge of the simplified blade model, about the cutter axis. The blade model is called simplified,

18

because the rake, relief and hook angles are neglected, and it is assumed that the tooth cutting cutting edge of the cutter blade lay on the normal plane of the cutter as shown in the Fig. 2.4(a).
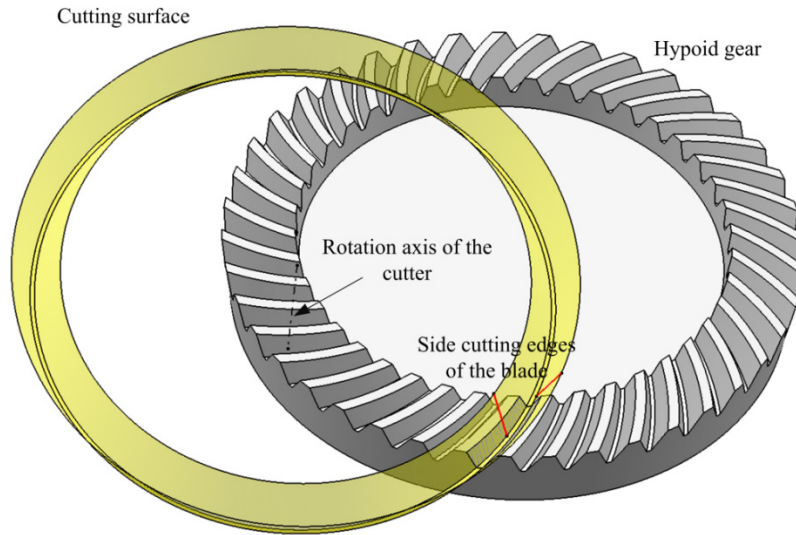
Figure 2.3. Hypoid gear tooth formed by the cutter sweep envelope in a non-generated machining process.
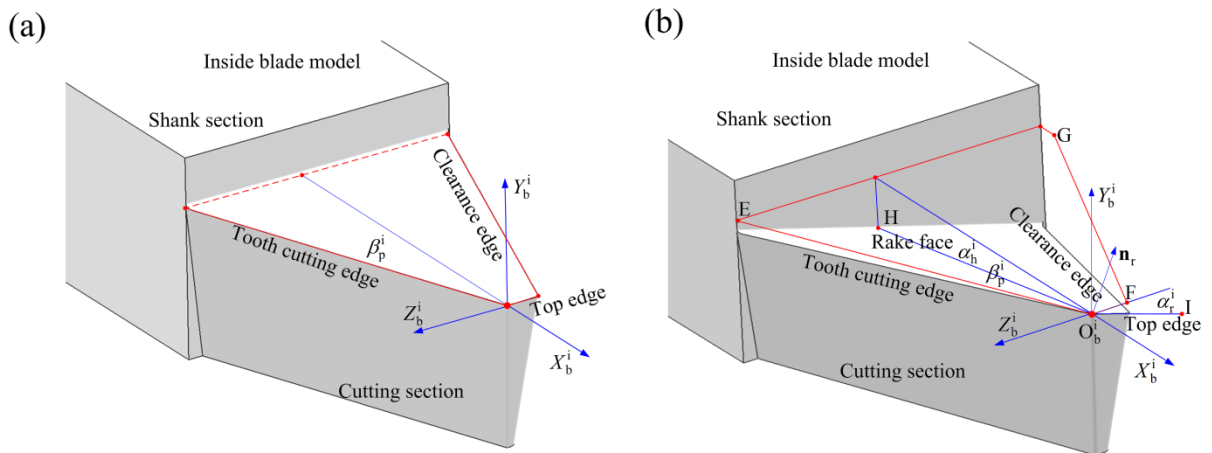
Figure 2.4. Inside blade, (a) simplified blade model, (b) accurate blade model.

In practical gear machining, the top and the tooth cutting edge of the blade lay on the rake plane of the blade, which is the function of the pressure (β_p), the rake (α_r) and the hook (α_h) angles as shown in the Fig. 2.4(b). The pressure angle (β_p) controls the cross section of the cutter sweep surface that forms the tooth flank and depends on the rake (α_r) and the hook angles (α_h), which are essential for the efficient metal cutting [66]. The normal cross section of a cutting surface formed by revolving the tooth cutting edge of an accurate blade model, are the hyperboloids, on the convex and concave side of the gear teeth flanks [67], rather than the straight flanks, as assumed in the previous research. Due to the hyperboloid geometry of the cutting surface, the pressure angle is not equal to the gear flank angle. Therefore, for the precise machining of the gear teeth, it is needed to calculate the cutter parameters for the given design of the gear and the pinion teeth.

For the machining analysis of hypoid gears, specialized software are used to determine cutter system parameters and to calculate machine settings. Unfortunately, the software is developed specifically for certain machine tools, not be able to cope up with different machine tools. A few published technical articles clearly address the CNC programming and the post-processing for the multi-axis face-milling of hypoid gears, such as the cutter system determination, the cutter location and orientation calculation, and the CNC machining codes generation. It is in high demand from industry to develop generic CAM software for face-milling hypoid gears on different hypoid gear machine tools.

2.2.2 Proposed objectives

Objectives of this research are focussed on the mentioned technical challenge. Following objectives are set to overcome the current research problems;

1. Developing a CAD based mathematical model to determine the cutter geometry, for the given design of the hypoid gear and the pinion teeth.

2. Developing a generic approach to CNC programming and post-processing for the CNC face-milling of hypoid gears.

These new approaches provide a general and accurate methodology for the face-milling of hypoid gears on any machine tools with the accurate cutter geometry, and can be directly applied to the hypoid gear manufacturing for the better quality.

This dissertation thesis is divided into following three chapters, chapter 3 addresses the method of local synthesis [7], which relates the geometry of two tangent surfaces at a specified point; it is used to determine the cutter geometry for the face milling of gears and pinions. The cutter determination model is presented in the chapter 4, which presents the selection of the cutter radius and the pressure angle of the tooth cutting edge for the face-milling of hypoid gears and the conjugate pinion. Chapter 5 of the thesis contains, the CNC programming and the post-processing model for the face milling of the hypoid gears. In this chapter, the designed cutter model is taken into consideration for the face-milling of the given tooth geometry of the gear, in a generic multi-axis CNC machine.

Chapter 3

Local synthesis between the gear, pinion and the cutter surfaces

Local synthesis is a method of applying tangency between two mating surfaces at a specified mean point, which relates the principal curvatures, and directions of the two surfaces [7]. Determination of cutter geometry and machining parameters are performed using the local synthesis between the given geometry of the gear and the cutting surface. The surface parameters of the pinion teeth are evaluated using the local synthesis between the gear and the pinion. Finally, the cutting surface and machining parameters for the calculated geometry of the pinion are computed using the local synthesis between the pinion and the pinion-cutting surface at the mean point as shown in the Fig. 3.1.
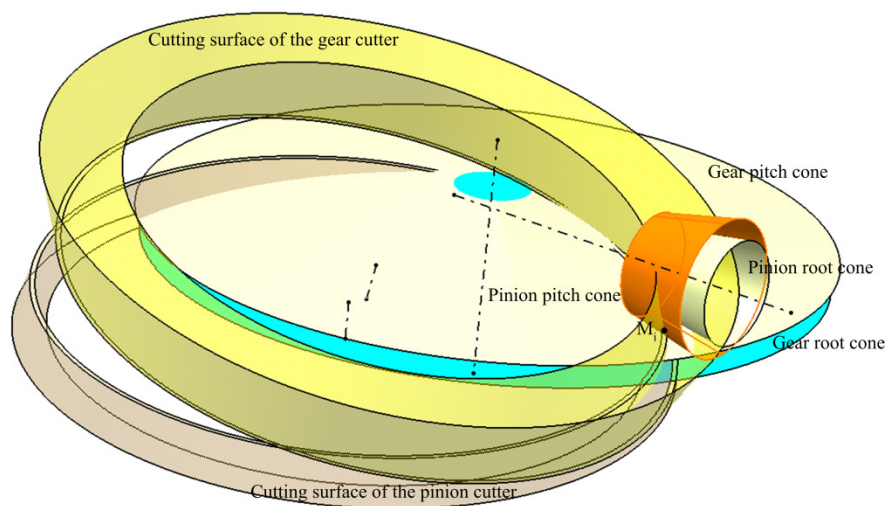
Figure 3.1. Local synthesis between gear cutting surface, gear, pinion and pinion cutting surface

The method of local synthesis is well developed in the previous research [7]. It is used in this research for the determination of surface geometries tangent to a known surface geometry. As mentioned above, the local synthesis is initiated from the known parameters of the hypoid gear; therefore, the geometry of the hypoid gears is discussed in the following section. Local synthesis between the gear and the gear cutting surface, the gear and the pinion, and the pinion and the pinion cutting surface are presented in the next sections.

3.1   Geometry of hypoid gears

Hypoid gear geometry can be divided into two major components, the blank, and the gear teeth. Hypoid gears machined with different machining processes have different parameters of gear geometries. A generalized model of the hypoid gear is discussed in this section, to illustrate the geometry of the gear blank and the teeth.

First a gear blank is defined using a coordinate system $X_w Y_w Z_w O_w$, which is attached with the centre face of the gear blank, having the X_w axis along the gear rotation axis, whereas $Y_w Z_w$ axes are on the blank face. The gear blank is defined by three cones; root cone, pitch cone and face cone, having the cone angles Γ_R, Γ and Γ_o with the apices O_r, O_p and O_f respectively, on the rotation axis of the gear blank. The cross section on the $X_w Y_w$ plane of the gear blank is shown in the Fig. 3.2. Length of the gear tooth is defined along the pitch cone generatrix, which is called face width and denoted by F. Location of a point N along the pitch cone generatrix is defined by the length L_p, which is located at the centre of the face width. A tooth section at the start of the face width is called toe, whereas, the tooth section at

the end of the face width is called heel. The gear tooth height is defined at the heel, which is the sum of addendum a_{oG} and the dedendum b_{oG}.

Figure 3.2. Illustration of a generalized hypoid gear blank.

The projection of the point N on the root cone generatrix is denoted by N_r. Location of a designated mean point M is calculated, which is chosen for the tangency of the gear and the pinion teeth surfaces. This mean point M lies on a line perpendicular to the root cone generatrix at the point N_r. The height of the point M along this line, measured from the point N_r is denoted by h_M, which is the average of the gear and the pinion dedendums at that point. The gear and the pinion dedendums are calculated using the AGMA formulations [68]

$$b_G = b_{oG} - \frac{1}{2} \cdot F \cdot \sin(\delta_G) \tag{3.1}$$

$$b_{\mathrm{P}} = a_{\mathrm{oG}} - \frac{1}{2} \cdot F \cdot \sin(\alpha_{\mathrm{G}}) + c \tag{3.2}$$

where α_{G} and δ_{G} are the gear addendum and dedendum angles, b_{G} and b_{P} are the gear and pinion dedendums at the mean point, and c is the clearance between the gear and the pinion. Thus, the height h_{M} can be calculated as

$$h_{\mathrm{M}} = \frac{b_{\mathrm{G}} + b_{\mathrm{P}}}{2} \tag{3.3}$$

The distance between the root and the pitch cone apices A_{l} can be calculated as

$$A_{\mathrm{l}} = \frac{L_{\mathrm{p}} \cdot \sin(\delta_{\mathrm{G}}) - b_{\mathrm{G}}}{\sin(\Gamma_{\mathrm{r}})} \tag{3.4}$$

The distance A_{w} between the top face centre and the root cone apex O_{r} can be calculated with the following equation

$$A_{\mathrm{w}} = A_{\mathrm{l}} + \left(L_{\mathrm{p}} - \frac{f_{\mathrm{w}}}{2} + h_{\mathrm{i}} + b_{\mathrm{iG}} \right) \cdot \cos(\Gamma) \tag{3.5}$$

where h_{i} is the tooth height at the toe, b_{iG} be the gear dedendum at the toe. Besides, the equation of the length $O_{\mathrm{r}} N_{\mathrm{r}}$, is

$$L_{\mathrm{r}} = L_{\mathrm{p}} \cdot \cos(\delta_{\mathrm{G}}) - A_{\mathrm{l}} \cdot \cos(\Gamma_{\mathrm{r}}) \tag{3.6}$$

Second, the gear tooth profile is defined, using a plane tangent to the root cone generatrix which is shown in the Fig. 3.3.
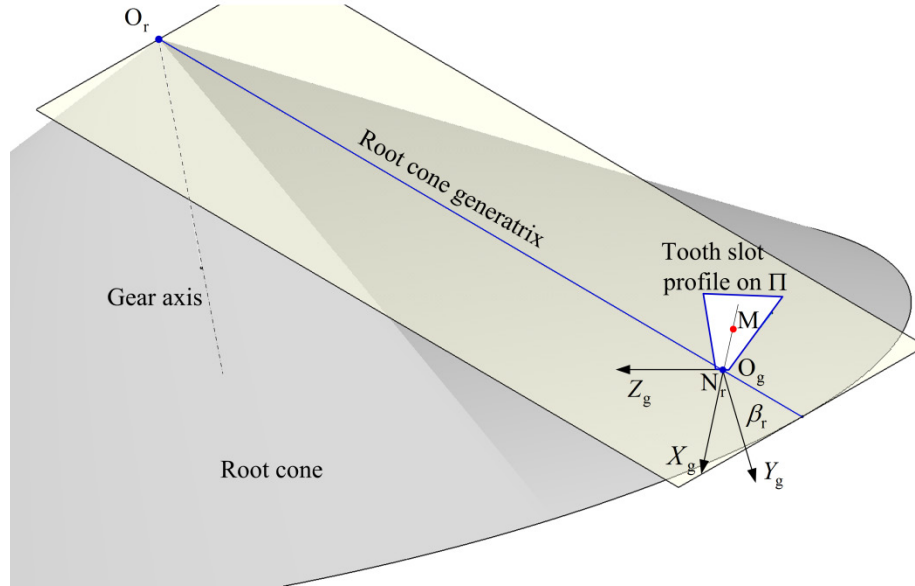
Figure 3.3. Gear tooth profile on the root cone of the hypoid gear.

A direction on the root cone tangent plane is considered that forms the root spiral angle β_r with the root cone generatrix. Based on its definition, the tooth profile plane Π is considered, which passes through O_gM and is normal to that direction. On this plane Π, a coordinate system $X_g Y_g Z_g O_g$ is set-up as follows: the X_g axis is on the line of O_gM and points downwards, the Y_g axis is normal to the plane Π and directed away from the root cone apex. Z_g axis is determined with the right-hand rule. The root land R_iR_o is on the Z_g axis and is equal to the point width P_w as shown in the Fig. 3.4. Point O_g is in the middle of R_iR_o. The inside and the outside flanks are drawn so that the angles between the flanks and the X_g

axis are equal to angles α_g^i and α_g^o. The points M_i and M_o on the flanks corresponding to

the mean point M are the intersection points between a line passing through point M and

parallel to the Z_g axis, and the two flanks. The height of the gear tooth in the plane Π is

measured as h. The curvatures $\kappa_{I,g}$ and $\kappa_{II,g}$ at the points M_i and M_o are defined. This is how

the gear tooth profile is calculated in the initial design of the hypoid gear.
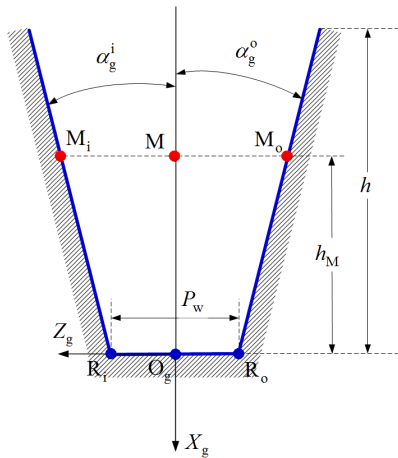
Figure 3.4. Cross section of the gear tooth.

3.2   Local synthesis between gear and gear-cutter

In the non-generated face milling of the gear, the cutter machines a tooth slot in a spiral way

by rotating and feeding along its axis to the gear root. After a tooth slot is completed, the

gear is rotated by an indexing angle of one tooth, and then the cutter starts to machine the

next tooth slot. In this machining method, the gear is intermittently indexed. Here, the

envelope surface of the blades, rotating about the cutter head axis is called the cutting

surface. Therefore, the gear teeth shape is the same as the cutting surface, which is the

geometric relationship between the gear and the cutter and shown in Fig. 3.5.
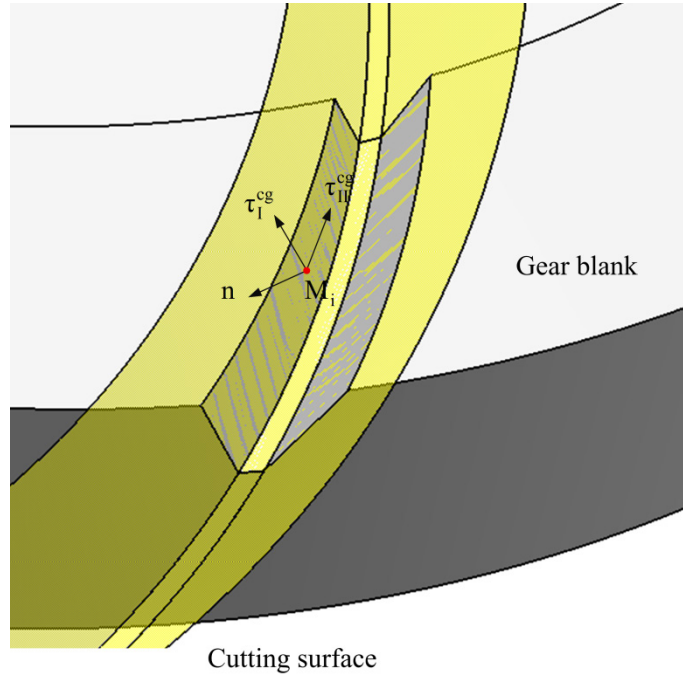
Figure 3.5. Gear tooth machined by a cutting surface using the non-generated face milling

Due to the mentioned geometrical relationship between the gear and the gear cutting surface, the cutting surface should satisfy the specified tooth profile at points M_i and M_o. Thus, the gear parameters, such as, the curvatures at these points (κ_g^i, κ_g^o) and the gear flank angle (α_g^i, α_g^o) are used to determine the geometry of the gear cutting surface at those points. Therefore, the principal directions of the gear ($\tau_{I,g}^i$, $\tau_{II,g}^i$, $\tau_{I,g}^o$, $\tau_{II,g}^o$) and the cutting surface ($\tau_{I,cg}^i$, $\tau_{II,cg}^i$, $\tau_{I,cg}^o$, $\tau_{II,cg}^o$) are same in magnitude as well as the directions.

3.3   Local synthesis between gear and pinion

Local synthesis between a gear and conjugated pinion is applied to relate the principal

28

curvatures and the direction of the gear and the pinion, on the points M_i and M_o. The geometrical relation between the gear and the pinion are shown in the Fig. 3.6. Coordinate systems O_g and O_{pn} are rigidly attached with the gear and the pinion, where, the axes X_g and X_{pn} are the rotation axes of the gear and the pinion respectively.
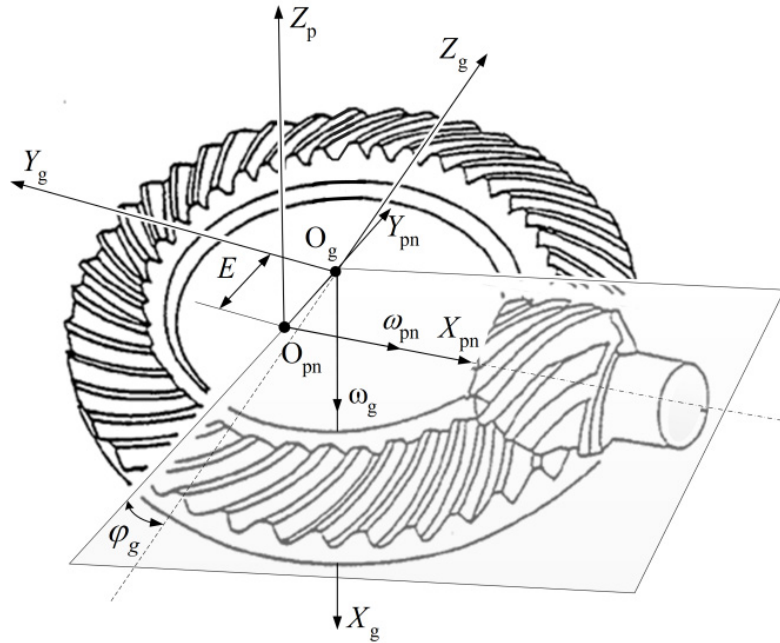
Figure 3.6. Hypoid gear and pinion assembly.

To align the axes of the gear and the pinion parallel to each other, the gear is to be rotated with an angle of φ_g about the rotation axis of the gear, whereas, E be the offset between the gear and the pinion. The parameter φ_g is calculated by applying the equation of meshing between the gear and the pinion at the point M_i on the driving side of the gear teeth. The equation of meshing defines the contact principal and states that the relative velocity V_{pg} of the gear and the pinion remains perpendicular to a common unit normal n at the point M_i,

where, the unit normal n is the cross product of the principal directions $\tau_{I,g}$ and $\tau_{II,g}$. The equation of meshing is given by

$$n.V_{pg} = 0 \qquad (3.7)$$

where,
$$V_{pg} = (\omega_p - \omega_g) \times M_i - R_p \times \omega_g \qquad (3.8)$$

The angular velocities of the gear ω_g and the pinion ω_p are related with each other by a velocity ratio I_{pg}, and vector R_p represents the offset between the O_g and O_{pn}.
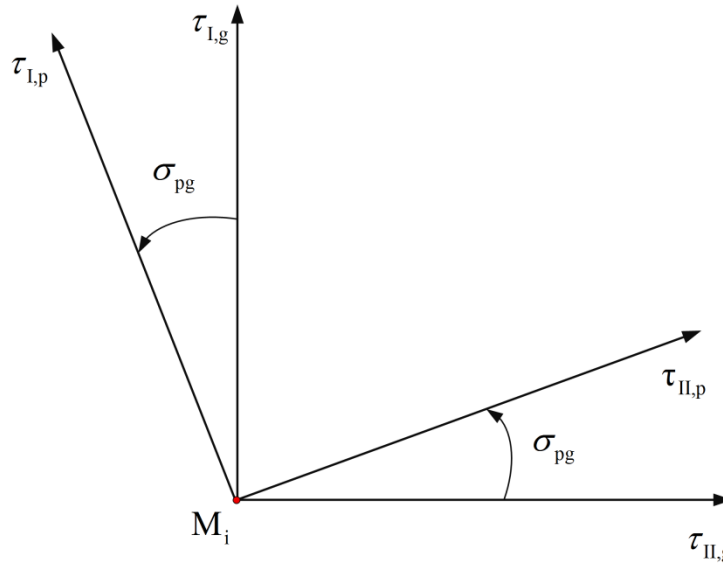
Figure 3.7. Principal directions of a gear and conjugated pinion at the point M_i.

Since the angle φ_g is calculated using the equation of meshing, principal directions of the gear are transformed to the O_{pn} coordinate system. Due to the tangency of the gear and the pinion teeth surfaces at the point M_i, the principal directions of the two surfaces lie at a

common tangent plane, passing through the point M_i and the points O_g and O_{pn}. Therefore, the principal directions of the gear ($\tau_{I,g}$, $\tau_{II,g}$) and the pinion ($\tau_{I,p}$, $\tau_{II,p}$) on the common tangent plane are related to each other, and are shown in the Fig. 3.7.

Angle σ_{pg} between the principal directions of the two gears can be determined by considering the contact ellipse theory and the local synthesis equations [5], which relate the contact velocity v_r and transfer velocity v_t with the geometrical parameters of the gear and the pinion. These equations are given by

$$v_{r,g} = v_{r,p} + V_{pg} \tag{3.9}$$

$$\dot{n}_{r,g} = \dot{n}_{r,p} + (\omega_{pg} \times n_g) \tag{3.10}$$

$$\frac{d}{dt}(n \cdot V_{pg}) = 0 \tag{3.11}$$

where, ω_{pg} is the relative angular velocity of the gear pair, $\dot{n}_{r,g}$ and $\dot{n}_{r,p}$ be the velocities of the normals tip on the contact point of the gear and the pinion respectively. The above equations are transformed in terms of the pinion contact velocity $v_{r,p}$ and are resolved into the components along the principal directions of the pinion ($\tau_{I,p}$, $\tau_{II,p}$) as shown in the Fig. 3.8.
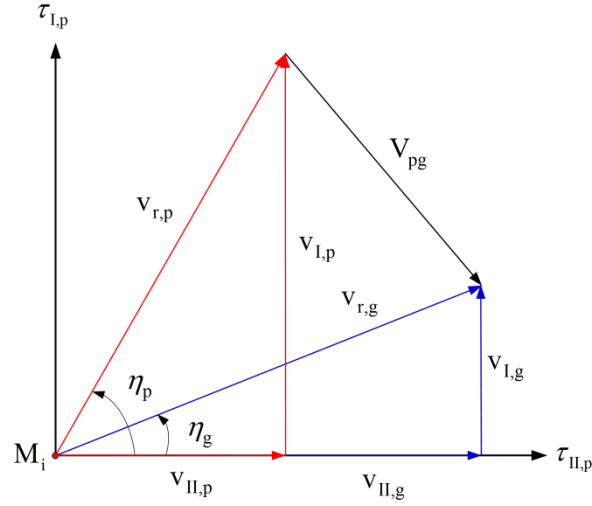
Figure 3.8. Contact velocities along the principal directions of the pinion.

where, η_g and η_p are the tangent directions of the contact paths on the gear and pinion teeth, mathematically the Eqs. 3.9 to 3.11 in resolved form are given by [6],

$$\begin{bmatrix} b_{11} & b_{12} \\ b_{21} & b_{22} \\ b_{31} & b_{32} \end{bmatrix} \cdot \begin{bmatrix} V_{I,p} \\ V_{I,p} \end{bmatrix} = \begin{bmatrix} b_{13} \\ b_{23} \\ b_{33} \end{bmatrix}$$ (3.12)

where,

$$b_{11} = \kappa_{I,g} - 0.5(\kappa_{I,p} + \kappa_{II,p}) - 0.5(\kappa_{I,p} - \kappa_{II,p}).\cos 2\sigma_{pg}$$

$$b_{12} = b_{21} = 0.5(\kappa_{I,p} - \kappa_{II,p}).\sin 2\sigma_{pg}$$

$$b_{22} = \kappa_{II,g} - 0.5(\kappa_{I,p} + \kappa_{II,g}) + 0.5(\kappa_{I,p} - \kappa_{II,p}).\cos 2\sigma_{pg}$$

$$b_{13} = -\kappa_{I,g}.V_{I,pg} + (n \times \omega_{pg}).\tau_{I,g}$$

$$b_{23} = -\kappa_{II,g}.V_{II,pg} + (n \times \omega_{pg}).\tau_{II,g}$$

$$b_{33} = \kappa_{II,g}.\left(V_{I,pg}\right)^2 + \kappa_{II,g}.\left(V_{II,pg}\right)^2 + n \cdot (\omega_{pg} \times V_{pg}) - n.(\omega_p \times v_{t,g} - \omega_g \times v_{t,p}) - \frac{I'_{pg}}{I_{pg}}.\omega_p.(n.v_{t,g})$$

$$I_{pg} = N_p/N_g \,; V_{I,pg} = V_{pg} \cdot \tau_{I,g} \,; V_{II,pg} = V_{pg} \cdot \tau_{II,g}$$

Since the principal curvatures of the pinion $\kappa_{I,p}$, $\kappa_{II,p}$ and the angle σ_{pg} are unknown, therefore, the coefficients b_{11}, b_{12} and b_{22} are also unknown. The other coefficients can be calculated using the pre-defined parameters of the contact path, which are, the tangent direction of the contact path η_g, length of semi major axis D_L formed during the instantaneous contact, as shown in the Fig. 3.9, and the derivative of the transmission ratio I'_{pg}, which defined the transmission path of the contact.

(a)   (b)
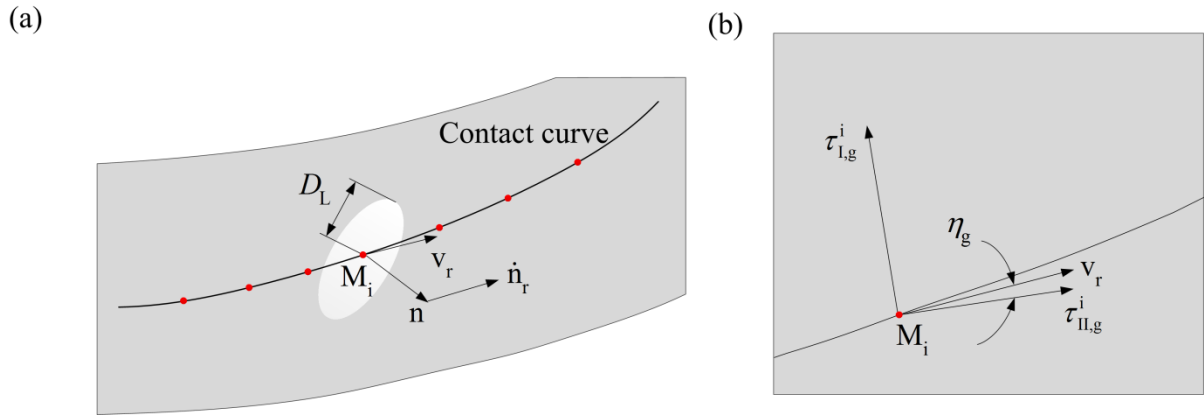
Figure 3.9. Contact curve between the gear and pinion, (a) contact ellipse and the contact velocities, (b) principal directions of the gear tooth and the contact direction.

Using the known parameters and coefficients, following relationship are established [3];

$$\tan \eta_p = \frac{\left(b_{33} + b_{13} \cdot V_{I,pg}\right) \cdot \tan \eta_g - b_{13} \cdot V_{II,pg}}{b_{33} + b_{23} \cdot \left(V_{II,pg} - V_{I,pg} \cdot \tan \eta_g\right)} \tag{3.13}$$

$$V_{I,p} = \frac{b_{33}}{b_{13} + b_{23}.\tan \eta_p} \tag{3.14}$$

$$\mathrm{v}_{\mathrm{II,p}} = \frac{b_{33}.\tan\eta_p}{b_{13} + b_{23}.\tan\eta_p} \tag{3.15}$$

$$K_{\Sigma} = (\kappa_{\mathrm{I,g}} + \kappa_{\mathrm{II,g}}) - (\kappa_{\mathrm{I,p}} + \kappa_{\mathrm{II,p}}) = \frac{\dfrac{(b_{13})^2 + (b_{23})^2}{(\mathrm{v}_{\mathrm{I,p}})^2 + (\mathrm{v}_{\mathrm{II,p}})^2} - 4A^2}{\dfrac{b_{13}\cdot\mathrm{v}_{\mathrm{I,p}} + b_{23}\cdot\mathrm{v}_{\mathrm{II,p}}}{(\mathrm{v}_{\mathrm{I,p}})^2 + (\mathrm{v}_{\mathrm{II,p}})^2} + 2A} \tag{3.16}$$

$$A = \frac{\delta_{\mathrm{D}}}{D_{\mathrm{L}}^{\ 2}} \tag{3.17}$$

$$b_{11} = \frac{b_{13}.\mathrm{v}_{\mathrm{I,p}} - b_{23}.\mathrm{v}_{\mathrm{II,p}} + K_{\Sigma}(\mathrm{v}_{\mathrm{II,p}})^2}{\left(\mathrm{v}_{\mathrm{I,p}}\right)^2 + \left(\mathrm{v}_{\mathrm{II,p}}\right)^2} \tag{3.18}$$

$$b_{22} = \frac{-b_{13}.\mathrm{v}_{\mathrm{I,p}} + b_{23}.\mathrm{v}_{\mathrm{II,p}} + K_{\Sigma}(\mathrm{v}_{\mathrm{I,p}})^2}{\left(\mathrm{v}_{\mathrm{I,p}}\right)^2 + \left(\mathrm{v}_{\mathrm{II,p}}\right)^2} \tag{3.19}$$

$$b_{12} = \frac{b_{13}.\mathrm{v}_{\mathrm{II,p}} + b_{23}.\mathrm{v}_{\mathrm{I,p}} - K_{\Sigma}.\mathrm{v}_{\mathrm{I,p}}.\mathrm{v}_{\mathrm{II,p}}}{\left(\mathrm{v}_{\mathrm{I,p}}\right)^2 + \left(\mathrm{v}_{\mathrm{II,p}}\right)^2} \tag{3.20}$$

Since unknown coefficients (b_{11}, b_{12} and b_{22}) are in terms of known coefficients (b_{13}, b_{23} and

b_{33}) and can be calculated, therefore, by solving the unknown coefficients

$$\kappa_{\mathrm{I,p}} - \kappa_{\mathrm{II,p}} = \frac{2b_{12}}{\sin 2\sigma_{\mathrm{pg}}} \tag{3.21}$$

$$\tan 2\sigma_{\mathrm{pg}} = \frac{2b_{12}}{\kappa_{\mathrm{I,g}} + \kappa_{\mathrm{II,g}} - (b_{11} - b_{22})} \tag{3.22}$$

Therefore, from the Fig. 3.7, principal directions of the pinion can be calculated by,

$$\tau_{I,p} = \tau_{I,g}.\cos\sigma_{pg} - \tau_{II,g}.\sin\sigma_{pg} \tag{3.23}$$

$$\tau_{II,p} = \tau_{I,g}.\sin\sigma_{pg} + \tau_{II,g}.\cos\sigma_{pg} \tag{3.24}$$

Using the equations 3.16 and the 3.21, the principal curvatures of the pinion ($\kappa_{I,p}$, $\kappa_{II,p}$) are determined. Therefore, the local synthesis between the gear and the pinion are completed with the calculated geometry parameters of the pinion at the point M_i, which are the parameters of the concave side of the pinion, these are the principal directions ($\tau_{I,p}$, $\tau_{II,p}$) and the principal curvatures ($\kappa_{I,p}$, $\kappa_{II,p}$).

3.4   Local synthesis between pinion and pinion cutter

During the face milling generation process of the pinion, the contact between the pinion tooth surface and the cutting surface is a line contact. Since the cutting surface is tangent to the pinion tooth surface along the cutting line, which contains the point M_i, therefore, the principal directions of the cutting surface, also lie on the same tangent plane defined by the points M_i, O_g and O_{pn}. It is to be noted that to cut the concave side of the pinion tooth tangent to the convex side of the gear tooth, the outside cutting surface of the cutting surface is used. Therefore, the principal directions of the pinion-cutting surface ($\tau_{I,cp}$, $\tau_{II,cp}$) are related with the principal directions of the gear ($\tau_{I,g}$, $\tau_{II,g}$) and the pinion ($\tau_{I,p}$, $\tau_{II,p}$), as shown in the Fig. 3.10.
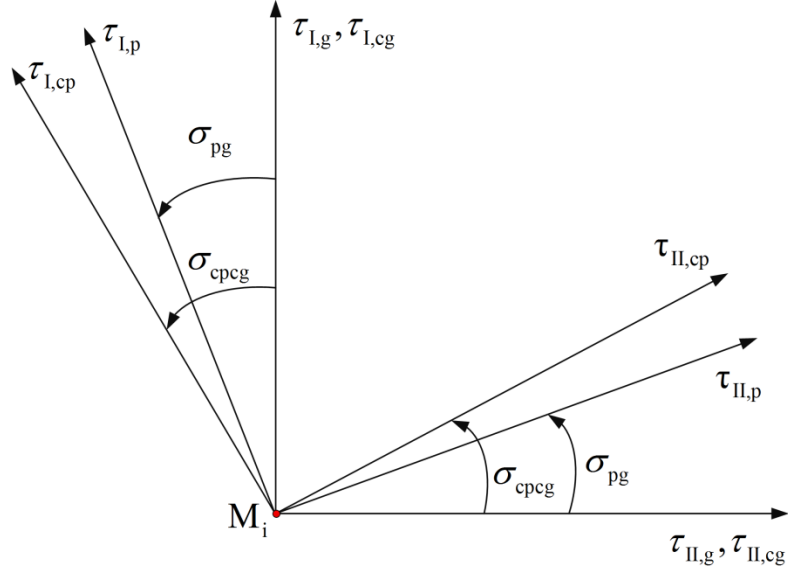
Figure 3.10. Principal directions of the gear, gear cutter, pinion and pinion cutter

Since the rotation axes of the gear cutter and the pinion cutter are perpendicular to the root cone tangent planes of the gear and the pinion respectively. Therefore, the angle σ_{cpcg} between the principal directions of the gear cutter and the pinion cutter, is equals to the difference between the root and face cone angles of the gear, angle σ_{cpcg} is given by

$$\cos \sigma_{cpcg} = \cos \sigma_{cpg} = \Gamma_{\circ} - \Gamma_{R} \tag{3.25}$$

Therefore, at the point M_i, the principal directions of the pinion cutting surface, and the angle between the principal directions of the pinion and the pinion cutting surface are given by [8]

$$\tau_{I,cp} = \tau_{I,g} . \cos \sigma_{cpcg} - \tau_{II,g} . \sin \sigma_{cpcg} \tag{3.26}$$

36

$$\tau_{\text{II,cp}} = \tau_{\text{I,g}}.\sin\sigma_{\text{cpcg}} + \tau_{\text{II,g}}.\cos\sigma_{\text{cpcg}} \tag{3.27}$$

$$\sigma_{\text{cpp}} = \cos^{-1}\left(\tau_{\text{I,cp}} \cdot \tau_{\text{I,p}}\right) \tag{3.28}$$

To calculate the pinion principal curvatures, equation of meshing and the contact velocity relations between the pinion and the pinion-cutting surface are applied at the point M_i which are

$$v_{\text{r,cp}} = v_{\text{r,p}} + V_{\text{pcp}} \tag{3.29}$$

$$\dot{n}_{\text{r,cp}} = \dot{n}_{\text{r,p}} + \left(\omega_{\text{pcp}} \times n\right) \tag{3.30}$$

$$\frac{d}{dt}(n.\vec{V}_{\text{pcp}}) = 0 \tag{3.31}$$

where, ω_{pcp} is the relative angular velocity of the pinion and the pinion cutter, $\dot{n}_{\text{r,p}}$ and $\dot{n}_{\text{r,cp}}$ be the velocities of the normals tip on the contact point of the pinion and the cutter respectively. The above equations are transformed in terms of pinion contact velocity $v_{\text{r,cp}}$ and are resolved into the components along the principal directions of the pinion ($\tau_{\text{I,cp}}$, $\tau_{\text{II,cp}}$)

$$\begin{bmatrix} d_{11} & d_{12} \\ d_{21} & d_{22} \\ d_{31} & d_{32} \end{bmatrix} \cdot \begin{bmatrix} v_{\text{I,cp}} \\ v_{\text{II,cp}} \end{bmatrix} = \begin{bmatrix} d_{13} \\ d_{23} \\ d_{33} \end{bmatrix} \tag{3.32}$$

where,

$$d_{12} = d_{21} = 0.5(\kappa_{I,p} - \kappa_{II,p}) \cdot \sin(2\sigma_{pcp})$$

$$d_{11} = \kappa_{I,cp} - 0.5(\kappa_{I,p} + \kappa_{II,p}) - 0.5(\kappa_{I,p} - \kappa_{II,p}) \cdot \cos(2\sigma_{pcp})$$

$$d_{22} = \kappa_{II,cp} - 0.5(\kappa_{I,p} + \kappa_{II,p}) + 0.5(\kappa_{I,p} - \kappa_{II,p}) \cdot \cos(2\sigma_{pcp})$$

$$d_{13} = -\kappa_{I,cp} \cdot V_{I,pcp} + (n \times \omega_{pcp}) \cdot \tau_{I,p}$$

$$d_{23} = -\kappa_{II,cp} \cdot V_{II,pcp} + (n \times \omega_{pcp}) \cdot \tau_{II,p}$$

$$d_{33} = \kappa_{I,cp} \cdot \left(V_{I,pcp}\right)^2 + \kappa_{II,cp} \cdot \left(V_{II,pcp}\right)^2 - V_{pcp} \cdot (n \times \omega_{pcp}) - n \cdot (\omega_{cp} \times v_{t,p} - \omega_p \times v_{t,cp}) - n. \frac{m'_f}{m_f} \cdot (\omega_p \cdot \omega_{cp})$$

where, m_f be the roll ratio, which is the ratio between the pinion and cradle angular velocity.

Since the principal curvatures of the pinion cutting surface ($\kappa_{I,cp}$ and $\kappa_{II,cp}$) are unknown, therefore, all the coefficients are the unknown. But due to the line contact between the pinion and the cutting surface, the Eq. 3.32 does not have a unique solution, and have augmented matrix of rank equal to 1 [3], therefore, it provides the relation

$$\kappa_{II,cp} = \frac{\kappa_{I,p} \cdot \kappa_{II,p} - \kappa_{I,cp} \cdot \left[\kappa_{I,p} \cdot \sin^2\left(\sigma_{pcp}\right) + \kappa_{II,p} \cdot \cos^2\left(\sigma_{pcp}\right)\right]}{-\kappa_{I,cp} + \kappa_{I,p} \cdot \cos^2\left(\sigma_{pcp}\right) + \kappa_{II,p} \cdot \sin^2\left(\sigma_{pcp}\right)} \tag{3.33}$$

This relation is used in the pinion-cutter determination model for the curvatures of pinion-cutting surface. Using the current local synthesis, the local geometry of the inside cutting surface of the pinion cutter is determined which includes, the principal directions ($\tau_{I,cp}$, $\tau_{II,cp}$) and the relationship between the principal curvatures (Eq. 3.33) of the cutting surface. The similar local synthesis method is also applied on the concave side of the gear, which determines the local geometry of the inside cutting surface of the pinion cutter.

Chapter 4

An Accurate Approach to Determine Average Cutter Radius and Blade Pressure Angle for the CNC Face-Milling of Hypoid Gears

Unlike conventional milling cutters, a face-milling cutter of hypoid gears includes a group of inside and outside blades set up around the axis of the cutter head as shown in the Fig. 4.1. To reduce the machining error of the gear and pinion, the cutter systems are crucial; unfortunately, the current methods determine the cutter systems in an approximate way.
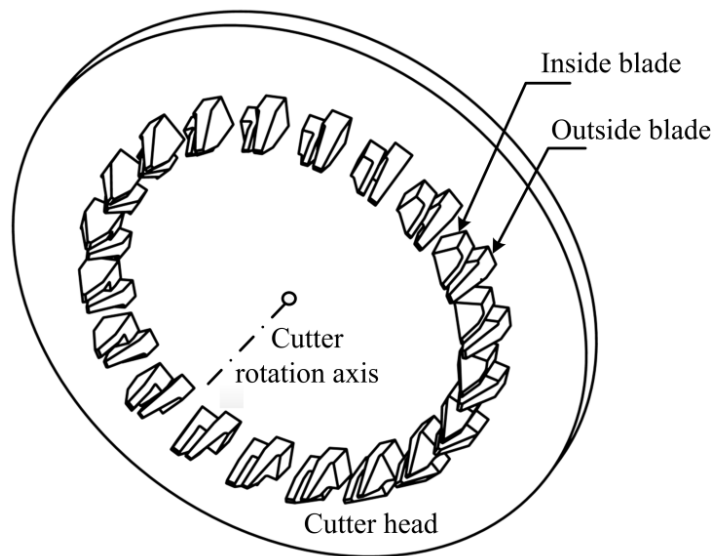
Figure 4.1. Cutter head for the face milling of hypoid gears.

The existing hypoid gear methods use the simplified model of inside and outside blades, resulting in large errors in the machined hypoid gears. It is assumed that the cutting

edges of the cutter blade lay on the normal plane of the cutter as shown in the Fig. 4.2(a). Whereas, in practical gear machining, the top and the tooth cutting edge of the blade lay on the rake plane of the blade, which is the function of pressure (β_p), hook (α_h), rake (α_r) and relief angles (γ_f and γ_o) as shown in the Fig. 4.2(b). The pressure angle controls the cross section of the cutter sweep surface that forms the tooth flank, the selection of pressure angle depends on the rake, hook and relief angles, which are essential for the efficient metal cutting.
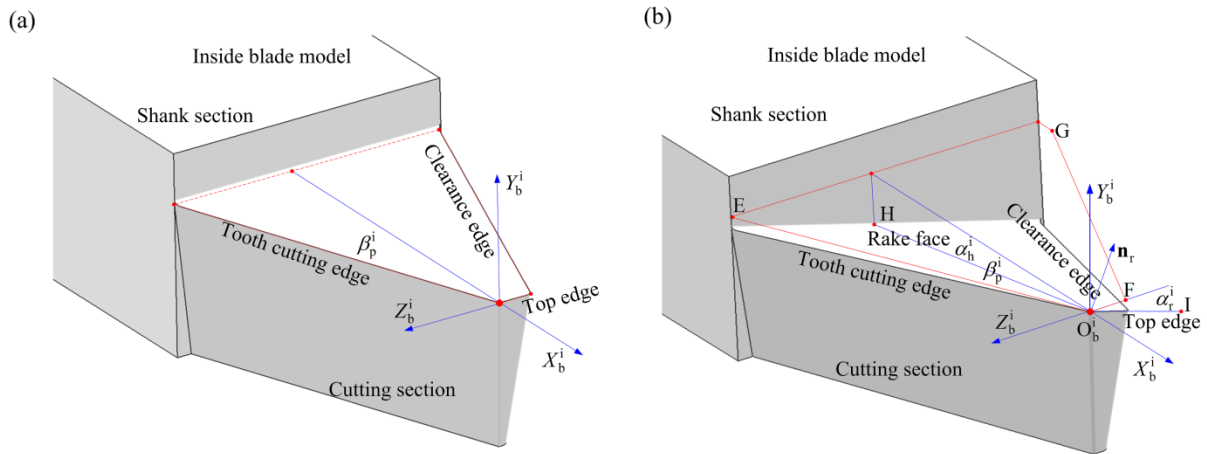
Figure 4.2. Inside blade, (a) simplified blade model, (b) accurate blade model.

In this research, for the given gear and pinion tooth geometry, selection of the average cutter radius R_{ac}, inside and outside pressure angles (β_p^i and β_p^o) are addressed. Whereas, the rake, hook and relief angles are assumed to be already calculated using a cutting force or FEA simulation methods, and it is not the scope of this research. The generalized gear geometry is already presented in the section 3.1 of the chapter 3. Therefore, this chapter consists of three major sections, section 4.1 addresses the mathematical

formulation of the cutting system, section 4.2 is based on the determination of the cutting system parameters for the given geometry of the gear and the pinion teeth. In the last section, industrial application of the new approach is presented.

4.1   Mathematical formulation of the cutting surface

For the CNC face-milling of hypoid gears, a special type of cutting system has to be used, which usually consists of a disk-shaped cutter head and many high-speed-steel or carbide tick-type blades. These blades are grouped with an inside and an outside blade, and are set up group by group in slots patterned around the cutter head axis. In machining the gear tooth slots, the blades are rotated around the cutter head axis, and geometrically, the envelope of the revolving blades is called the cutting surface of the cutting system in this work. Due to the complex relationship between the cutting surface and the cutting system parameters, the parameters cannot be directly determined based on the local geometry of the cutting surface. Unfortunately, many existing methods simplify the geometric representation of the cutting system, in order to easily attain the cutting surface geometry. In this work, the blade geometry is accurately modelled and the cutting surface is precisely formulated.

4.1.1   Mathematical representations of tooth cutting edges of the blades

Although cutting systems of different hypoid gear companies are not the same, the structures of their cutter heads and blades share a lot of common features. For example, their blades are classified into two types, the inside and outside blades, which are similar in geometry. Generally, the cutting sections of the blades are defined with the key parameters: rake angle

(α_r^i and α_r^o), hook angle (α_h^i and α_h^o), tooth cutting edge pressure angle (β_{tcp}^i and β_{tcp}^o), clearance edge pressure angle (β_{cp}^i and β_{cp}^o), top edge length (c_{tw}^i and c_{tw}^o), tooth cutting edge relief angle (γ_{tcr}^i and γ_{tcr}^o), top edge relief angle (γ_{tr}^i and γ_{tr}^o) and clearance edge relief angle (γ_{cr}^i and γ_{cr}^o). Of the parameters notations, the superscript "o" refers to the outside blade, and the superscript "i" refers to the inside blade. Since the cutting surfaces are generated with the tooth cutting edges of the inside and outside blades, it is crucial to formulate mathematical representations of these edges. In this work, two common types of inside and outside blades are adopted, and their tooth cutting edge equations are derived.

First, assume a rectangular bar stock of the inside blade, its dimensions are length s_l^i, width s_w^i and height s_h^i, which is shown in Fig. 4.3.
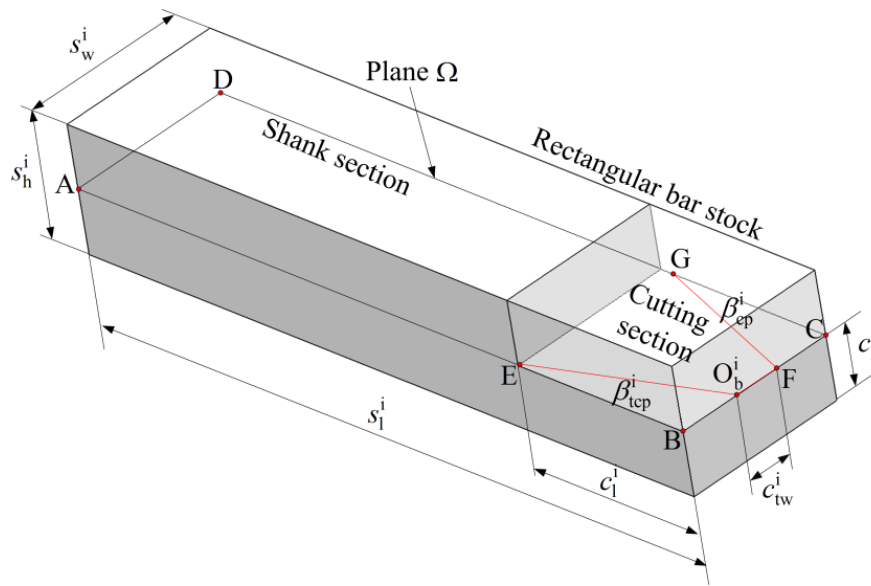
Figure 4.3. An illustrative diagram for constructing an inside blade model.

A plane Ω is drawn parallel to the plane of the length and width at a height c_h^i, which is the

height of the blade cutting tip. This plane intersects with the bar stock at a rectangle ABCD.

Second, point E is located on line AB so that EB is equal to the length c_l^i of the blade

cutting section A point O_b^i is located on line BC with the angle between lines EO_b^i and AB

as the tooth cutting edge pressure angle β_{tcp}^i. Then, point F is located on line BC with the

length of $\mathrm{O}_b^i\mathrm{F}$ being equal to the top edge width c_{tw}^i, point G is the intersection between the

rectangle ABCD and line FG that forms an angle with line CD being equal to the clearance

pressure angle β_{cp}^i. The blade coordinate system is set up in the following way. Point O_b^i is

the origin, the Y_b^i axis is normal to the plane Ω and points upwards, and the Z_b^i axis is along

the direction of CB. The X_b^i axis is determined with the right hand rule. This coordinate

system is plotted in Fig. 4.4.
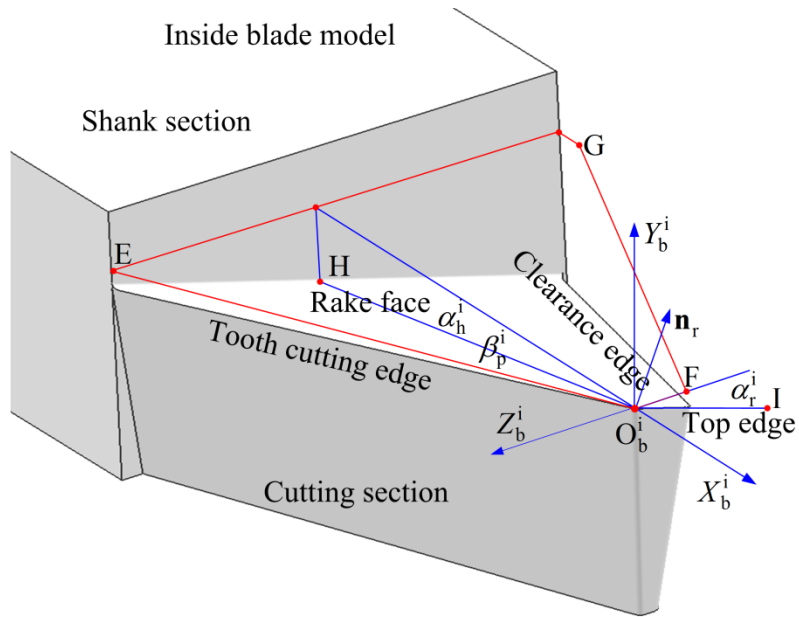
Figure 4.4. Key parameters of an inside blade model in its coordinate system.

According to the hook angle α_h^i definition, line $O_b^i H$ is drawn on plane $X_b^i Y_b^i$ from the

X_b^i axis by angle an $180° + \alpha_h^i$. Thus the unit vector of $O_b^i H$ is represented as

$$O_b^i H = \begin{bmatrix} -\cos\left(\alpha_h^i\right) \\ -\sin\left(\alpha_h^i\right) \\ 0 \end{bmatrix} \tag{4.1}$$

Meanwhile, according to the rake angle definition, line $O_b^i I$ is drawn on plane $Y_b^i Z_b^i$

from the Z_b^i axis by angle an $180° + \alpha_r^i$. So the unit vector of $O_b^i I$ is represented as

$$O_b^i I = \begin{bmatrix} 0 \\ -\sin\left(\alpha_r^i\right) \\ -\cos\left(\alpha_r^i\right) \end{bmatrix} \tag{4.2}$$

The rake face is spanned with $O_b^i I$ and $O_b^i H$, thus, the unit normal of the rake face is

$$\mathbf{n}_r = \begin{bmatrix} -\cos\left(\alpha_r^i\right) \cdot \sin\left(\alpha_h^i\right) \\ \cos\left(\alpha_r^i\right) \cdot \cos\left(\alpha_h^i\right) \\ -\sin\left(\alpha_r^i\right) \cdot \cos\left(\alpha_h^i\right) \end{bmatrix} \tag{4.3}$$

The tooth cutting edge CE^i is the project of line EO_b^i on the rake face along the Y_b^i axis. A

parametric equation of this edge is

$$CE^i = \begin{bmatrix} l \cdot e_1^i \\ l \cdot e_2^i \\ l \cdot e_3^i \end{bmatrix} \tag{4.4}$$

44

where,

$$\begin{bmatrix} e_1^i \\ e_2^i \\ e_3^i \end{bmatrix} = \begin{bmatrix} -\cos\left(\alpha_r^i\right)\cdot\cos\left(\alpha_h^i\right)\cdot\cos\left(\beta_{tcp}^i\right) \\ \sin\left(\alpha_r^i\right)\cdot\cos\left(\alpha_h^i\right)\cdot\sin\left(\beta_{tcp}^i\right) - \cos\left(\alpha_r^i\right)\cdot\sin\left(\alpha_h^i\right)\cdot\cos\left(\beta_{tcp}^i\right) \\ \cos\left(\alpha_r^i\right)\cdot\cos\left(\alpha_h^i\right)\cdot\sin\left(\beta_{tcp}^i\right) \end{bmatrix},$$

and parameter l is within the range of $\left[0, c_i^i \big/ \left[\cos\left(\alpha_r^i\right)\cdot\cos\left(\alpha_h^i\right)\cdot\cos\left(\beta_{tcp}^i\right)\right]\right]$.

Similarly, the tooth cutting edge, the top edge and the clearance edge can be constructed with their relief angles. Therefore, a parametric model of the outside blade can be built with CAD/CAM software. The geometries of the inside and the outside blades are symmetric. To attain an equation of the tooth cutting edge of the outside blade, a blade coordinate system $O_b^o - X_b^o - Y_b^o - Z_b^o$ is established and shown in Fig. 4.5.
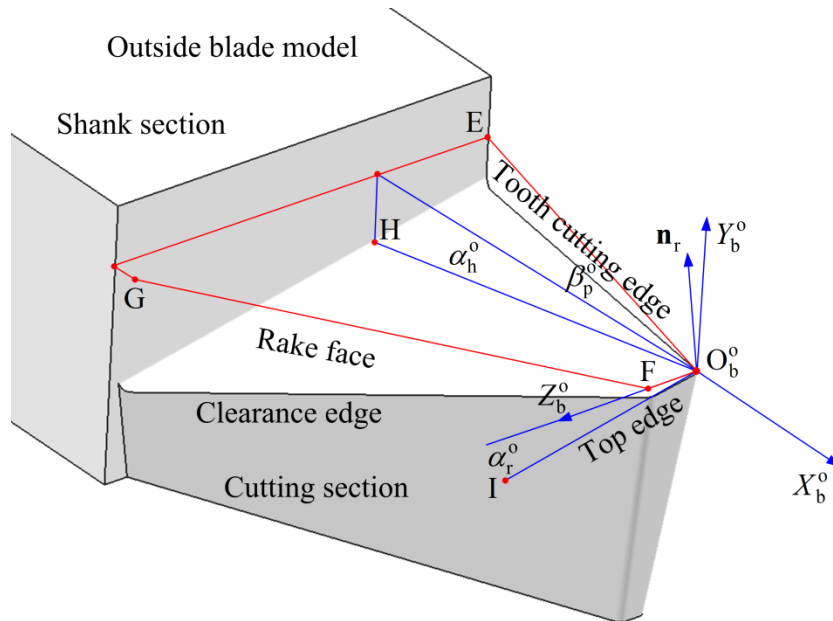
Figure 4.5. Illustration of an outside blade model in its coordinate system.

45

Similar to the way of deriving the equation of the tooth cutting edge $\mathrm{CE^o}$ of the inside blade, an parametric equation of the tooth cutting edge of the outside blade is

$$\mathrm{CE^o} = \begin{bmatrix} l \cdot e_1^o \\ l \cdot e_2^o \\ l \cdot e_3^o \end{bmatrix} \tag{4.5}$$

where

$$\begin{bmatrix} e_1^o \\ e_2^o \\ e_3^o \end{bmatrix} = \begin{bmatrix} -\cos\left(\alpha_r^o\right)\cdot\cos\left(\alpha_h^o\right)\cdot\cos\left(\beta_{tcp}^o\right) \\ \sin\left(\alpha_r^o\right)\cdot\cos\left(\alpha_h^o\right)\cdot\sin\left(\beta_{tcp}^o\right) - \cos\left(\alpha_r^o\right)\cdot\sin\left(\alpha_h^o\right)\cdot\cos\left(\beta_{tcp}^o\right) \\ -\cos\left(\alpha_r^o\right)\cdot\cos\left(\alpha_h^o\right)\cdot\sin\left(\beta_{tcp}^o\right) \end{bmatrix},$$

and parameter l is within a range of $\left[0, c_l^o \big/ \left[\cos\left(\alpha_r^o\right)\cdot\cos\left(\alpha_h^o\right)\cdot\cos\left(\beta_{tcp}^o\right)\right]\right]$.

4.1.2   Equations of the cutting surfaces of inside and outside blades

In the cutting systems of hypoid gears and pinions, each group of one inside and one outside blade should be precisely set up in slots of the cutter head around its axis in pattern. In the face-milling of hypoid gears, an elementary motion is that, the blades rotates about the cutting system axis. It can be represented, from the geometric perspective, as the tooth cutting edges of the inside blades generating an imaginary envelope surface cut convex shape in the tooth slot, and the tooth cutting edges of the outside blades generating an imaginary envelope surface cut concave shape in the tooth slot. In this work, these imaginary envelope surfaces are called cutting surfaces. In the prior research, the blades models were simplified. Although the cutting surfaces can be easily found, they are not accurate, resulting in large machining error in hypoid gears. In this section, a conventional cutting system is adopted,

46

and the cutting surfaces of the inside and outside blades are formulated.

Among various cutting systems in the market, a conventional cutting system is adopted, and its structure is introduced here. First, a coordinate system $O_{ch} - X_{ch} - Y_{ch} - Z_{ch}$ is established on the cutter head face with its origin at the face centre as shown in the Fig. 4.6. In the cutter head, a number of slot groups are distributed around the cutter head axis, and each group includes a slot for an inside blade and a slot for an outside blade. The inside blade slots are oriented so that the blade cutting tip velocity is normal to the shank face of the length and width; and the central angle between the inside blade slot and the outside blade slot is λ_1, the central angle between the outside blade and the inside blade of the next group is λ_2. The blade cutting tip is away from the blade face by a distance h_b. The radius of the inside blade cutting tip is $R_{ac} - 0.5P_w$, and the radius of the outside blade cutting tip is $R_{ac} + 0.5P_w$, where R_{ac} is the average cutter radius and P_w is the tooth point width. According to the cutting system structure, the relationships between the cutter head and the blade coordinate systems can be found, which are shown in Fig. 4.6. According to the above mentioned relationships, the cutting surface generated with the tooth cutting edge of the inside blade (also called inside cutting surface) is formulated with parameters l and λ. as

$$\mathrm{CS}^i(l,\lambda) = \begin{bmatrix} X_{CS}^i \\ Y_{CS}^i \\ Z_{CS}^i \end{bmatrix} = \begin{bmatrix} l \cdot e_1^i + h_b \\ e_2^i \cdot l \cdot \cos\lambda - e_3^i \cdot l \cdot \sin\lambda + e_4^i \cdot \sin\lambda \\ e_2^i \cdot l \cdot \sin\lambda + e_3^i \cdot l \cdot \cos\lambda - e_4^i \cdot \cos\lambda \end{bmatrix} \qquad (4.6)$$

where $e_4^i = R_{ac} - 0.5P_w$, the parameter λ is the rotation angle about the X_{ch} in the range of $[0, 2 \cdot \pi]$.
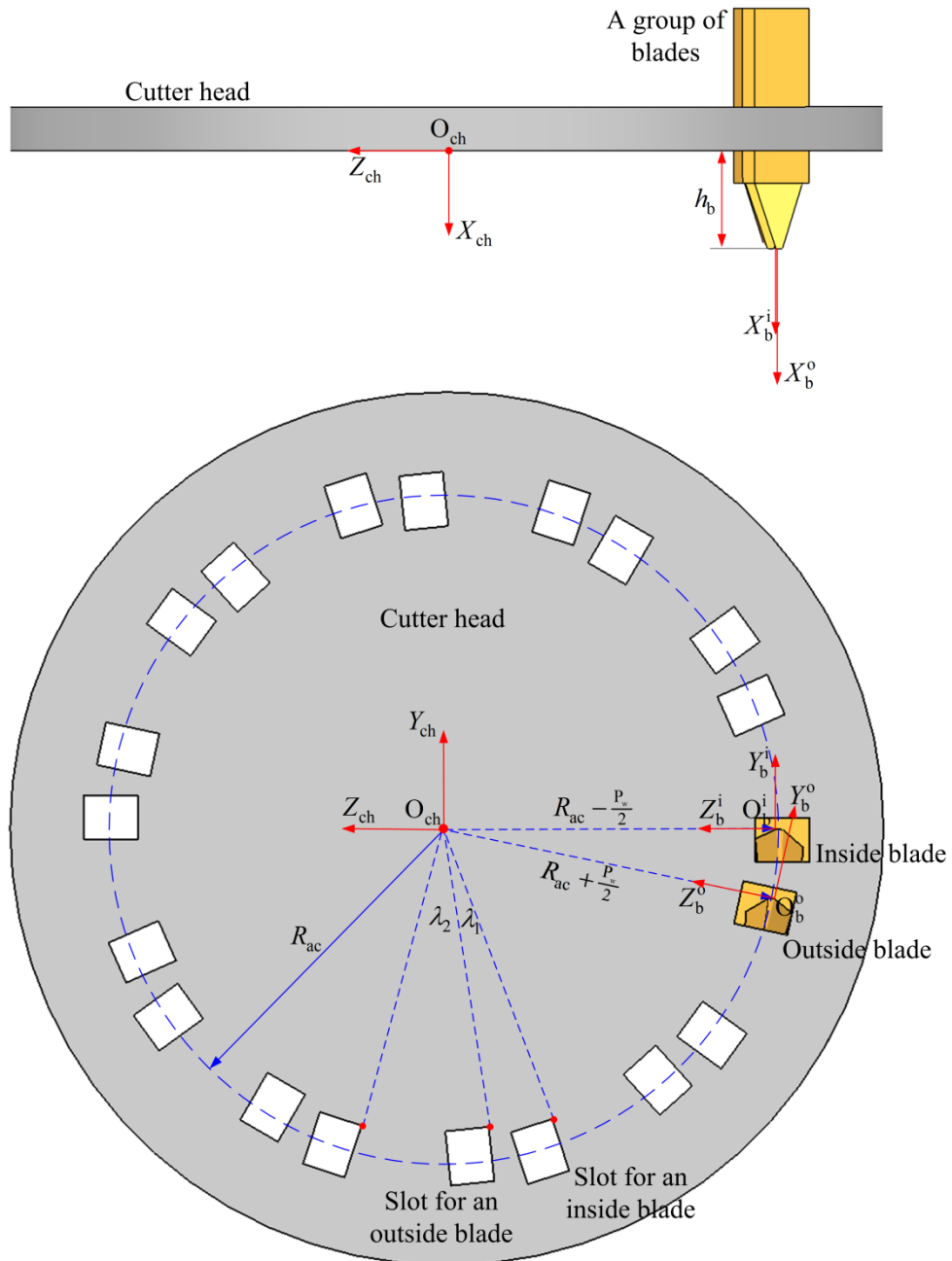
Figure 4.6. The cutting system structure and the relationship between the cutter head and the blade coordinate systems.

Similarly, the parametric equation of the tooth cutting edge of the outside blade is

$$\mathrm{CS^o}\left(l,\lambda\right) = \begin{bmatrix} X_{\mathrm{CS}}^{\mathrm{o}} \\ Y_{\mathrm{CS}}^{\mathrm{o}} \\ Z_{\mathrm{CS}}^{\mathrm{o}} \end{bmatrix} = \begin{bmatrix} l \cdot e_1^{\mathrm{o}} + h_{\mathrm{b}} \\ e_2^{\mathrm{o}} \cdot l \cdot \cos\lambda - e_3^{\mathrm{o}} \cdot l \cdot \sin\lambda + e_4^{\mathrm{o}} \cdot \sin\lambda \\ e_2^{\mathrm{o}} \cdot l \cdot \sin\lambda + e_3^{\mathrm{o}} \cdot l \cdot \cos\lambda - e_4^{\mathrm{o}} \cdot \cos\lambda \end{bmatrix} \qquad (4.7)$$

where $e_4^{\mathrm{o}} = R_{\mathrm{ac}} + 0.5 P_{\mathrm{w}}$, and the parameter λ is the rotation angle about the X_{ch} in the range of $[0, 2 \cdot \pi]$.

4.1.3   Geometric characteristics of the cutting surfaces

To determine the cutter system parameters in the next section, it is crucial to attain the geometric characteristics of the inside and the outside cutting surfaces, such as tangent vectors, the maximum and the minimum curvatures and directions. Since the cutting surfaces are revolutionary, their geometric characteristics can be typically represented with those of their axial cross-sections. With help of the previously mentioned parametric equations of the cutting surfaces, the closed-form equations of the surface geometric characteristics are derived in the following.

Based on the inside and the outside cutting surfaces of the cutting system, which is adopted in Section 4.1.2, can be used for the machining of hypoid gears and pinions (Fig. 4.7), its geometric characteristics can be represented with those of the cutting surface profile on any axial cross-section. In Fig. 4.7, the $X_{\mathrm{ch}} - Z_{\mathrm{ch}}$ plane cuts through the cutting surface at the profile ABCD. The profiles of inside and outside cutting surface are given by the angle

$$\tan \lambda = \frac{e_2^{\mathrm{i}} \cdot l}{e_3^{\mathrm{i}} - e_4^{\mathrm{i}}} \tag{4.8}$$

$$\tan \lambda = \frac{e_2^{\mathrm{o}} \cdot l}{e_3^{\mathrm{o}} - e_4^{\mathrm{o}}} \tag{4.9}$$

(a)
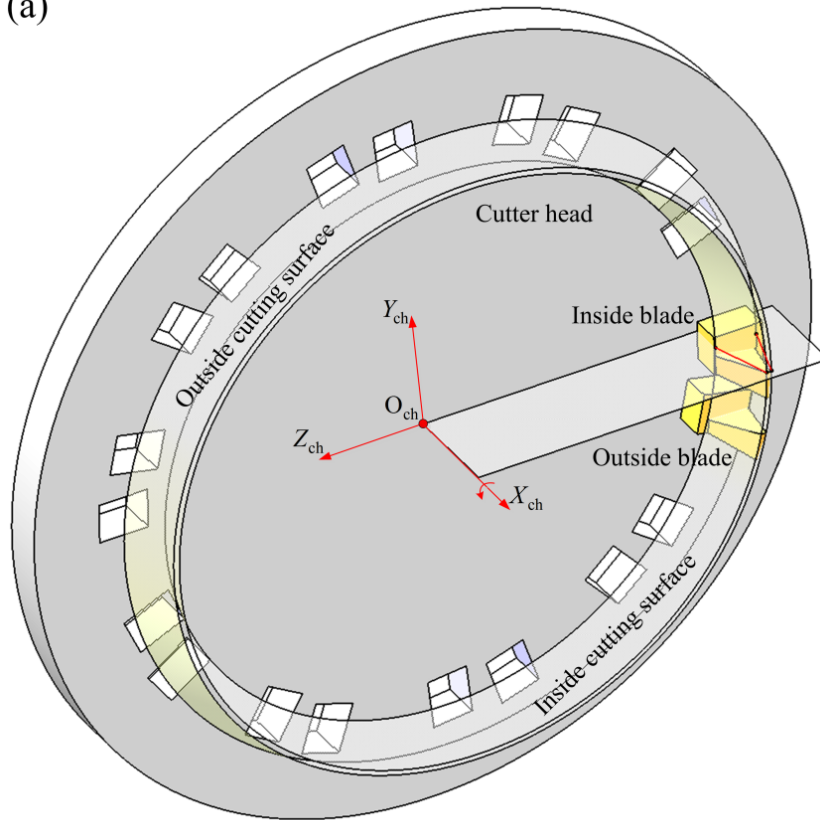
(b)
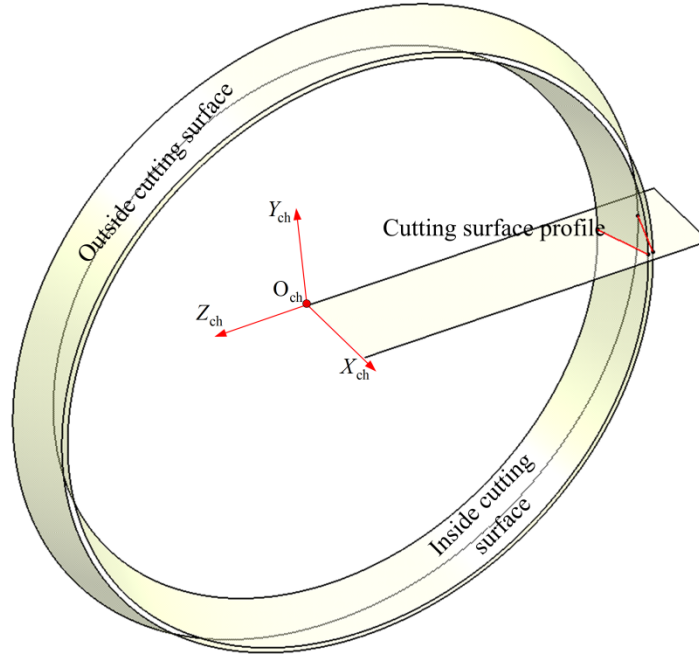
Figure 4.7. (a) The inside and the outside cutting surfaces of the blades, (b) The cross section of the cutting surface on the X_{ch}-Z_{ch} plane.

According to the equation of the inside cutting surface profile, the first and the second derivatives of λ in terms of l can be found as

$$\frac{d\lambda}{dl} = \frac{e_2^i \cdot \cos\lambda - e_3^i \cdot \sin\lambda}{e_2^i \cdot l \cdot \sin\lambda + e_3^i \cdot l \cdot \cos\lambda - e_4^i \cdot \cos\lambda} \tag{4.10}$$

$$\frac{d^2\lambda}{dl^2} = \frac{\left(e_3^i \cdot l \cdot \sin\lambda - e_2^i \cdot l \cdot \cos\lambda - e_4^i \cdot \sin\lambda\right) \cdot \dfrac{d\lambda}{dl} - 2 \cdot e_2^i \cdot \sin\lambda - 2 \cdot e_3^i \cdot \cos\lambda}{e_2^i \cdot l \cdot \sin\lambda + e_3^i \cdot l \cdot \cos\lambda - e_4^i \cdot \cos\lambda} \cdot \frac{d\lambda}{dl} \tag{4.11}$$

Then, the inside flank angle can be calculated with the following equation

$$\tan\left(\alpha_{\mathrm{g}}^{\mathrm{i}}\right) = \frac{dZ_{\mathrm{CS}}^{\mathrm{i}}/dl}{dX_{\mathrm{CS}}^{\mathrm{i}}/dl} \tag{4.12}$$

where,

$$\frac{dX_{\mathrm{CS}}^{\mathrm{i}}}{dl} = e_1^{\mathrm{i}} \text{ and}$$

$$\frac{dZ_{\mathrm{CS}}^{\mathrm{i}}}{dl} = \left(e_2^{\mathrm{i}} \cdot l \cdot \cos\lambda - e_3^{\mathrm{i}} \cdot l \cdot \sin\lambda + e_4^{\mathrm{i}} \cdot \sin\lambda\right) \cdot \frac{d\lambda}{dl} + e_2^{\mathrm{i}} \cdot \sin\lambda + e_3^{\mathrm{i}} \cdot \cos\lambda .$$

$$\kappa_{\min}^{\mathrm{i}} = \frac{\dfrac{dX_{\mathrm{CS}}^{\mathrm{i}}}{dl} \cdot \dfrac{d^2 Z_{\mathrm{CS}}^{\mathrm{i}}}{dl^2}}{\left[\left(\dfrac{dX_{\mathrm{CS}}^{\mathrm{i}}}{dl}\right)^2 + \left(\dfrac{dZ_{\mathrm{CS}}^{\mathrm{i}}}{dl}\right)^2\right]^{\frac{3}{2}}} \tag{4.13}$$

where,

$$\frac{d^2 Z_{\mathrm{CS}}^{\mathrm{i}}}{dl^2} = \left(e_2^{\mathrm{i}} \cdot l \cdot \cos\lambda - e_3^{\mathrm{i}} \cdot l \cdot \sin\lambda + e_4^{\mathrm{i}} \cdot \sin\lambda\right) \cdot \frac{d^2\lambda}{dl^2} - \left(e_2^{\mathrm{i}} \cdot l \cdot \sin\lambda + e_3^{\mathrm{i}} \cdot l \cdot \cos\lambda - e_4^{\mathrm{i}} \cdot \cos\lambda\right) \cdot \left(\frac{d\lambda}{dl}\right)^2 + 2 \cdot \left(e_2^{\mathrm{i}} \cdot \cos\lambda - e_3^{\mathrm{i}} \cdot \sin\lambda\right) \cdot \frac{d\lambda}{dl}$$

Meanwhile, the equation of the maximum curvature of the inside cutting surface profile is

$$\kappa_{\max}^{\mathrm{i}} = \frac{2}{2 \cdot R_{\mathrm{ac}} - P_{\mathrm{w}}} \tag{4.14}$$

The formula of the geometric characteristics of the outside cutting surface profile are the same as those for the inside cutting surface profile, except that e_1^{i} to e_4^{i} are replaced with e_1^{o} to e_4^{o}. The equation of the maximum curvature of the outside cutting surface profile is

$$\kappa_{max}^{o} = \frac{2}{2 \cdot R_{ac} + P_{w}}$$

<div align="right">(4.15)</div>

Therefore, these geometric characteristics at the mean point can be easily found, and the cutter system parameters can be accurately determinate.

4.1.4   Sensitivity study of the cutting system parameters on the cutting surface shape

In the above sections, the formula of the cutting surface profiles in terms of the cutting system parameters, such as the hook angle, the rake angle, the tooth cutting edge pressure angle and the average cutter radius, have been derived. Since the mathematical models of the inside and outside blades are accurate, the cutting surface representations are exact. By changing the hook and the rake angles, the cutting surface shape varies accordingly. A sensitivity study of the hook and the rake angles on the cutting surface shape is conducted here. Meanwhile, since none of the existing methods has provided accurate blade geometric models, they ignored the hook and the rake angles by setting their values as zeros. Consequently, the cutting surfaces represented with these methods are inaccurate, and the deviation of these cutting surface representations (including geometric characteristics), compared to those of our approach, is called cutting surface representation error. Therefore, this sensitivity study can demonstrate the cutting surface error of the prior methods in order to highlight the advantage of our approach.

First, to understand how the hook angle affects the cutting surface representation error, four tests with four cutting systems are planned (see Table 4.1). In Test 1, the hook and the

rake angles are zeros, which is the simplified cutter system model used in the prior methods to approximate cutter systems. Thus, the geometric characteristics and the cutting surface profiles calculated with this method are the same as those calculated with the prior methods. In Tests 2 to 4, the hook angles of the cutter systems are different, and the geometric characteristics and the cutting surface profiles are accurately calculated with our approach, which are presented in Table 4.1.

Table 4.1. Calculated geometric characteristics of the cutting surfaces at the mean point.

Cutter system parameters	Test 1	Test 2	Test 3	Test 4
Hook angle (α_h^i and α_h^o)	$0°$	$10°$	$15°$	$25°$
Rake angle (α_r^i and α_r^o)	$0°$	$15°$	$15°$	$15°$
Cutting edge pressure angle (β_{tcp}^i and β_{tcp}^o)	$18°$	$18°$	$18°$	$18°$
Average cutter radius (R_{ac}, mm)	152.4	152.4	152.4	152.4
Tooth point width (P_w, mm)	2.54	2.54	2.54	2.54
Calculated geometric characteristics of the inside cutting surface at the mean point				
Inside flank angle (α_g^i)	$18°$	$17°59'$	$17°55'$	$17°38'$
The maximum curvature (κ_{max}^i, mm^{-1})	0.00672	0.00672	0.00672	0.00672
The minimum curvature (κ_{min}^i, mm^{-1})	0	0.00004	0.00019	0.00086
Calculated geometric characteristics of the outside cutting surface at the mean point				
Outside flank angle (α_g^o)	$18°$	$18°1'$	$18°5'$	$18°20'$
The maximum curvature (κ_{max}^o, mm^{-1})	0.00641	0.00641	0.00641	0.00641
The minimum curvature (κ_{min}^o, mm^{-1})	0	0.00004	0.00017	0.00076

Therefore, the cutting surface errors of the existing methods for the blades in Tests 2 to 4 are the deviations between the cutting surface profiles in Test 1 and those in Tests 2 to 4 (shown in Fig. 4.8). In Fig. 4.9, it is evident that with increment of the hook angle, the cutting surface representation error is increased accordingly.
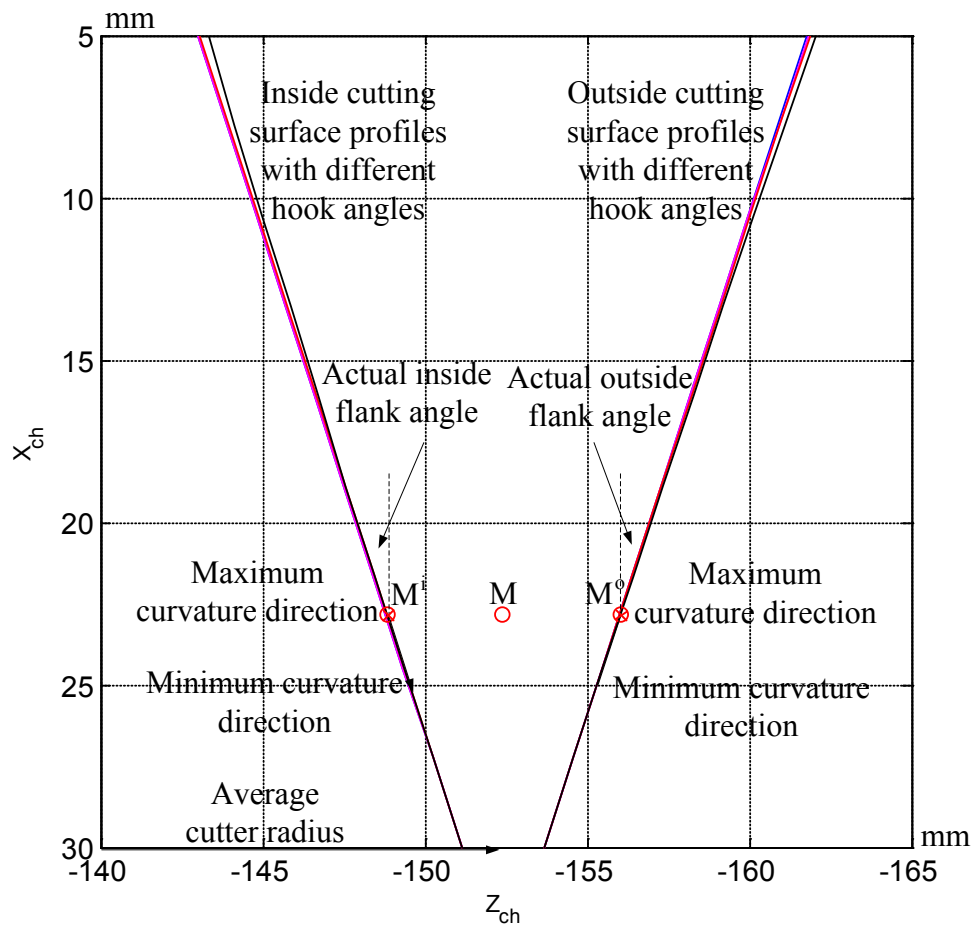
Figure 4.8. The cutting surface profiles of the four cutter systems in Tests 1 to 4.

(a)

Cutting surface error of the current methods

$\alpha_h^i = 25°$

$\alpha_h^i = 15°$

$\alpha_h^i = 0°$

$\alpha_h^i = 10°$

Outside cutting edge profile with the current methods

Zoom in of the outside cutting edge profiles

X_{ch}

Z_{ch}

mm

mm

(b)

Inside cutting surface error is the difference between this new approach and the existing methods

Cutting surface error of the current methods

$\alpha_h^i = 25°$

$\alpha_h^i = 15°$

$\alpha_h^i = 10°$

X_{ch}

mm

mm
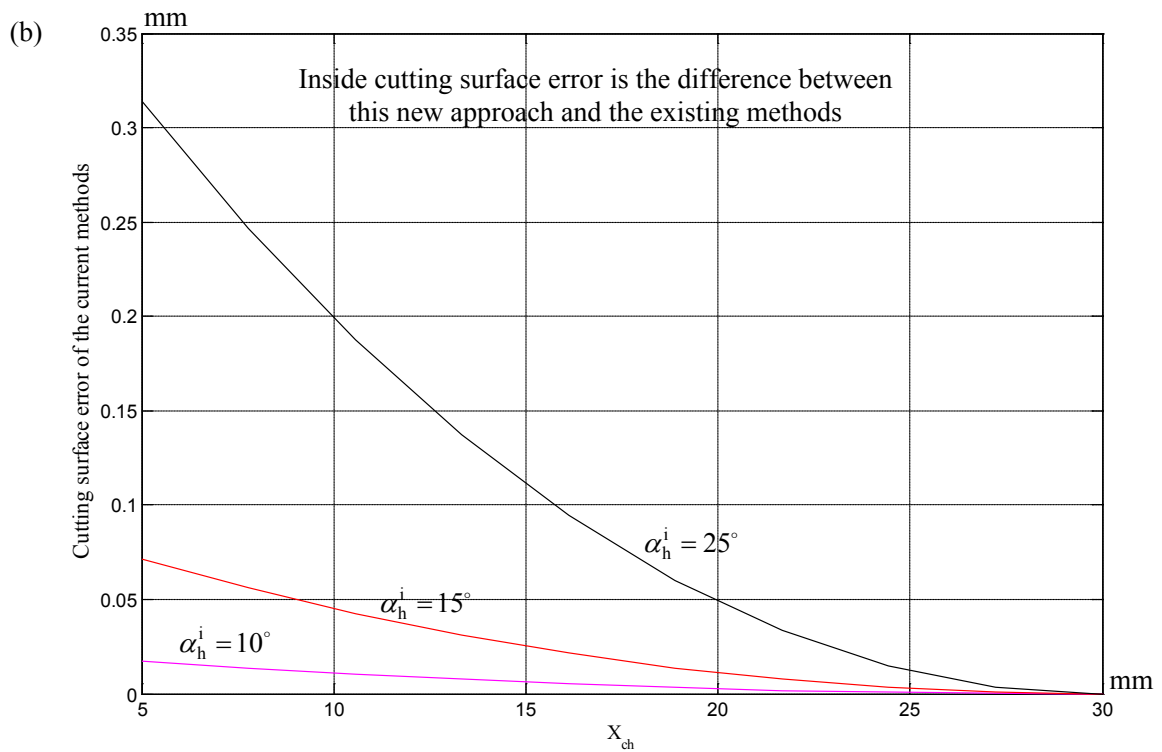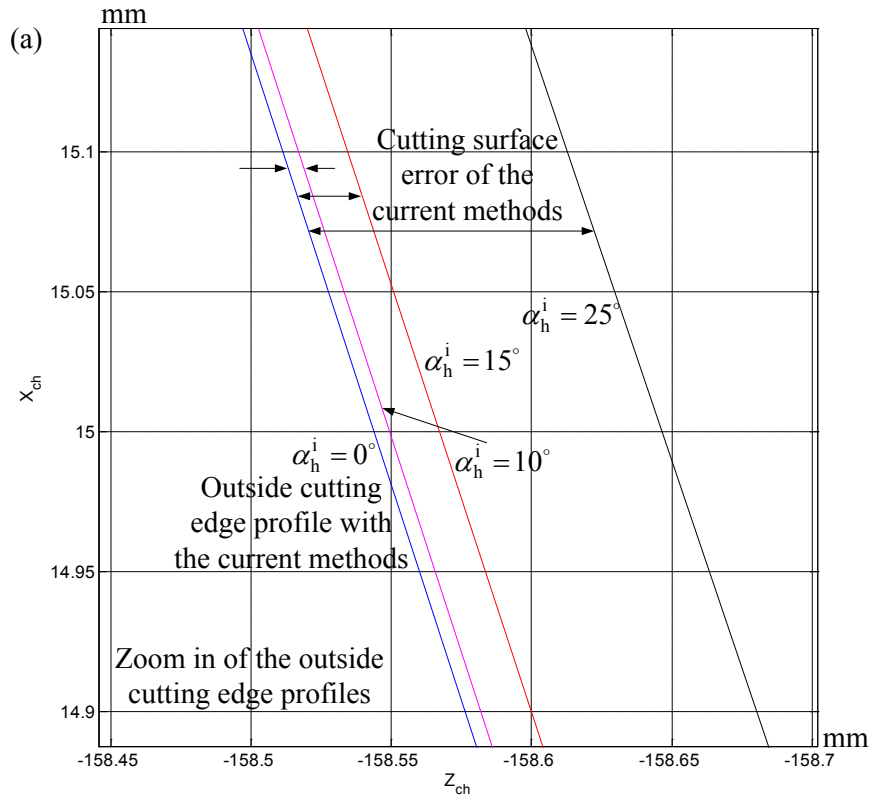
Figure 4.9. (a) A zoom-in of the cutting surface profiles in Tests 1 to 4, (b) the inside cutting surface errors of the existing methods for the blades in Tests 1 to 4, and (c) the outside cutting surface errors of the existing methods for the blades in Tests 1 to 4.

Similar to the above sensitivity study of the hook angle, a study of the rake angle is conducted in four tests with the four blades, which parameters are listed in Table 4.2. Using this approach, the geometric characteristics of the cutting surfaces are calculated and listed in Table 4.2. The cutting surface profiles in Tests 5 to 8 are plotted in Fig. 4.10, and the cutting surface error curves are plotted in Fig. 4.11.

Table 4.2. Calculated geometric characteristics of the cutting surfaces at the mean point.

Cutter system parameters	Test 5	Test 6	Test 7	Test 8
Hook angle (α_h^i and α_h^o)	0°	15°	15°	15°
Rake angle (α_r^i and α_r^o)	0°	10°	15°	25°
Cutting edge pressure angle (β_{tcp}^i and β_{tcp}^o)	18°	18°	18°	18°
Average cutter radius (R_{ac}, mm)	152.4	152.4	152.4	152.4
Tooth point width (P_w, mm)	2.54	2.54	2.54	2.54
Calculated geometric characteristics of the inside cutting surface at the mean point				
Inside flank angle (α_g^i)	18°	17°53′	17°55′	17°57′
The maximum curvature (κ_{max}^i, mm^{-1})	0.00672	0.00672	0.00672	0.00672
The minimum curvature (κ_{min}^i, mm^{-1})	0	0.00026	0.00019	0.00008
Calculated geometric characteristics of the outside cutting surface at the mean point				
Outside flank angle (α_g^o)	18°	18°6′	18°5′	18°2′
The maximum curvature (κ_{max}^o, mm^{-1})	0.00641	0.00641	0.00641	0.00641
The minimum curvature (κ_{min}^o, mm^{-1})	0	0.00024	0.00017	0.00007
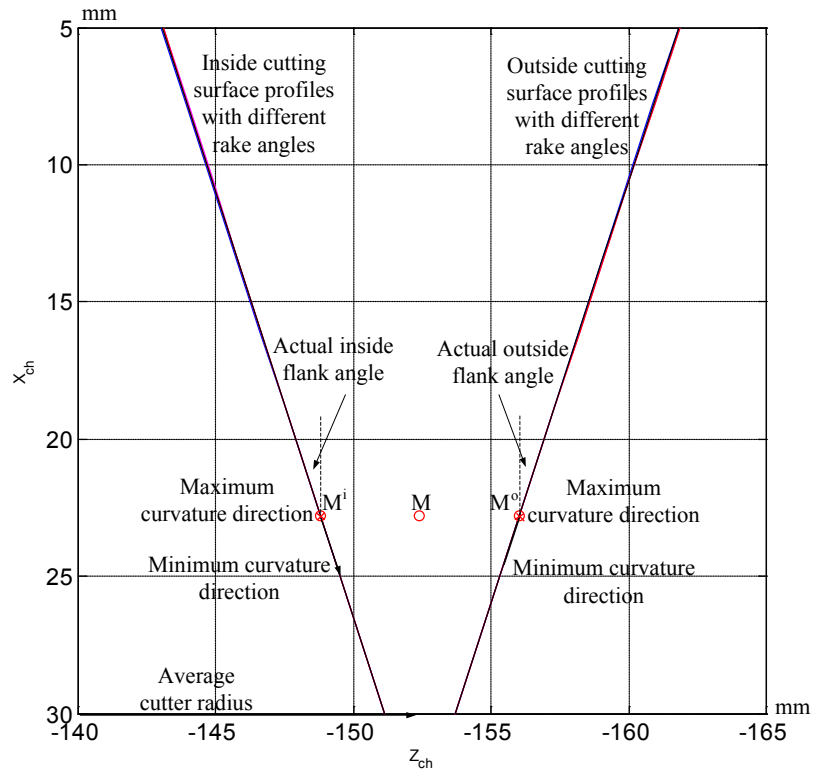
Figure 4.10. The cutting surface profiles of the four cutter systems in Tests 5 to 8.

(b)

$\alpha_r^i = 10°$

$\alpha_r^i = 15°$

$\alpha_r^i = 25°$

Inside cutting surface error is the difference between this new approach and the existing methods

Cutting surface error of the current methods

X_{ch}

(c)

$\alpha_r^i = 10°$

$\alpha_r^i = 15°$

$\alpha_r^i = 25°$

Outside cutting surface error is the difference between this new approach and the existing methods

Cutting surface error of the current methods

X_{ch}
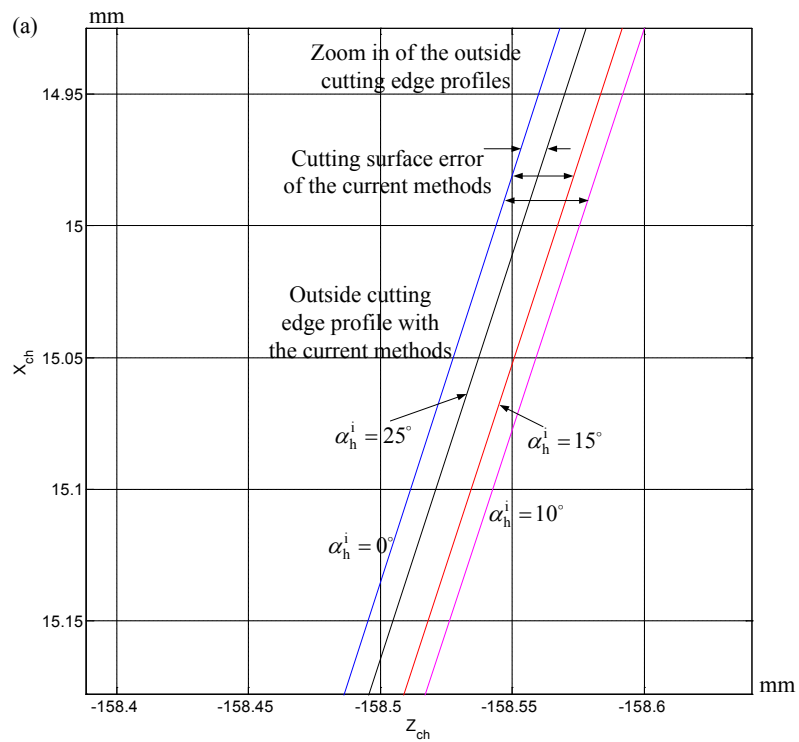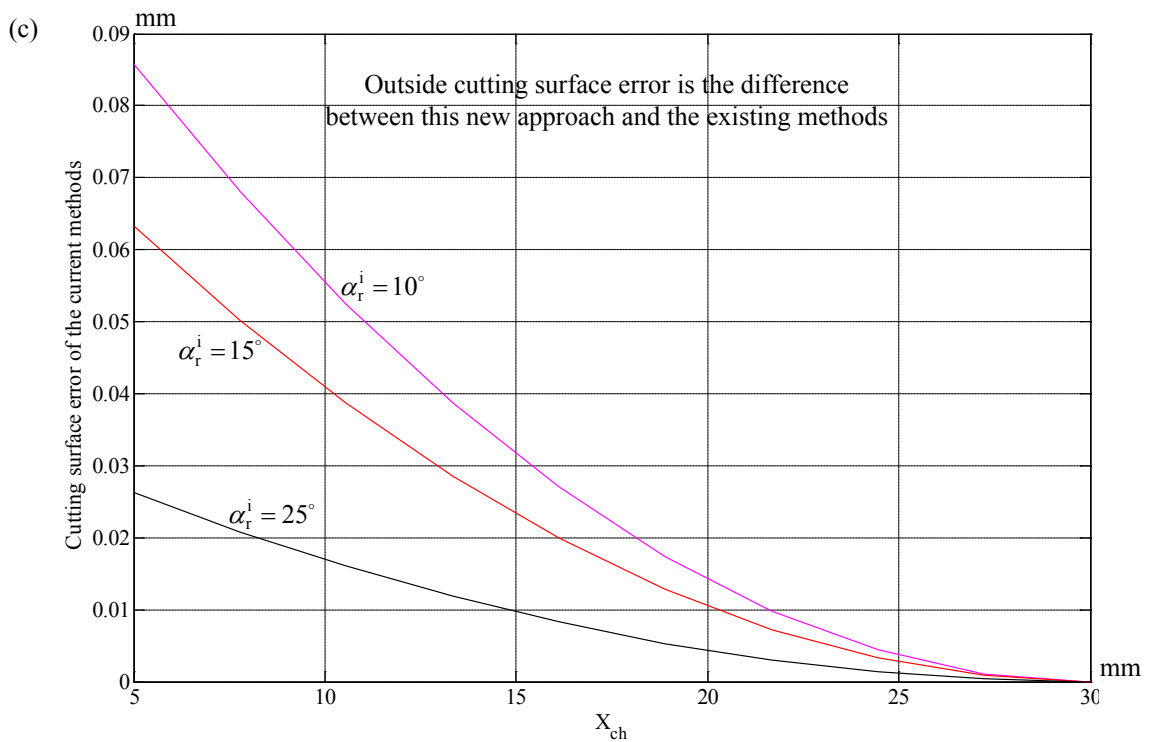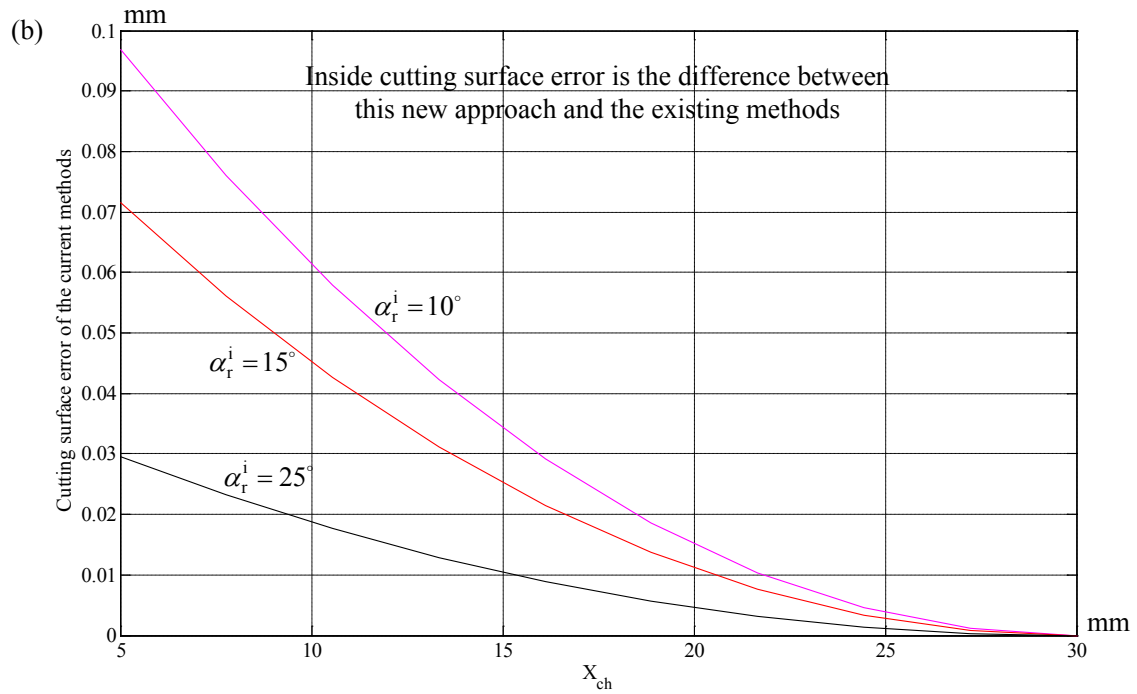
Figure 4.11. (a) A zoom-in of the cutting surface profiles in Tests 5 to 8, (b) the inside cutting surface errors of the existing methods for the blades in Tests 5 to 8, and (c) the outside cutting surface errors of the existing methods for the blades in Tests 5 to

61

4.2 Determination of average cutter radius and blade pressure angle

To face-mill hypoid gears and pinions with high tooth shape accuracy, low cutting forces and long cutter life, it is important to determine the cutter system parameters precisely, according to the physics of metal removing and the gear/pinion local geometry at the mean point. Among the cutter parameters, the parameters, such as the hook and the rake angles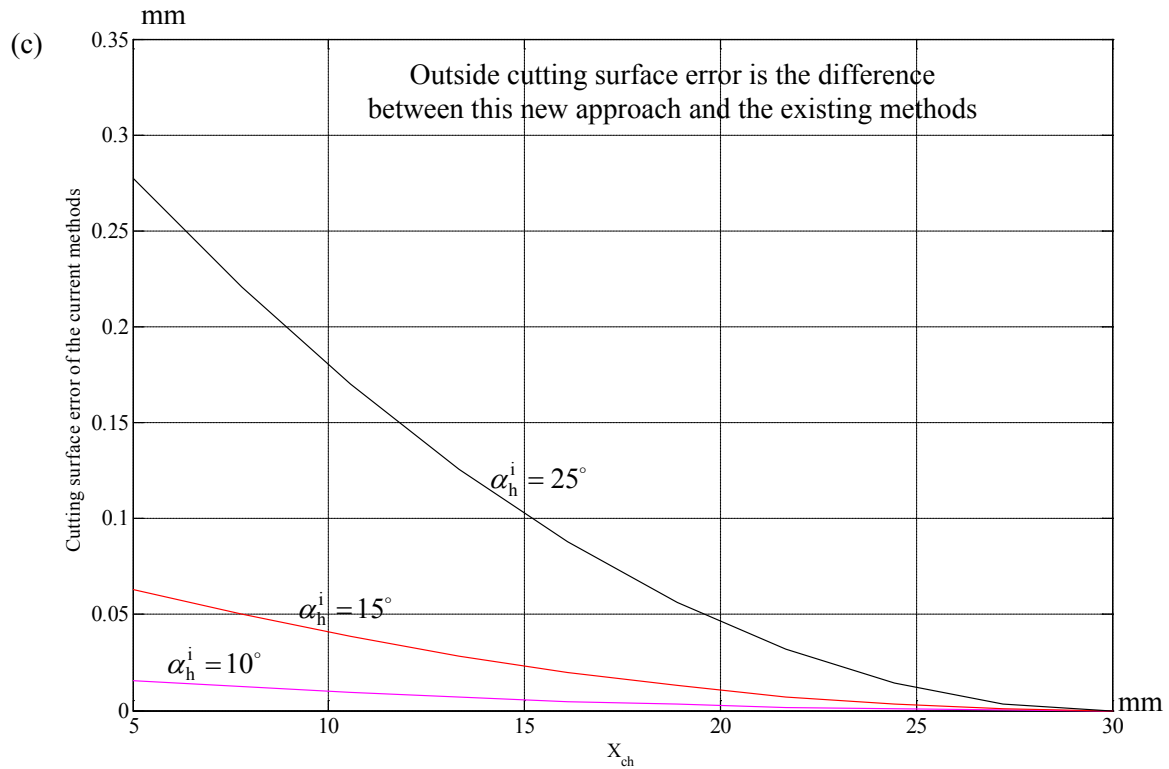, and the tooth cutting edge, the top edge and the clearance relief angles, directly affect the machining performance, for example, the cutting force, the cutting temperature, wear, and the cutter system life. This topic is out of the scope of this work. In this work, the focus is on the determination of tooth cutting edge pressure angle and the average cutter radius, for the gear and pinion cutter systems, which is based on the local geometry of the cutter surfaces at the mean point as calculated in gear geometry (section 3.1).

4.2.1 The parameters determination for the gear cutting system

In chapter 3, the local geometry of the inside and outside cutting surfaces on the points M_i and M_o has been calculated, including the inside and the outside flank angles (α_g^i and α_g^o), and the curvatures, which are shown in Fig. 4.12. The procedure of determining the average cutter radius and the tooth cutting edge pressure angles of the inside and the outside blades is as follows. First, based on the curvatures, the radii at these points can be computed, the average of these radii are calculated. Second, the average radius is compared to the standard cutter system radii (AGMA), and the standard cutter radius closet to the average radius is

taken as the average cutter radius R_{ac} .
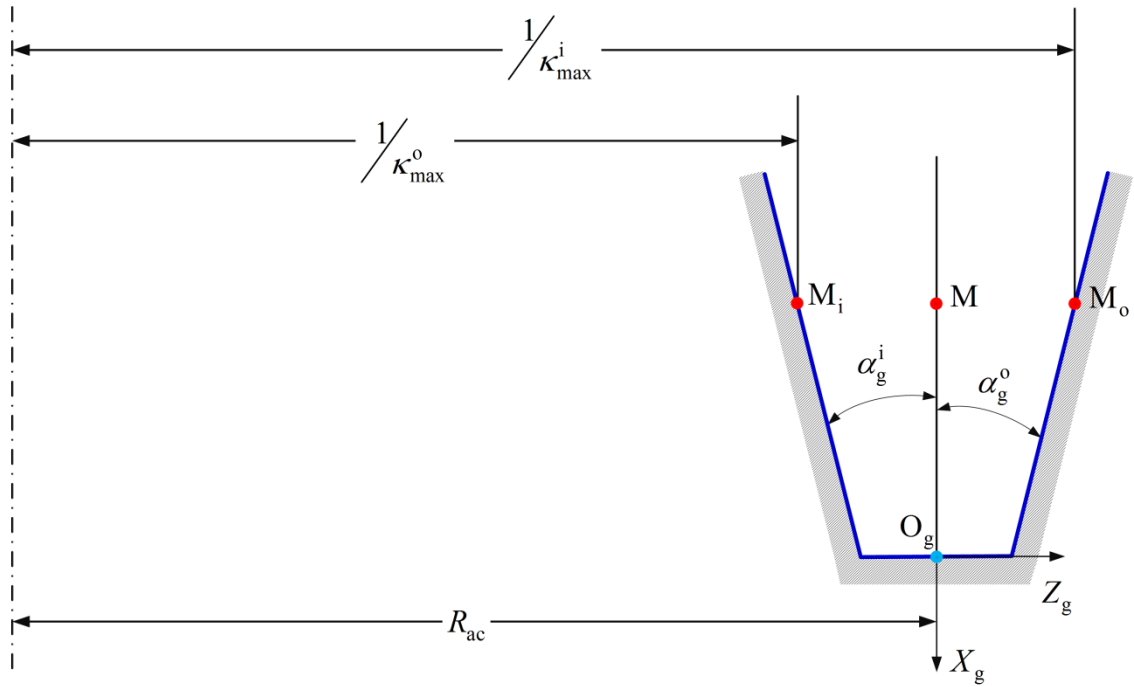
Figure 4.12. Illustration of determining the average cutter radius and the tooth cutting edge pressure angles of the inside and the outside blades.

The parameters l and λ of the inside and outside cutting surfaces are calculated for the point M_i .

$$l = \frac{h_M}{e_1^i} , \text{ and } \lambda = \tan^{-1}\left(\frac{e_2^i}{e_3^i - e_4^i} \cdot l\right). \tag{4.16}$$

Thus, the coordinates $\left[x_{M_i}^{ch}, y_{M_i}^{ch}, z_{M_i}^{ch}\right]^T$ of point M_i in the cutter head coordinate system can be calculated by substituting Eq. (4.16) into Eqs. 4.6 and 4.7. An iterative process of determining the inside blade's pressure angle at the point M_i is performed, to calculate the

inside flank angle (4.12). Pressure angle is changed until the inside flank angle is equal to the specified value of the gear flank angle on the point M_i. The same process applies to determine the outside blade pressure angle at the point M_o.

4.2.2 The parameters determination for the pinion cutting system

In Section 3.4, for the local geometry of the outside cutting surface of the pinion cutter, such as the minimum and the maximum curvature directions ($\tau_{I,cp}$ and $\tau_{II,cp}$), and the relationship between the minimum and the maximum curvatures ($\kappa_{I,cp}$ and $\kappa_{II,cp}$) has been developed (Eqs. 3.23,3.24 and 3.30). The flank angles of the pinion are given by the designers (α_p^i and α_p^o). It is to be noted that the outside cutting surface of the pinion cutter is tangent to the inside cutting surface of the gear cutter. Based on the local geometry, the average cutter radius and the tooth cutting edge pressure angle of the inside blade can be determined in the following procedure. First, an axial cross section is constructed to be normal to the plane of the curvature directions and passing through the minimum curvature direction as shown in the Fig. 4.13(a). Second, the x_{cp} axis is generated on the cross section forming an angle of $180^\circ - \alpha_p^o$ with the direction $\tau_{I,cp}$. Therefore, the x_{cp} axis is parallel to the cutter system axis as shown in the Fig. 4.13. Third, given an average cutter radius and the pressure angle, the maximum and the minimum curvatures are calculated. If the given parameters cannot meet Eq. 3.33, the radius and angle are modified until the equation is satisfied.

(a)

(b)
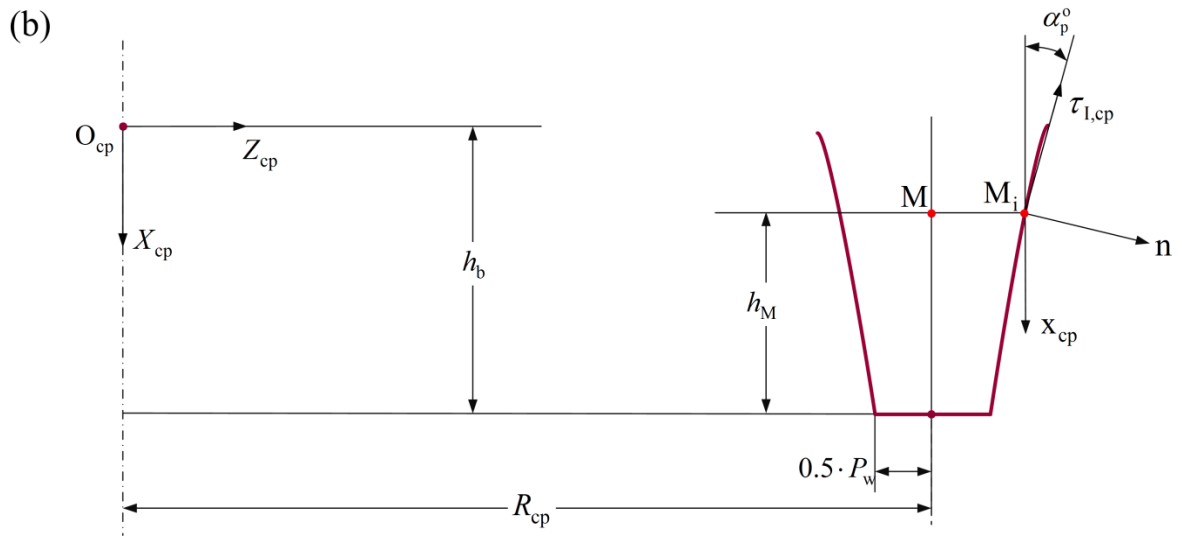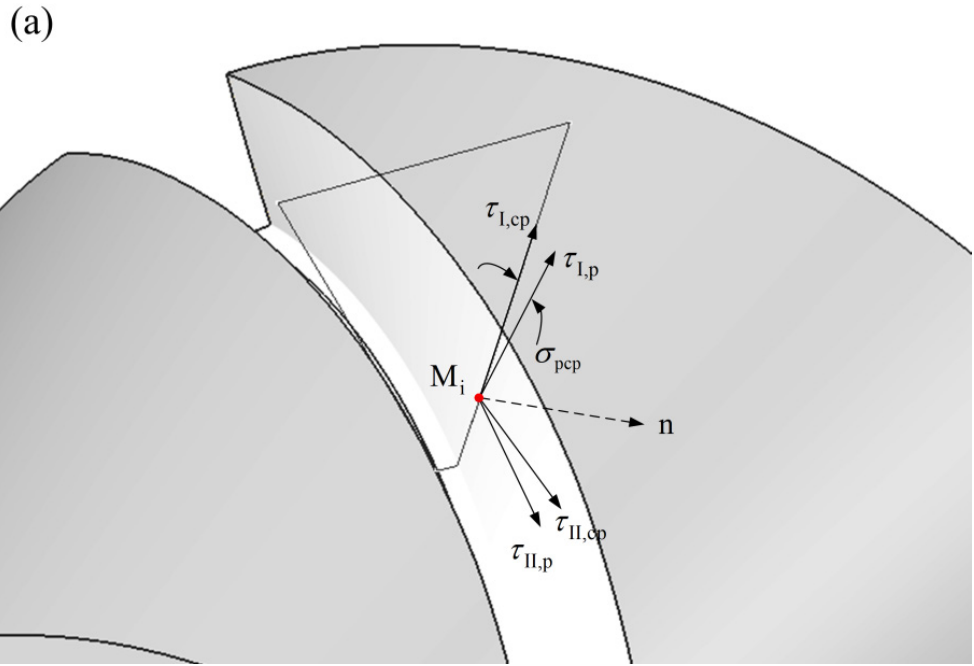
Figure 4.13. Illustration of determining the average cutter radius and the blade pressure angle for the pinion cutter system.

4.3   Applications

To verify the validity of our new approach, an example is provided. In this example, the gear parameters are specified and listed in Table 4.3. By using this new approach, a gear cutting system is determined and the parameters are listed in Table 4.4.

Table 4.3. Pre-specified parameters of the hypoid gear.

Gear parameters	Convex tooth	Concave tooth
Gear flank angle (α_g^i, α_g^o)	23°11′	21°49′
Gear tooth curvature at the mean points (κ_g^i, κ_g^o)	0.0067 mm^{-1}	0.0064 mm^{-1}
Gear face angle (Γ_o)	81°6′	
Gear root angle (Γ_R)	75°28′	
Gear dedendum angle (δ_G)	4°54′	
Gear addendum at outside (a_{oG})	1.700 mm	
Gear dedendum at outside (b_{oG})	13.100 mm	
Face width (F)	43.000 mm	
Clearance between gear and pinion (c)	1.680 mm	
Root spiral angle (β_r)	32°30′	
Height of the mean points (h_M)	7.184 mm	

Table 4.4. The parameters of the gear cutting system.

Gear cutting system parameters	Litvin's method		Our approach	
	Inside blade	Outside blade	Inside blade	Outside blade
Average cutter radius (R_{ac}, mm)	152.400		152.400	
Hook angles (α_h^i, α_h^o)	0°	0°	12°0′	12°0′
Rake angles (α_r^i, α_r^o)	0°	0°	14°0′	14°0′
Length of cutting section (c_1^i, c_1^o, mm)	45.0	45.0	45.0	45.0
Cutting surface flank angles (α_e)	23°11′0″	21°49′0″	23°11′1″	21°48′59″
Tooth cutting edge pressure angle (β_{tcp}^i, β_{tcp}^o)	23°11′0″	21°49′0″	23°12′35″	21°47′17″

The local synthesis between the gear and the pinion is conducted, and the local geometry of the pinion tooth surface is found which is shown in the Table 4.6.

Table 4.5. Blades parameters for the pinion cutter

Parameters	Litvin's Method		Our approach	
	Convex tooth (Inside blade)	Concave tooth (Outside blade)	Convex tooth (Inside blade)	Concave tooth (Outside blade)
Height of the mean points (h_M)	7.184 mm		7.184 mm	
Pinion flank angle (α_p^i, α_p^o)	14°0′	14°0′	14°0′	14°0′
Pinion tooth curvature at the mean points (κ_p^i, κ_p^o, mm^{-1})	-0.03417	0.00527	-0.03696	0.00506
Angle between the minimum curvature directions of pinion and gear ($\sigma_{p,g}$)	16°38′40″		18°18′4″	
Angle between the minimum curvature directions of cutting surface and gear ($\sigma_{pc,g}$)	5°38′0″		5°38′0″	

Table 4.6. The parameters of the pinion cutting system.

Pinion cutting system parameters	Litvin's method		Our approach	
	Inside blade	Outside blade	Inside blade	Outside blade
Average cutter radius (R_{ac}, mm)	153.001		157.162	
Hook angles (α_h^i, α_h^o)	0°	0°	12°0′	12°0′
Rake angles (α_r^i, α_r^o)	0°	0°	14°0′	14°0′
Length of cutting section (c_1^i, c_1^o, mm)	45.0	45.0	45.0	45.0
Cutting surface flank angles (α_e)	14°0′	14°0′	14°0′	13°59′59″
Tooth cutting edge pressure angle ($\beta_{tcp}^i, \beta_{tcp}^o$)	14°0′	14°0′	14°3′25″	13°56′43″

In face-milling simulation, a gear is virtually machined with this cutting system, and its parameters are measure, which are shown in the Fig. 4.15 and 4.16. It is clear that the measured parameters are close to the specified values within tolerance.
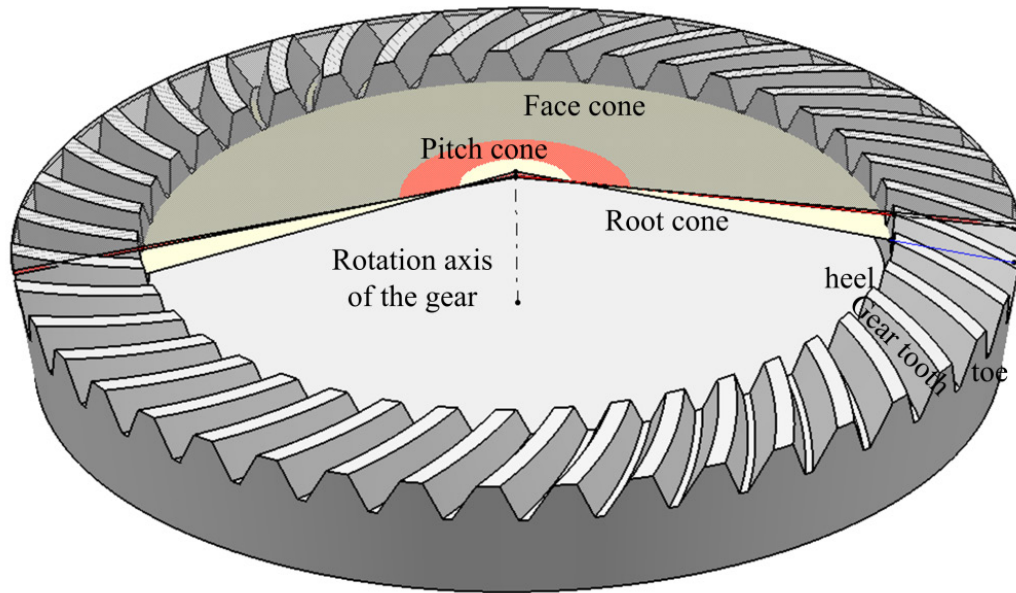
Figure 4.14. Virtually machined hypoid gear with the accurate cutter system.
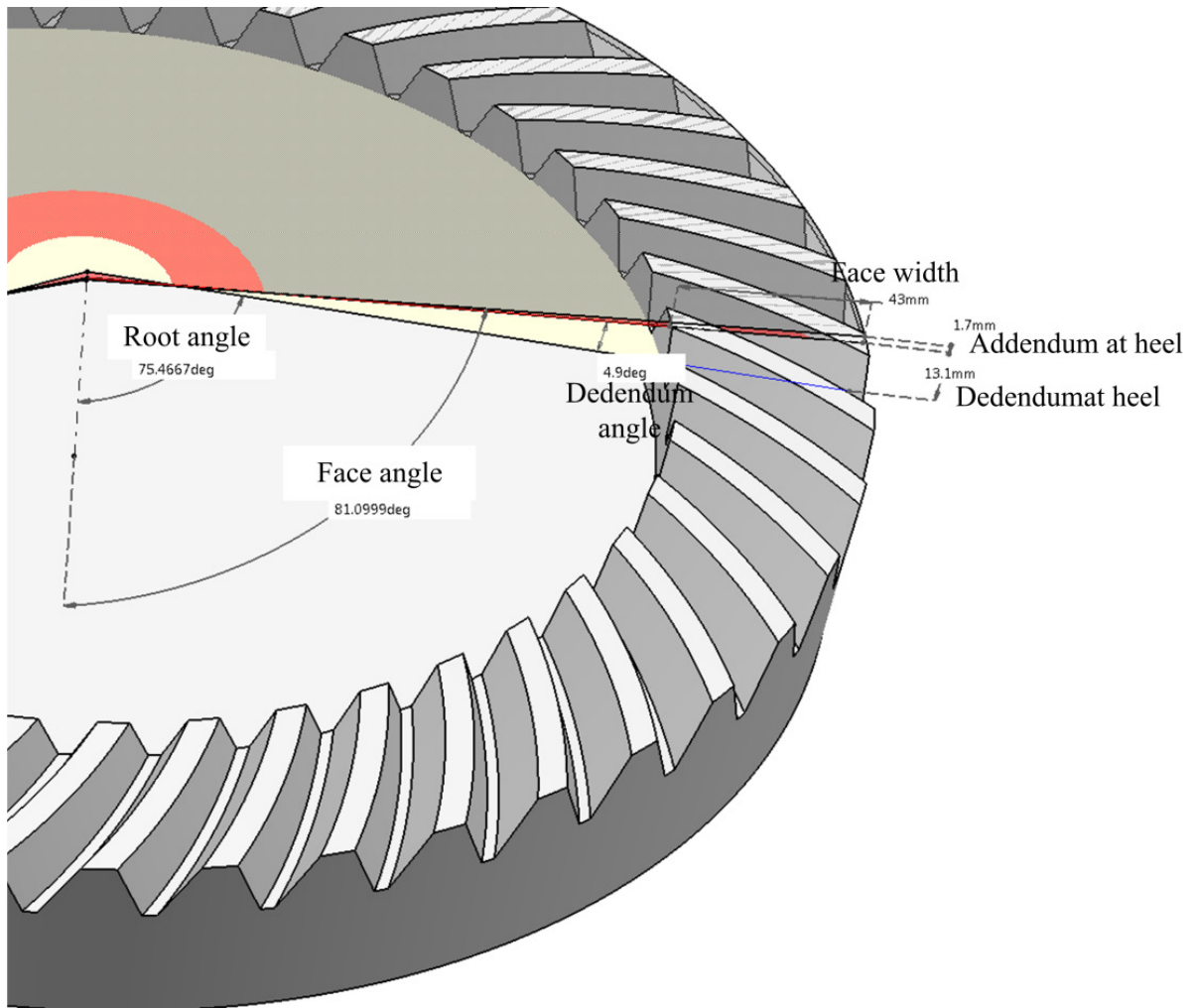
Figure 4.15. Gear blank parameters measured on a virtually machined hypoid gear using a CAD/CAM software.
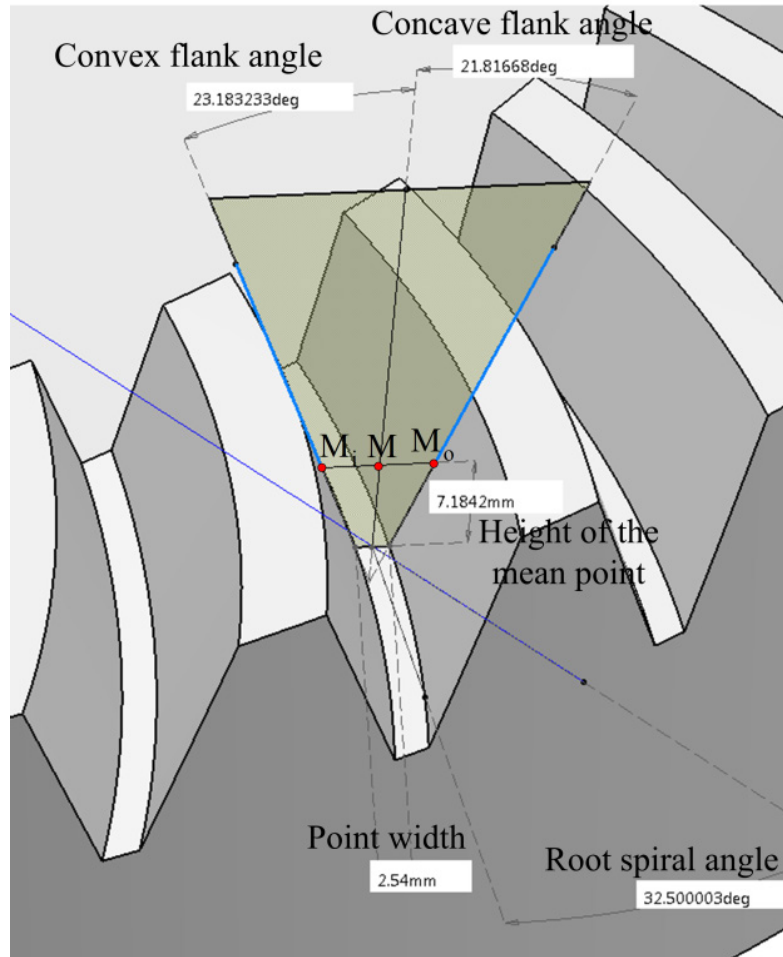
Figure 4.16. Gear tooth parameters measured on a virtually machined hypoid gear using a CAD/CAM software.

Chapter 5

A Generic and Theoretical Approach to CNC Programming and Post-Processing for Multi-Axis Face-Milling of Hypoid Gears

It is a high demand from industry, to develop generic CAM software for the face-milling of hypoid gears on different machine tools. To find an effective solution to the CNC face-milling of hypoid gears, it is useful to employ the conventional methodology for the CNC part milling, which is to calculate the cutter system's location and orientation in the gear coordinate system and to post-process them for the coordinates of the machine axes. Since the face-milling of hypoid gears with cutter systems is quite different from part milling with end-mills, it is essential to understand the complicate hypoid gear geometry and the current methods of designing and manufacturing hypoid gears.

Currently, hypoid gear engineers can use special CAD/CAM software to design the gears, to determine cutter system parameters and to calculate machine settings. Unfortunately, the software is developed only for a particular machine tools; it cannot be used for machine tools of different configurations. Moreover, few technical articles has been published to clearly address challenges in the CNC programming and the post-processing for multi-axis face-milling of hypoid gears, such as the cutter system's parameters determination, its location and orientation calculation and the CNC programs generation. To

solve the current problems, this research proposes a generic approach to CNC programming and post-processing for face-milling of hypoid gear. The main contributions of this research include (1) a new mathematical model to calculate the cutter system location and orientation and (2) a generic post-processing method to establish the machine kinematics chain and to compute the coordinates of the machine axes in face-milling. This approach provides a general and accurate methodology for the face-milling hypoid gears on any machine tools and can be directly applied to the hypoid gear manufacturing for better quality.

The outline of this paper is as follows. In Section 5.1, a new mathematical model of CNC programming to calculate the cutter system location and orientation in the gear coordinate system is established. In Section 5.2, the kinematics chain of a typical hypoid gear machine tool is built up and a solution of the coordinates of the machine axes is rendered. An example is provided in Section 5.3 to demonstrate the validity of this new approach.

5.1 CNC programming model for the face-milling of hypoid gears

Conventionally, a pair of hypoid gears refers to a gear and a pinion. This work is focused on CNC face-milling of gears, not pinions; thus, hypoid gears merely imply gears in this work. As a major contribution of this work, a mathematical model of CNC programming for gear face-milling, which includes closed-form equations of the cutter system location and orientation in the gear coordinate system, is first established and is now introduced here. For clarity, it is necessary to consider the hypoid gear geometry, which is already addressed in

the Section 3.1.

To determine the cutter system orientation, it is important to clearly define the spiral angle β_i on driving side of the gear tooth at the point M_i, and the root spiral angle β_r, which are illustrated in Fig. 5.1. This diagram shows a tangent plane at a root cone generatrix, the tooth slot profile on plane the Π, the mean point M, and its corresponding point on the convex flank M_i. Thus, the tangent plane is perpendicular to the plane Π. Fig. 5.1 shows the pitch spiral angle β_i is the angle between O_pM_i and the normal n_p of the plane Π, and the root spiral angle β_r is the angle between O_rN_r and the normal n_p. In gear design, the pitch spiral angle is specified, and the relationship between the pitch and root spiral angles is derived later.
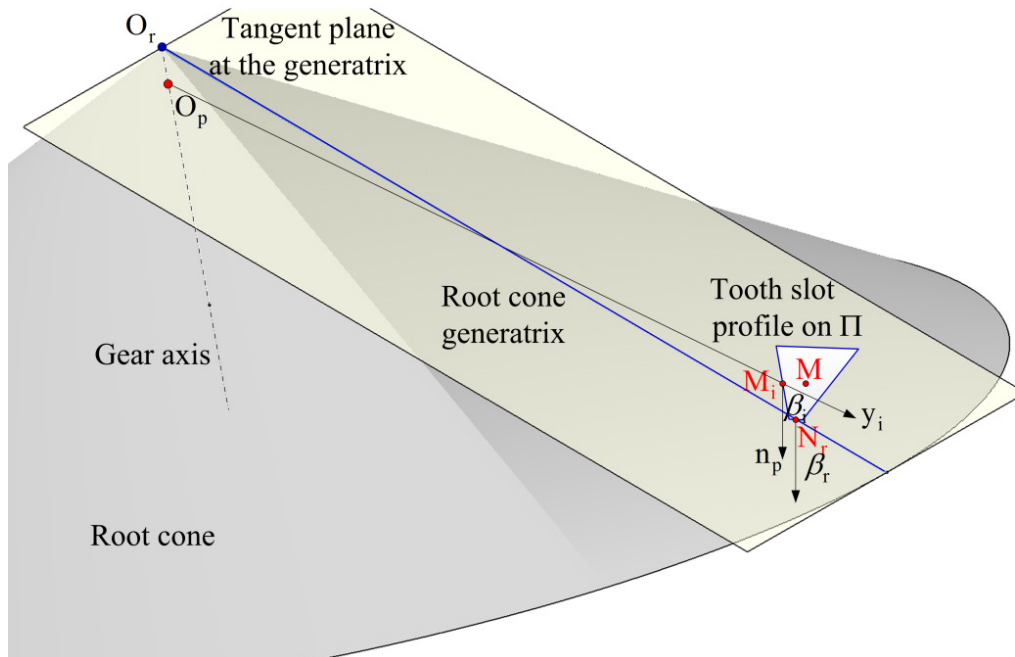
Figure 5.1. Definitions of the pitch spiral and root spiral angles.

5.1.1 The cutting surface profile of the inside blades

Different from the conventional end-mills used in milling operations, the structure of cutter systems for gear face-milling is that a number of blade groups, each of which includes one inside and one outside blades, are set up in the slots of a cutter head around its axis in a circular pattern (see Fig. 5.2).
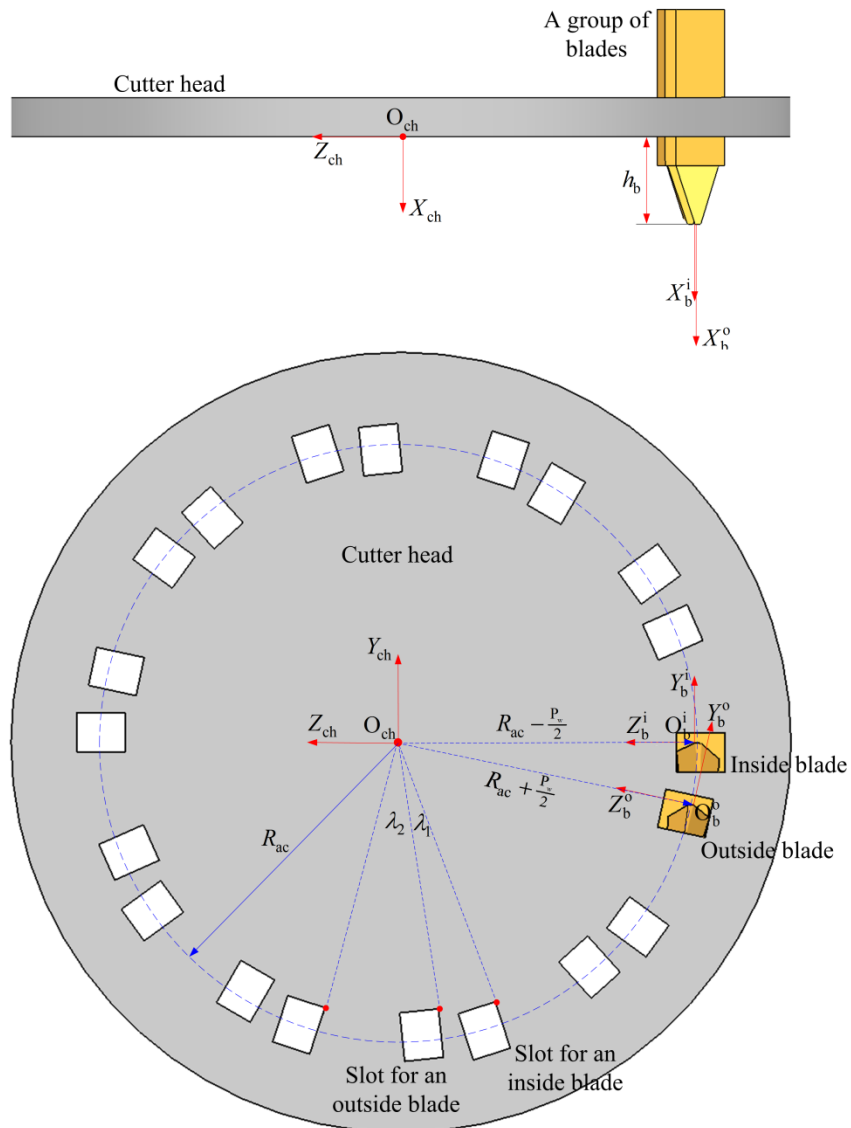
Figure 5.2. The cutting system structure and the relationship between the cutter head and the blade coordinate systems.

While a cutter system self-rotates in face-milling, the inside and outside cutting surfaces are virtually generated by the inside and outside blades. The intersection of an axial cross-section and the surfaces is called the cutting surface profile. The details about the cutting surface profile are provided in the Section 4.1, and the equations of the cutting surface profile are directly adopted here. Fig. 5.2 shows the cutter head coordinate system $O_{ch} - X_{ch} - Y_{ch} - Z_{ch}$, which is established on the cutter head face with its origin at the face centre. All of the blade cutting tips are away from the blade face by a distance h_b. The radius of the inside blade cutting tips is $R_{ac} - 0.5 \cdot P_w$, where R_{ac} is the average cutter radius and P_w is the tooth point width. For the inside blades, the rake angle α_r^i, the hook angle α_h^i, the tooth cutting edge pressure angle β_{tcp}^i, and the length c_l^i of the blade cutting section are determined before machining. The cutting surface generated with the tooth cutting edge of the inside blade is called inside cutting surface $CS^i(l, \lambda)$ and is formulated with parameters l and λ as

$$CS^i(l,\lambda) = \begin{bmatrix} X_{CS}^i \\ Y_{CS}^i \\ Z_{CS}^i \end{bmatrix} = \begin{bmatrix} h_b - l \cdot e_1^i \\ e_2^i \cdot l \cdot \cos \lambda - e_3^i \cdot l \cdot \sin \lambda + e_4^i \cdot \sin \lambda \\ e_2^i \cdot l \cdot \sin \lambda + e_3^i \cdot l \cdot \cos \lambda - e_4^i \cdot \cos \lambda \end{bmatrix}. \tag{5.1}$$

where,

$$\begin{bmatrix} e_1^i \\ e_2^i \\ e_3^i \\ e_4^i \end{bmatrix} = \begin{bmatrix} -\cos(\alpha_r^i) \cdot \cos(\alpha_h^i) \cdot \cos(\beta_{tcp}^i) \\ \sin(\alpha_r^i) \cdot \cos(\alpha_h^i) \cdot \sin(\beta_{tcp}^i) - \cos(\alpha_r^i) \cdot \sin(\alpha_h^i) \cdot \cos(\beta_{tcp}^i) \\ \cos(\alpha_r^i) \cdot \cos(\alpha_h^i) \cdot \sin(\beta_{tcp}^i) \\ R_{ac} - \frac{1}{2} \cdot P_w \end{bmatrix},$$

76

Parameter l is within the range of $\left[0, c_1^i / \left[\cos\left(\alpha_r^i\right) \cdot \cos\left(\alpha_h^i\right) \cdot \cos\left(\beta_{tcp}^i\right) \right] \right]$, and the parameter λ is

the rotation angle about the X_{ch} axis in the range of $[0, \ 2\pi]$. To find the mean point M_i on

the inside flank of the cutting surface profile, the $X_{ch} - Z_{ch}$ plane intersects the cutting

surfaces at the cutting surface profile H-I-J-K as shown in Fig. 5.3.
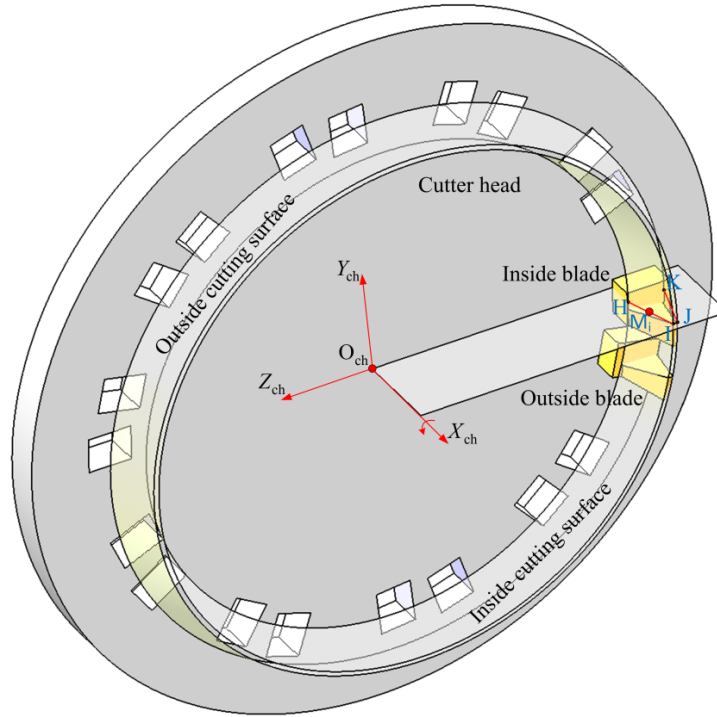
Figure 5.3. The inside and the outside cutting surfaces of the blades and the mean point on the inside flank of the cutting surface profile.

The mean point M_i on the inside flank H-I can be found with their parameters as

$$l = \frac{h_M}{e_1^i}, \text{ and } \lambda = \tan^{-1}\left(\frac{e_2^i}{e_3^i - e_4^i} \cdot l \right)$$

(5.2)

Thus, the coordinates $\left[x_{M_i}^{ch}, y_{M_i}^{ch}, z_{M_i}^{ch} \right]^T$ of point M_i in the cutter head coordinate system can

be calculated by substituting Eq. (5.2) into Eq. (5.1).

5.1.2   Determination of the cutter system location and orientation

As the core of the CNC programming model for gear face-milling, the formulation of the

cutter system location and orientation is established here. The geometric principle of this

model is that the cutter system is located and oriented in terms of the gear so that the profile

of a gear tooth slot at its mean point is coincided with a cutting surface profile of the cutter

system. Fig. 5.4 illustrates this principle. Based on this principle, the formula of the cutter

system location and orientation can be derived.
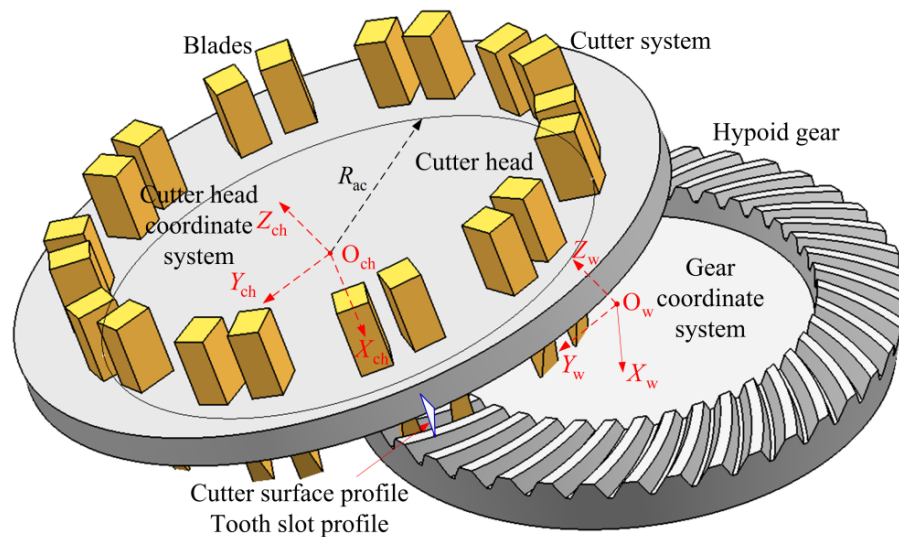
Figure 5.4. Illustration of the geometric principle for determining the cutter system location and orientation in the gear coordinate system.

78

To establish the CNC programming model, a gear coordinate system $O_w - X_w - Y_w - Z_w$ is defined as follows and shown in Fig. 5.5(a). The coordinate system origin O_w is at the centre of the gear top face, and the X_w axis is along the gear axis pointing to the bottom face. The Y_w and Z_w axes are on the top face and normal to each other. The cross-section of the gear on the $X_w - Y_w$ plane is plotted in Fig. 5.5(a). To locate and orient the cutter system so that the tooth slot profile is coincided with the cutting surface profile, a procedure of five steps is needed. Assume the cutter head coordinate system is coincided with the gear coordinate system. The procedure is,

(1) Translating the cutter system along the negative X_w axis by $-A_w$, to coordinate system $O_1 - X_1 - Y_1 - Z_1$.

(2) Rotating the cutter along the Z_1 axis by $-\left(90^\circ - \Gamma_r\right)$, to coordinate system $O_2 - X_2 - Y_2 - Z_2$ as shown in Fig. 5.5(a).

(a)
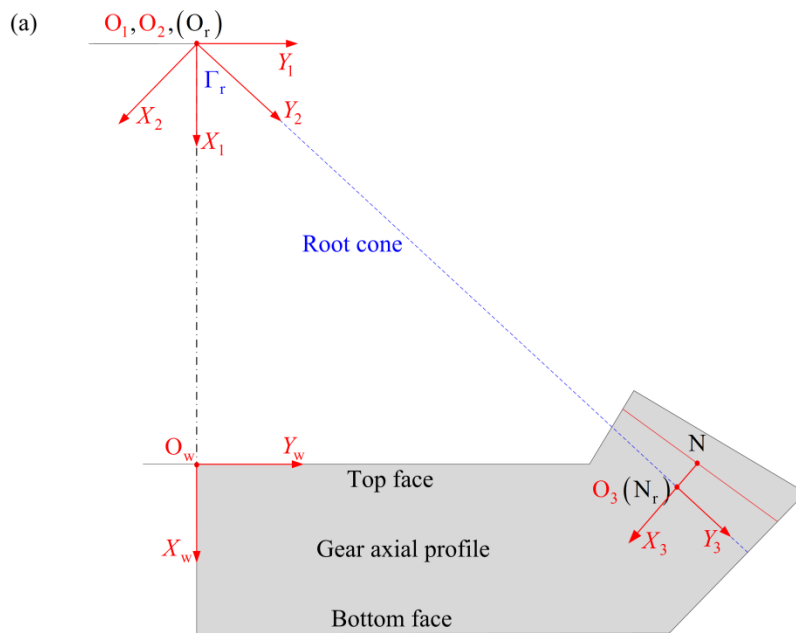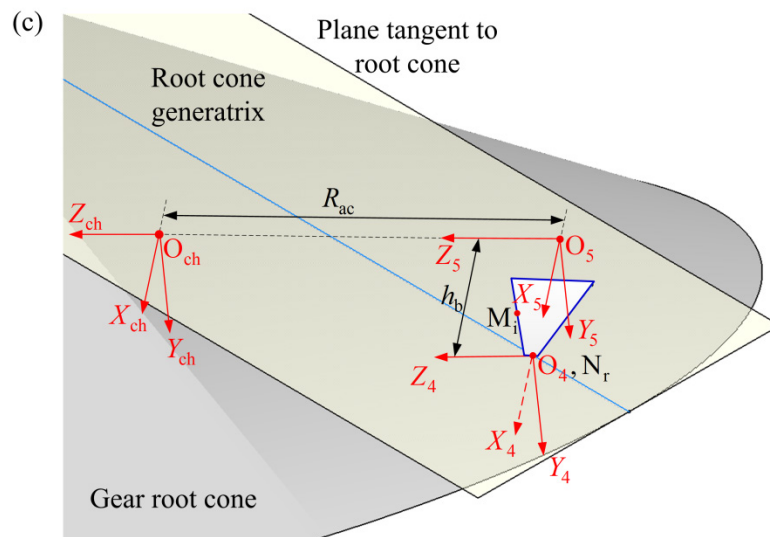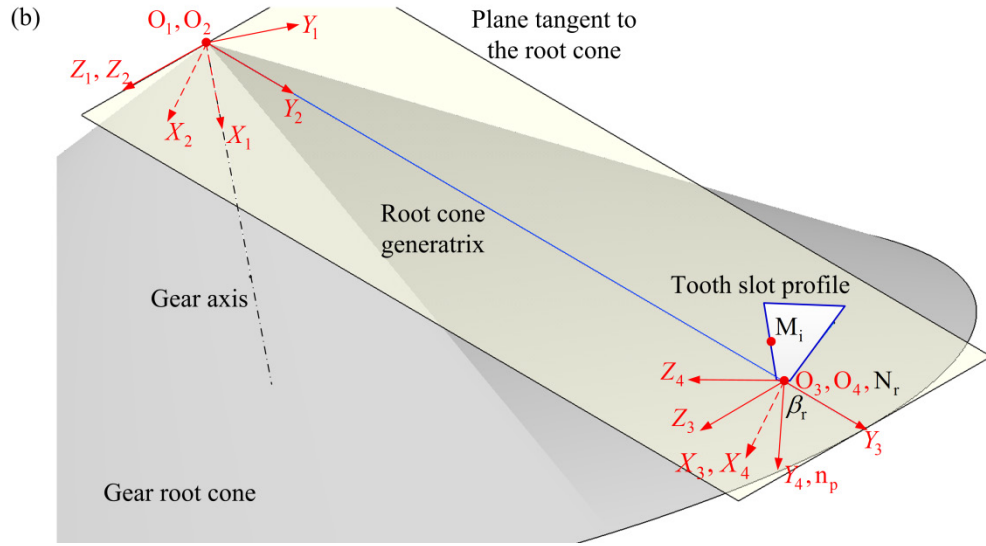
Figure 5.5. The procedure of deriving the formula of the cutter system location and orientation in the gear coordinate system.

(3) Translating the cutter along the Y_2 axis by L_r, to coordinate system $O_3 - X_3 - Y_3 - Z_3$ as shown in Fig. 5.5(b).

(4) Rotating the cutter along the X_3 axis by β_r to coordinate system $O_4 - X_4 - Y_4 - Z_4$,

(5) Translating the cutter along the negative X_4 axis by h_b to coordinate system $O_5 - X_5 - Y_5 - Z_5$ (see Fig. 5.5(c)), and

(6) Translating the cutter along the Z_5 axis by R_{ac} to coordinate system $O_{ch} - X_{ch} - Y_{ch} - Z_{ch}$.

Therefore, the equivalent transformation matrix is derived as

$$\mathbf{M}_{w,ch} = \begin{bmatrix} \sin(\Gamma_r) & \cos(\beta_r)\cdot\cos(\Gamma_r) & -\sin(\beta_r)\cdot\cos(\Gamma_r) & a_1 \\ -\cos(\Gamma_r) & \cos(\beta_r)\cdot\sin(\Gamma_r) & -\sin(\beta_r)\cdot\sin(\Gamma_r) & a_2 \\ 0 & \sin(\beta_r) & \cos(\beta_r) & a_3 \\ 0 & 0 & 0 & 1 \end{bmatrix}$$

(5.3)

where, $a_1 = L_r \cdot \cos(\Gamma_r) - h_b \cdot \sin(\Gamma_r) - R_{ac} \cdot \cos(\Gamma_r) \cdot \sin(\beta_r) - A_w$,

$a_2 = L_r \cdot \sin(\Gamma_r) + h_b \cdot \cos(\Gamma_r) - R_{ac} \cdot \sin(\Gamma_r) \cdot \sin(\beta_r)$ and $a_3 = R_{ac} \cdot \cos(\beta_r)$

With the equivalent transformation matrix, the coordinates of the point M_i in the gear coordinate system can be found as $\begin{bmatrix} x^w_{M_i}, y^w_{M_i}, z^w_{M_i} \end{bmatrix}^T$. The coordinate of point O_r in the gear coordinate system is $\begin{bmatrix} -A_w, 0, 0 \end{bmatrix}^T$. The unit vector of $O_r M_i$ can be calculated as $\begin{bmatrix} x^w_{O_r M_i}, y^w_{O_r M_i}, z^w_{O_r M_i} \end{bmatrix}^T$. The normal n_p of the tooth slot profile can be calculated as

$$n_p = \begin{bmatrix} \cos(\beta_r)\cdot\cos(\Gamma_r) \\ \cos(\beta_r)\cdot\sin(\Gamma_r) \\ \sin(\beta_r) \end{bmatrix}$$

(5.4)

According to the definition of the pitch spiral angle β_i, the equation of the root spiral angle can be derived as

$$\beta_r = -\xi + \sin^{-1}\left(\frac{\cos(\beta_i)}{\sqrt{\left[x_{O_r M_i}^w \cdot \cos(\Gamma_r) + y_{O_r M_i}^w \cdot \sin(\Gamma_r)\right]^2 + \left(z_{O_r M_i}^w\right)^2}}\right) \qquad (5.5)$$

where,

$$\sin\xi = \frac{x_{O_r M_i}^w \cdot \cos(\Gamma_r) + y_{O_r M_i}^w \cdot \sin(\Gamma_r)}{\sqrt{\left[x_{O_r M_i}^w \cdot \cos(\Gamma_r) + y_{O_r M_i}^w \cdot \sin(\Gamma_r)\right]^2 + \left(z_{O_r M_i}^w\right)^2}}$$

and

$$\cos\xi = \frac{z_{O_r M_i}^w}{\sqrt{\left[x_{O_r M_i}^w \cdot \cos(\Gamma_r) + y_{O_r M_i}^w \cdot \sin(\Gamma_r)\right]^2 + \left(z_{O_r M_i}^w\right)^2}}$$

Therefore, the equation of the cutter system location, which is the origin of the cutter head coordinate system, in the gear coordinate system is expressed as

$$O_{ch}^w = \begin{bmatrix} L_r \cdot \cos(\Gamma_r) - A_w - h_b \cdot \sin(\Gamma_r) - R_{ac} \cdot \cos(\Gamma_r) \cdot \sin(\beta_r) \\ L_r \cdot \sin(\Gamma_r) + h_b \cdot \cos(\Gamma_r) - R_{ac} \cdot \sin(\Gamma_r) \cdot \sin(\beta_r) \\ R_{ac} \cdot \cos(\beta_r) \end{bmatrix} \qquad (5.6)$$

The cutter system orientation is the representation of the X_{ch} axis in the gear coordinate system. Since the X_{ch} axis is represented as $\begin{bmatrix} 1 & 0 & 0 \end{bmatrix}^T$ in the cutter head coordinate system, it can be represented in the gear coordinate system by using the equivalent transformation matrix. The equation of the X_{ch} axis in the gear coordinate system is

$$X_{ch}^{w} = \begin{bmatrix} \sin\left(\Gamma_r\right) \\ -\cos\left(\Gamma_r\right) \\ 0 \end{bmatrix} \tag{5.7}$$

5.2   A new approach to post-processing for CNC face-milling of hypoid gears

A conventional way of CNC programming for machining a part is to calculate the cutting tool's locations and orientations in the part coordinate system and convert them into the machine coordinate system using a post-processor. Unfortunately, little research has been published provide a CNC programming solution for gear face-milling. The equations of the cutter system's location and orientation are rendered in Section 5.1, and a post-processing solution is proposed here.

5.2.1   The kinematics chain of the hypoid gear machine tool

To develop a post-processing method for multi-axis face-milling machines of hypoid gears, a general hypoid gear machine is adopted (see Fig. 5.6), and its kinematics chain is established. Based on the previously mentioned equations of the cutter system location and orientation in

the gear coordinate system, closed-form equations are derived to compute the cutter system location and orientation in the machine coordinate system. The basic structure of the machine is defined by the following axes; (1) the machine table moves along the z axis, (2) the carriage assembly moves along the x axis, (3) the workpiece spindle moves along the y axis, (4) the cutter system is set up on the cradle, which rotates along its axis by angle C, and (5) the sliding base rotates about its axis by angle B.

In face-milling gears, the cutting system rotates in high speed, and the gear blank is indexed with an intermittent rotation after a tooth slot is completed cut.
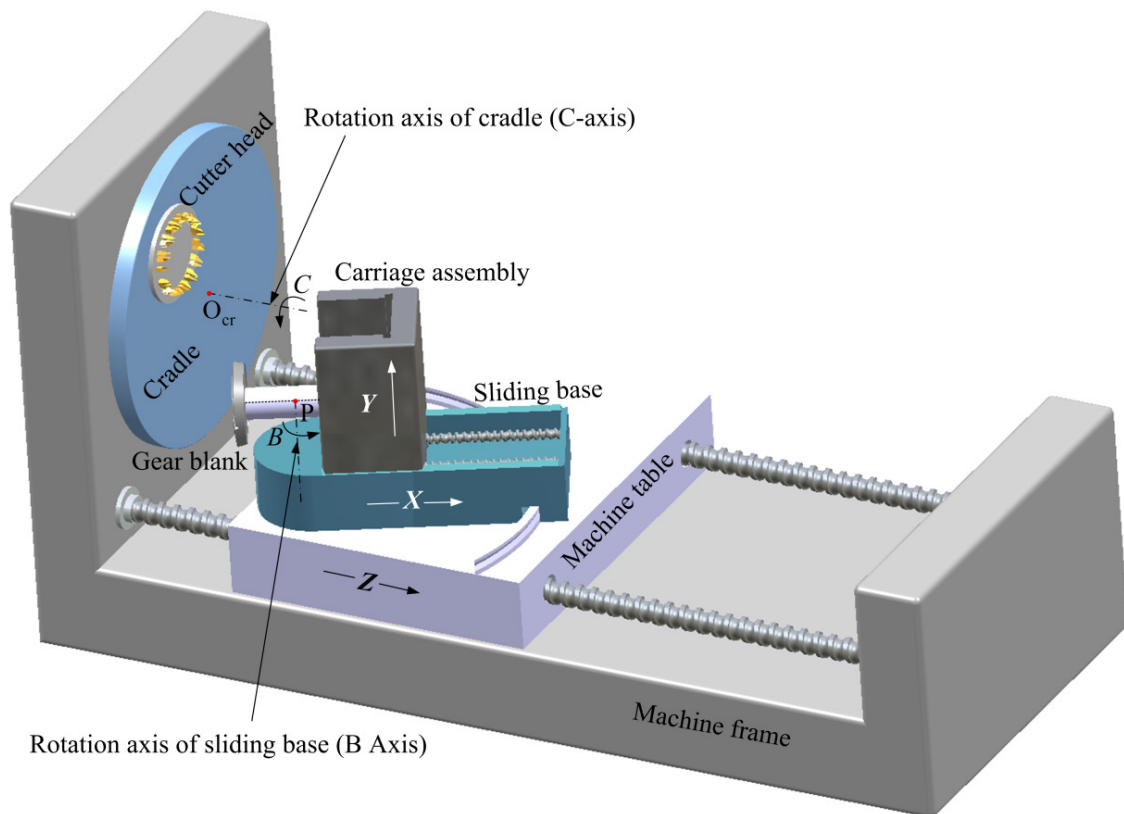
Figure 5.6. Structure of the multi-axis hypoid gear face-milling machine.

One of the machine features is the cradle with the cutter system set up off the centre. To represent this feature, a cradle coordinate system $O_1 - X_1 - Y_1 - Z_1$ is built, and the cutter system coordinate system $O_{ch} - X_{ch} - Y_{ch} - Z_{ch}$ is used (see Fig. 5.7). The distance between the centres of the cradle and the cutter system is d_c, and the angle between the line O_1O_{ch} and the X_1 axis is C_0. The cutter head thickness is t_{ch}. In gear machining, the cradle is fixed, and the cutter system rotates with the cutting velocity.
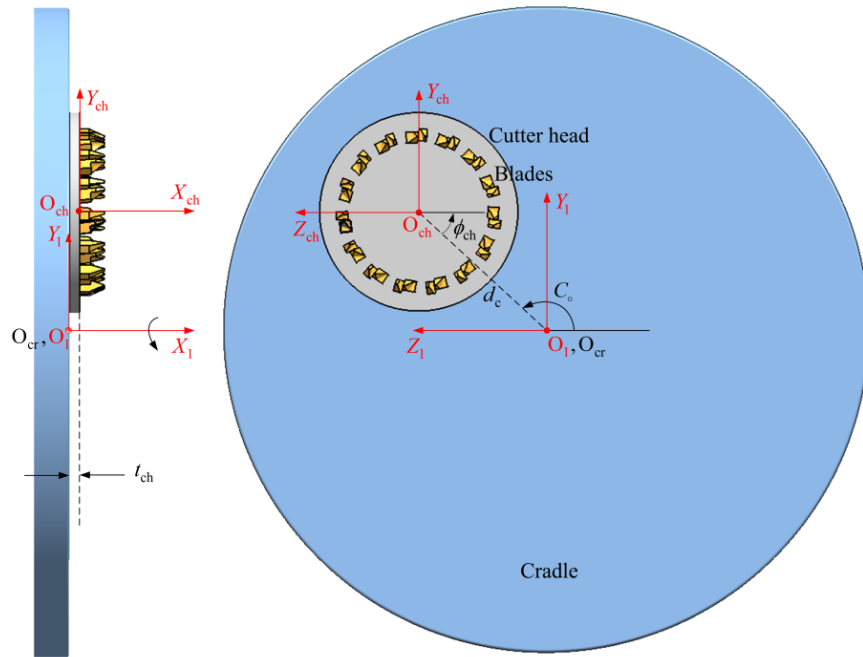
Figure 5.7. Structure of the cradle and the cutter system.

The machine configuration of all functional assemblies at their initial positions is shown in Fig. 5.8, this configuration dimensions are fixed during the assembly of machine. The distance between the axes of the cradle and the gear spindle in the horizontal direction is d_1, the distance between these axes in the vertical direction is d_3. The distance between the

cradle face and the gear spindle end face is d_2, whereas, the distance between this face and the B axis is l_s.

(a) Top view of the hypoid gear face-milling machine tool

Machine configuration when the machine is at home position

Point O_3 is the intersection between the B and the spindle axes

Point P is fixed on the gear spindle

(b) Rotating coordinate system O_3 about the B axis by angle B to coordinate system O_4.

(c)

Kinematics chain of the
machine tool

The machine tool is in a
machining position

Cradle axis

X_6, X_7

X_4, X_5

x

P O_4, O_5

Z_4, Z_5

$t_w + l_s + x$

Z_6, Z_7

(d)

Rotating coordinate system O_6 about the
spindle to coordinate system O_7.

Y_7 Y_6

θ_w

Y_5

y

X_6, X_7

$d_3 + y$

O_6, O_7 O_5 X_5

X_4

O_4

B axis

z

Figure 5.8. The kinematics chain of the machine; (a) top view and (b) front view of the
coordinate system O_1 to O_4 , (c) top view and (d) front view of the coordinate system O_4 to O_7.

87

By using Euler's method, the equivalent matrix for transforming from the gear coordinate system to the cutter system coordinate system is derived as

$$\mathbf{M}_{\text{w,ch}}\left(x,y,z,B,\phi_{\text{ch}},\theta_{\text{w}}\right)=\begin{bmatrix} \cos(B) & 0 & -\sin(B) & g_1 \\ \sin(B)\cdot\sin(\theta_{\text{w}}) & \cos(\theta_{\text{w}}) & \cos(B)\cdot\sin(\theta_{\text{w}}) & g_2 \\ \sin(B)\cdot\cos(\theta_{\text{w}}) & -\sin(\theta_{\text{w}}) & \cos(B)\cdot\cos(\theta_{\text{w}}) & g_3 \\ 0 & 0 & 0 & 1 \end{bmatrix} \qquad (5.8)$$

where,

$$g_1 = x - \left(z + l_s - t_{\text{ch}} + d_2\right)\cdot\cos(B) + \left(d_1 - d_c\cdot\cos\phi_{\text{ch}}\right)\cdot\sin(B) + l_s + t_{\text{w}},$$

$$g_2 = -\left[\left(z + l_s - t_{\text{ch}} + d_2\right)\cdot\sin(B) + d_1.\cos(B) - d_c\cdot\cos(\phi_{\text{ch}})\cdot\cos(B)\right]\cdot\sin(\theta_{\text{w}}) - \left[y - d_c\cdot\sin(\phi_{\text{ch}})\right]\cdot\cos(\theta_{\text{w}}),$$

$$g_3 = -\left[\left(z + l_s - t_{\text{ch}} + d_2\right)\cdot\sin(B) - d_1.\cos(B) + d_c\cdot\cos(\phi_{\text{ch}})\cdot\cos(B)\right]\cdot\cos(\theta_{\text{w}}) + \left[y - d_c\cdot\sin(\phi_{\text{ch}})\right]\cdot\sin(\theta_{\text{w}})$$

With this machine kinematics chain, the cutter system location and orientation represented in the gear coordinate system can be converted the representations in the machine coordinate system.

5.2.2 Equations of the cutter system location and orientation in the machine coordinate system

As the post-processing function, the conversion of the cutter system location and orientation in the gear coordinate system calculated in the aforementioned CNC programming is to compute the corresponding coordinates of the machine axes in order to maintain the relative location and orientation between the cutter system and the gear. Thus, a system of equations can be established based on that the cutter system location and orientation represented in the gear coordinate system by using the machine kinematics is equal to the location and

orientation calculated in the CNC programming. By solving these equations, the machine axes coordinates can be found, and then CNC machining codes can be generated.

To build the system of equations about the cutter system location and orientation, their representations in the gear coordinate system can be found by using the machine kinematics. The origin of the cutter system coordinate system is its location, which is $O_{ch} = \begin{bmatrix} 0 & 0 & 0 \end{bmatrix}^T$ in its own coordinate system. By using the equivalent transformation matrix of the machine kinematics chain, the cutter system location can be represented in the gear coordinate system as

$$O_{ch}^w = \begin{bmatrix} x - (z + l_s - t_{ch} + d_2) \cdot \cos(B) + \left[d_1 - d_c \cdot \cos(\phi_{ch}) \right] \cdot \sin(B) + l_s + t_w \\ \\ -\left[(z + l_s - t_{ch} + d_2) \cdot \sin(B) + d_1 \cdot \cos(B) - d_c \cdot \cos(\phi_{ch}) \cdot \cos(B) \right] \cdot \sin(\theta_w) \\ -\left[y - d_c \cdot \sin(\phi_{ch}) \right] \cdot \cos(\theta_w) \\ \\ -\left[(z + l_s - t_{ch} + d_2) \cdot \sin(B) + d_1 . \cos(B) - d_c \cdot \cos(\phi_{ch}) \cdot \cos(B) \right] \cdot \cos(\theta_w) \\ + \left[y - d_c \cdot \sin(\phi_{ch}) \right] \cdot \sin(\theta_w) \end{bmatrix} \quad (5.9)$$

Meanwhile, the cutter system orientation can be represented with the X_{ch} axis $X_{ch} = \begin{bmatrix} 1 & 0 & 0 \end{bmatrix}^T$ in its own coordinate system. Using the equivalent transformation matrix, the cutter system orientation can be represented in the gear coordinate system, and its equation is as

$$X_{ch}^w = \begin{bmatrix} \cos(B) \\ \sin(B) \cdot \sin(\theta_w) \\ \sin(B) \cdot \cos(\theta_w) \end{bmatrix} \quad (5.10)$$

In Section 5.1 of the CNC programming, the cutter system location O_{ch}^w in the gear coordinate system has been calculated as

$$O_{ch}^w = \begin{bmatrix} L_r \cdot \cos(\Gamma_r) - h_b \cdot \sin(\Gamma_r) - R_{ac} \cdot \cos(\Gamma_r) \cdot \sin(\beta_r) - A_w \\ L_r \cdot \sin(\Gamma_r) + h_b \cdot \cos(\Gamma_r) - R_{ac} \cdot \sin(\Gamma_r) \cdot \sin(\beta_r) \\ R_{ac} \cdot \cos(\beta_r) \end{bmatrix} \qquad (5.11)$$

Besides, the cutter system orientation is calculated in the CNC programming, and it is represented in the gear coordinate system as

$$X_{ch}^w = \begin{bmatrix} \sin(\Gamma_r) \\ -\cos(\Gamma_r) \\ 0 \end{bmatrix} \qquad (5.12)$$

Theoretically, there are infinitive solutions of the machine axes coordinates in gear machining. To simplify this problem, it is reasonable to assume that the gear is not rotated for the first tooth slot, in which θ_w is zero. Then, the equation of the cutter system location is simplified by substituting zero to θ_w, in the Eq. 5.9,

$$O_{ch}^w = \begin{bmatrix} x - (z + l_s - t_{ch} + d_2) \cdot \cos(B) + [d_1 - d_c \cdot \cos(\phi_{ch})] \cdot \sin(B) + l_s + t_w \\ d_c \cdot \sin(\phi_{ch}) - y \\ d_c \cdot \cos(B) \cdot \cos(\phi_{ch}) - (z + l_s - t_{ch} + d_2) \cdot \sin(B) - d_1 \cdot \cos(B) \end{bmatrix} \qquad (5.13)$$

Similarly, by substituting zero to θ_w in Eq. 5.10,

$$X_{ch}^{w} = \begin{bmatrix} \cos(B) \\ 0 \\ \sin(B) \end{bmatrix} \qquad (5.14)$$

Now, the cutter system orientation is represented with Eqs. 5.12 and 5.14, which should be equal to each other, this relation is given by

$$\begin{bmatrix} \cos(B) \\ 0 \\ \sin(B) \end{bmatrix} = \begin{bmatrix} \sin(\Gamma_r) \\ -\cos(\Gamma_r) \\ 0 \end{bmatrix} \qquad (5.15)$$

By solving this equation, the angle B is

$$B = 90^{\circ} - \Gamma_r \qquad (5.16)$$

At the same time, the cutter system location is represented with Eqs. 5.11 and 5.13, which are also equal to each other, the following equation is attained as

$$\begin{bmatrix} x - (z + l_s - t_{ch} + d_2) \cdot \cos(B) + [d_1 - d_c \cdot \cos(\phi_{ch})] \cdot \sin(B) + l_s + t_w \\ d_c \cdot \sin(\phi_{ch}) - y \\ d_c \cdot \cos(B) \cdot \cos(\phi_{ch}) - d_1 . \cos(B) - (z + l_s - t_{ch} + d_2) \cdot \sin(B) \end{bmatrix}$$
$$= \begin{bmatrix} L_r \cdot \cos(\Gamma_r) - A_w - h_b \cdot \sin(\Gamma_r) - R_{ac} \cdot \cos(\Gamma_r) \cdot \sin(\beta_r) \\ L_r \cdot \sin(\Gamma_r) + h_b \cdot \cos(\Gamma_r) - R_{ac} \cdot \sin(\Gamma_r) \cdot \sin(\beta_r) \\ R_{ac} \cdot \cos(\beta_r) \end{bmatrix} \qquad (5.17)$$

where,

$$x = \frac{1}{\sin(\Gamma_r)} \begin{bmatrix} z - [l_s + t_w + A_w + h_b \cdot \sin(\Gamma_r)] \cdot \sin(\Gamma_r) + (l_s - t_{ch} + d_2) - (d_1 - L_r) \cdot \cos(\Gamma_r) \cdot \sin(\Gamma_r) \\ + d_1 \cdot \sin(\Gamma_r) \cdot \cos(\Gamma_r) - R_{ac} \cdot [\sin(\beta_r) \cdot \sin(\Gamma_r) - \cos(\beta_r)] \cdot \cos(\Gamma_r) \end{bmatrix},$$

$$y = d_{c} \cdot \sin(\phi_{ch}) - L_{r} \cdot \sin(\Gamma_{r}) - h_{b} \cdot \cos(\Gamma_{r}) + R_{ac} \cdot \sin(\Gamma_{r}) \cdot \sin(\beta_{r}), \text{ and}$$

$$z = \frac{1}{\cos(\Gamma_{r})} \cdot \left[d_{c} \cdot \cos(\phi_{ch}) \cdot \sin(\Gamma_{r}) - d_{1} \cdot \sin(\Gamma_{r}) - (l_{s} - t_{ch} + d_{2}) \cdot \cos(\Gamma_{r}) - R_{ac} \cdot \cos(\beta_{r}) \right]$$

With the closed-form equations of the machine axes coordinates, the cutter system location and orientation can be presented in the machine coordinate system, and the cutter system can machine the gear tooth slots accurately.

5.3   Applications

To demonstrate this generic approach to the CNC programming and the post-processing for accurate face-milling of hypoid gears, a completed example is provided, which includes cutter system location and orientation, coordinates of the machine axes, machining simulation, and virtually machined gear inspection. First, a gear is designed with all its parameters listed in Table 5.1. To cut this gear, a cutter system is determined and its parameters are listed in Table 5.2. The details of determining the cutter system is explained in the chapter 4.

Table 5.1. Pre-specified parameters of the hypoid gear.

Gear parameters	Convex tooth	Concave tooth
Gear flank angle (α_g^i, α_g^o)	23°11′	21°49′
Gear tooth curvature at the mean points (κ_g^i, κ_g^o)	0.0067 mm^{-1}	0.0064 mm^{-1}
Gear face angle (Γ_o)	81°6′	
Gear root angle (Γ_r)	75°28′	
Gear dedendum angle (δ_G)	4°54′	
Gear addendum at outside (a_{oG})	1.700 mm	
Gear dedendum at outside (b_{oG})	13.100 mm	
Face width (f_w)	43.000 mm	
Distance from gear root apex to blank face (A_w)	43.071 mm	
Clearance between gear and pinion (c)	1.680 mm	
Height of the mean points (h_M)	7.184 mm	

Table 5.2. The parameters of the gear cutting system.

Gear cutting system parameters	Inside blade	Outside blade
Average cutter radius (R_{ac} , mm)	152.400	
Spiral angle at the mean point (β_i)	36°0′	
Root spiral angle (β_r)	37°12′9″	
Hook angles (α_h^i, α_h^o)	12°0′	12°0′
Rake angles (α_r^i, α_r^o)	14°0′	14°0′
Length of cutting section (c_l^i, c_l^o, mm)	30.0	30.0
Cutting surface flank angles (α_e)	23°11′1″	21°48′59″
Tooth cutting edge pressure angle (β_{tcp}^i, β_{tcp}^o)	23°12′35″	21°47′17″

Based on the gear and the cutter system parameters, the cutter system location and the orientation in the gear coordinate system are $\begin{bmatrix} -71.904 & 68.099 & 121.387 \end{bmatrix}^T$ and $\begin{bmatrix} 0.968 & -0.251 & 0 \end{bmatrix}^T$, respectively. Assume the adopted hypoid gear face-milling machine with its configuration parameters listed in Table 5.3. By using our approach, the coordinates of the machine axes, B, x, y and z are calculated and listed in Table 5.3. Comparison between the new approach and the previous method is also shown, which states that the accurate machine model is considered in this research with the pre-defined machine constant.

Table 5.3. Machine constants and the setting parameters

Machine parameters	Litvin's Method	Proposed Method
Distance b/w cradle centre and the pivot point P along the lateral direction of the table (d_1)		1000 mm
Vertical distance b/w cradle centre and Y axis datum (d_2)		300 mm
Horizontal distance b/w cradle centre and the pivot point P (d_3)		250 mm
Distance between the pivot point and the blank instalment position (l_s)		400 mm
Thickness of the cutter head plate (t_{cg})		25 mm
Thickness of the gear blank at centre (t_w)		50 mm
Radial distance b/w cradle centre and the cutter centre (d_c)	1200 mm	1200 mm
Radial angle of the cutter centre (ϕ_{cg})	32°50′	−5°0′
Angular displacement of the C axis (C)	75°28′	185°0′
Angular displacement of the B axis (B)	61°54′57″	14°32′
Displacement along the x axis (x)		-205.218 mm
Displacement along the y axis (y)		-162.787 mm
Displacement along the z axis (z)		-398.509 mm

To validate the results, a machining simulation for the face-milling on the adopted hypoid gear machine tool is conducted with commercial CAD/CAM software. The machine is constructed according to its configuration, which it is shown in Fig. 5.9. In machining, the cutter system engages with the gear blank, when the machine axes, such as B, x, y and z, are equal to the calculated coordinates. In this simulation, the face-milling process is not carried out, and the final cut in forming the tooth slot is presented. To demonstrate accuracy of this approach, The machined gear model is shown in Fig. 5.10(a), the inspection results of the gear model parameters are shown in Fig. 5.10(b), and the inspection results of the tooth slot parameters are shown in Fig. 5.10(c). It is evident that the machined gear parameters are accurate, compared to the gear design. Therefore, this approach is valid. This approach can be applied to any gear and the face-milling machines.
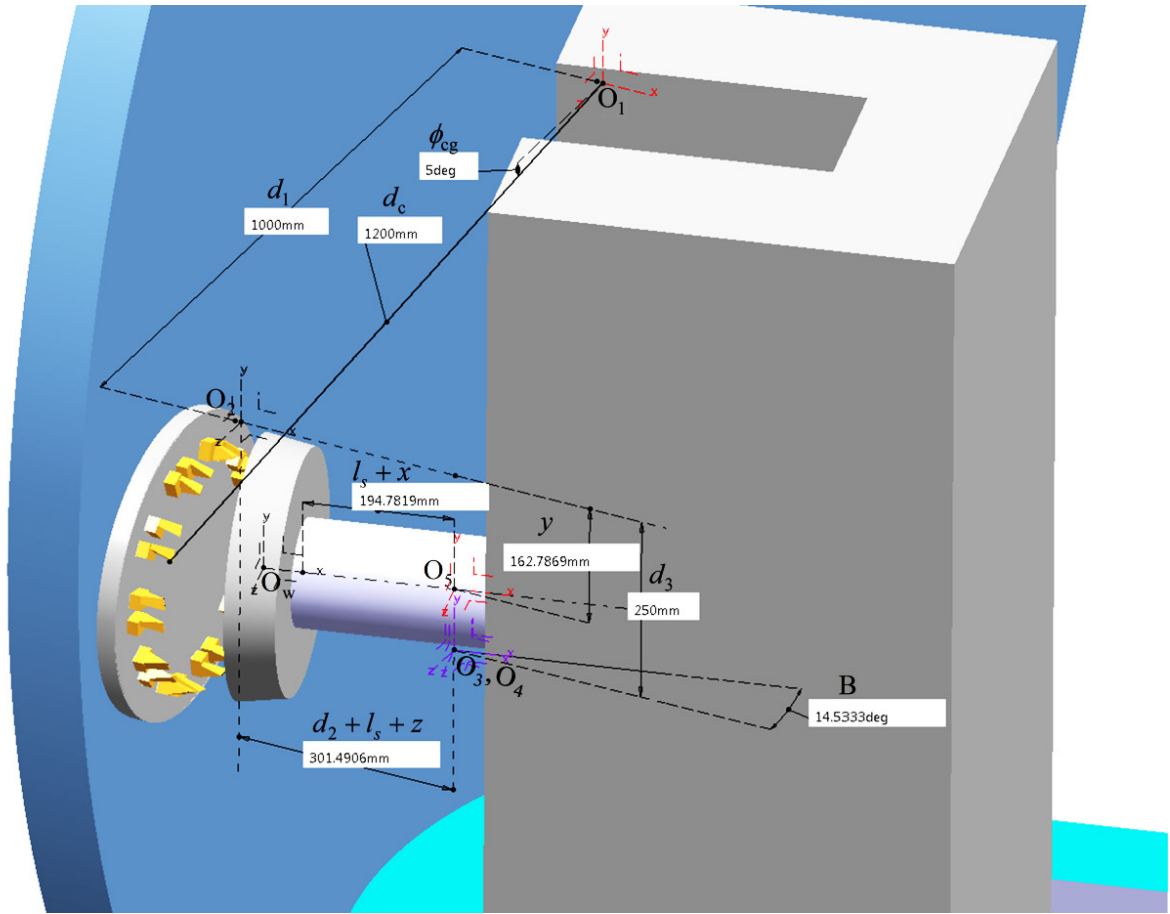
Figure 5.9. Machining simulation of the gear on the adopted hypoid gear face-milling machine with the calculated coordinates of the machine axes.

(a)

Face cone

Pitch cone

Rotation axis
of the gear

Root cone

heel

Gear tooth

toe

(b)

Root angle

75.4667deg

Face angle

80.3667deg

Dedendum
angle

4.9deg

Face width

43mm

Addendum at heel

1.7mm

Dedendumat heel

13.1mm

(c)

Convex flank angle
23.1832deg

Concave flank angle
21.8167deg

Height of the mean point
7.1842mm

Point width
2.54mm

37.2024deg
Root spiral angle
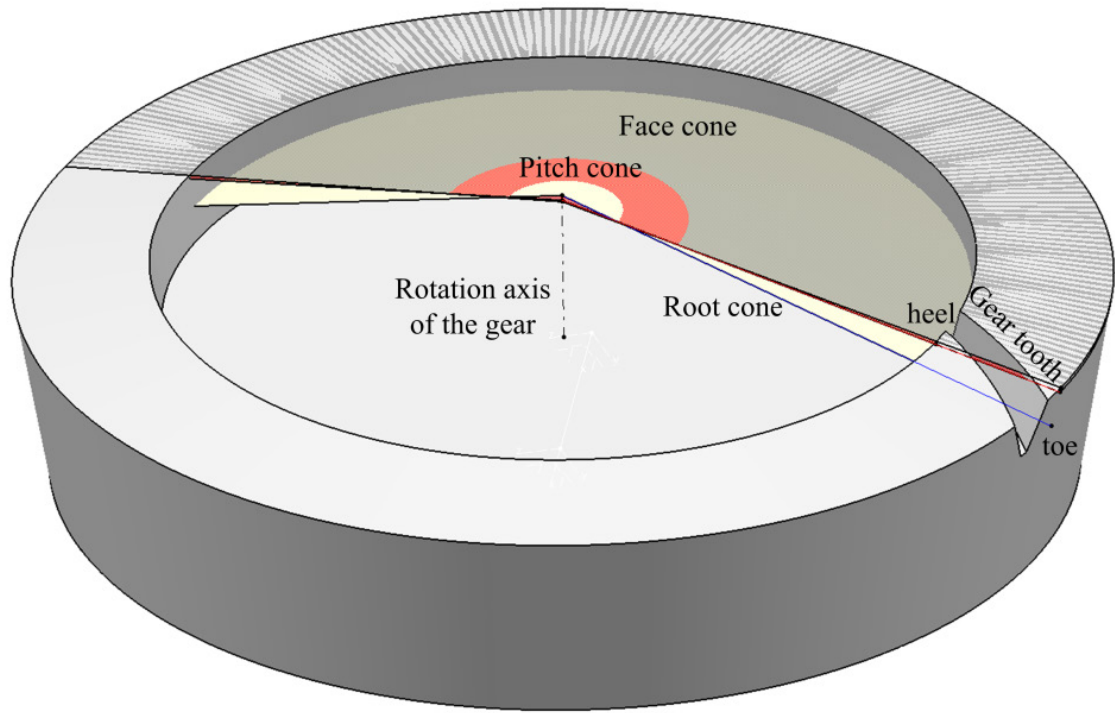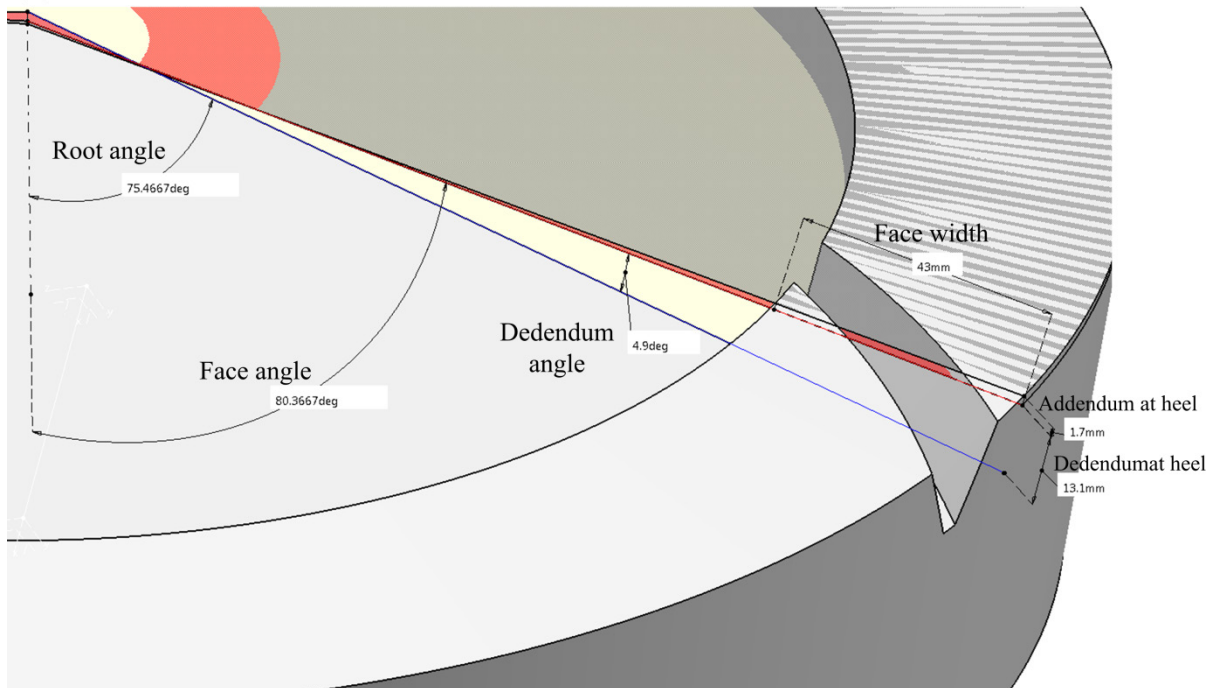
Figure 5.10. (a) An overview of the machined gear, (2) the inspection of the gear parameters, and (3) the inspection of the tooth slot parameters.

Contribution highlights

Unlike the previous research, pressure angles of the tooth cutting edges of the inside and outside blade are not equal to the convex and concave sides flank angles of the hypoid gear. The accurate selection of the pressure angle results in the precise machining of the gear teeth, and reduces the experimental iterations for the selection of appropriate inside and outside blades. In this research, parametric model of an accurate blade is built for the face milling of the hypoid gears, cutting surfaces of inside and outside blades are generated, by assembling the blade models in industrial cutter head and revolving it around the cutter rotation axis. Using the local synthesis method, the cutter geometry determination is performed which is based on the given parameters of the gear and the pinion. Sensitivity analysis is performed, to analyse the sensitivity of the cutting surface, with respect the blade rake and hook angle. Finally, an application of this new approach is presented. It shows the comparison between the new and the current approach, it clearly states that the cutter and the pressure angles are the key parameters to machine the precise gear and the pinion teeth, using a practical cutter system with the predefined rake, hook and relief angles.
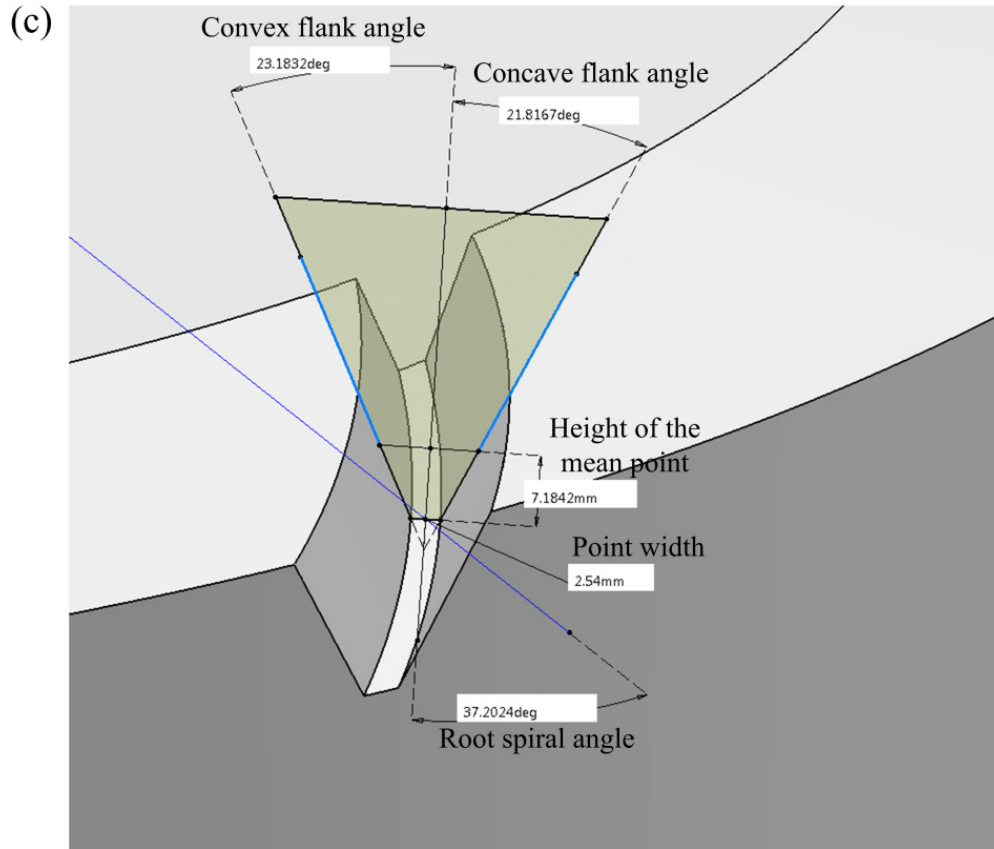
To solve the current problems, this research presented a generic approach to CNC programming and post-processing for gear face-milling. The main contributions of this research include (1) a new mathematical model to calculate the cutter system location and orientation and (2) a generic post-processing method to establish the machine kinematics chain and to compute the coordinates of the machine axes in face-milling. This approach

provides a general and accurate methodology for face-milling hypoid gears on any machine tools and can be directly applied to the hypoid gear manufacturing for better quality.

Future work

The kinematics model of the pinion-cutting machine is a potential scope of research, which can be performed to generate the CNC post processor.

The contact pattern between the gear pair, modelled with the accurate blade design with the mathematical model of the tooth contact analysis (TCA) is to be developed. It helps in optimizing the input parameters for the local synthesis between the gear pair and the cutters.

Cutting forces model for the face milling of hypoid gear pair is decided as another future work, which can be further used to optimize the rake. hook and relief angles of the blade for the efficient metal cutting, which is the need of current industry to prolong the life of the blades as well as less rejection on the shop floor.

References

[1] H. Stadtfeld, Handbook of bevel and gypoid gear: calculation, manufacturing, optimization, 1st ed., Rochester: Rochester Institute of Technology, 1990.

[2] Q. Fan, "Computerized Modeling and Simulation of Spiral Bevel and Hypoid Gears Manufactured by Gleason Face Hobbing Process", *Journal of Mechanical Design,* vol. 128, pp. 1315-1327, 2006.

[3] F. L. Litvin, "Development of Gear Technology and Theory of Gearing", NASA, Washington, DC, 1997.

[4] F. L. Litvin, "Theory of Gearing", NASA, Cleveland, 1989.

[5] F. L. Litvin, "Local Synthesis and Tooth Contact Analysis of Face-milled Spiral Bevel Gears", NASA, Cleveland, 1991.

[6] F. L. Litvin and A. Fuentes, Gear Geometry and Applied Theory, 2nd ed., Cambridge: Cambridge University press, 2004.

[7] F. L. Litvin and Y. Gutman, "Method of synthesis and analysis for hypoid gear-drives of "Formate" and "Helixform"; Part 1", *Journal of Mechanical Design,* vol. 103, pp. 83-88, 1981.

[8] F. L. Litvin and Y. Gutman, "Method of synthesis and analysis for hypoid gear-drives of "Formate" and "Helixform"; Part 2", *Journal of Mechanical Design,* vol. 103, pp. 89-101, 1981.

[9] F. L. Litvin and Y. Gutman, "A Method od Local Synthesis of Gears Grounded on the Connections Between the Principal and Geodetic Curvatures of Surfaces", *Journal of*

Mechanical Design, vol. 103, pp. 114-122, 1981.

[10] F. L. Litvin, N. X. Chen and J. S. Chen, "Computerized determination of curvature relations and contact ellipse for conjugate surfaces", *Computer methods in applied mechanics and engineering,* vol. 125, pp. 151-170, 1995.

[11] F. L. Litvin and Y. Gutman, "Method of synthesis and analysis for hypoid gear-drives of "Formate" and "Helixform"; Part 3", *Journal of Mechanical Design,* vol. 103, pp. 102-113, 1981.

[12] F. L. Litvin, A. G. Wang and R. F. Handschuh, "Computerized Design and Analysis of Face-Milled, Uniform Tooth Height Spiral Bevel Gear Drives", *Journal of Mechanical Design,* vol. 118, pp. 573-579, 1996.

[13] J. Argyris, A. Fuentes and F. L. Litvin, "Computerized integrated approach for design and stress analysis of spiral bevel gears", *Computer Methods in Applied Mechanics and Engineering,* vol. 191, pp. 1057-1095, 2002.

[14] F. L. Litvin, A. Fuentes and K. Hayasaka, "Design, manufacture, stress analysis, and experimental tests of low-noise high endurance spiral bevel gears", *Mechanism and Machine Theory,* vol. 41, pp. 83-118, 2006.

[15] A. Fuentes, F. L. Litvin, B. R. Mullins, R. Woods and R. F. Handschuh, "Design and Stress Analysis of Low-Noise Adjusted Bearing Contact Spiral Bevel Gears", *Journal of Mechanical Design,* vol. 124, pp. 524-532, 2002.

[16] Y. Zhang, F. L. Litvin and R. F. Handschuh, "Computerized design of low-noice face-milled spiral bevel gears", *Mechanism and Machine Theory,* vol. 30, no. 8, pp. 1171-1178, 1995.

[17] F. L. Litvin, F. Alfonso, Q. Fan and R. F. Handschuh, "Computerized design, simulation of meshing, and contact and stress analysis of face-milled formate generated spiral bevel

gears", *Mechanism and Machine Theory,* vol. 37, pp. 441-459, 2002.

[18] F. L. Litvin, A. G. Wang and R. F. Handschuh, "Computerized generation and simulation of meshing and contact of spiral bevel gears with improved geometry", *Computer Methods in Applied Mechanics and Engineering,* vol. 158, pp. 35-64, 1998.

[19] F. L. Litvin, M. D. Donno, Q. Lian and S. A. Lagutin, "Alternative approach for determination of singularity of envelope to a family of parametric surfaces", *Computer methods in applied mechanics and engineering,* vol. 167, pp. 153-165, 1998.

[20] R. L. Huston and J. J. Coy, "Surface Geometry of Circular Cut Spiral Bevel Gears", *Journal of Mechanical Design,* vol. 104, pp. 743-748, 1982.

[21] Z. H. Fong and C. Tsay, "A Mathematical Model for the Tooth Geometry of Circular-Cut Spiral Bevel Gears", *Journal of Mechanical Design,* vol. 113, pp. 174-181, 1991.

[22] K. Kawasaki and H. Tamura, "Duplex Spread Blade Method for Cutting Hypoid Gears with Modified Tooth Surface", *Journal of Mechanical Design,* vol. 120, pp. 441-447, 1998.

[23] Z. H. Fong, "Mathematical Model of Universal Hypoid Generator With Supplemental Kinematic Flank Correction Methods", *Journal of Mechanical Design,* vol. 122, pp. 136-142, 2000.

[24] F. D. Puccio, M. Gabiccini and M. Guiggiani, "Alternative formulation of the theory of gearing", *Mechanism and Machine Theory,* vol. 40, pp. 613-637, 2005.

[25] F. D. Puccio, M. Gabiccini and M. Guiggiani, "Generation and curvature analysis of conjugate surfaces via a new approach", *Mechanism and Machine Theory,* vol. 41, pp. 382-404, 2006.

[26] F. D. Puccio, M. Gabiccini and M. Guiggiani, "An invariant approach for gear generation with supplement motions", *Mechanism and Machine Theory,* vol. 42, pp.

275-295, 2007.

[27] M. Vimercati, "Mathematical model for tooth surfaces representation of face-hobbed hypoid gears and its application to contact analysis and stress calculation", *Mechanism and Machine Theory,* vol. 42, pp. 668-690, 2007.

[28] Y. P. Shih, Z. H. Fong and G. C. Lin, "Mathematical Model for a Universal Face Hobbing Hypoid Gear Generator", *Journal of Mechanical Design,* vol. 129, pp. 38-47, 2007.

[29] Q. Fan, "Optimization of Face Cone Element for Spiral Bevel and Hypoid Gears", *Journal of Mechanical Design,* vol. 133, pp. 091002-1-7, 2011.

[30] S. H. Suh, W. S. Jih, H. D. Hong and D. H. Chung, "Sculptured surface machining of spiral bevel gears with CNC milling", *International Journal of Machine Tools & Manufacture,* vol. 41, pp. 833-853, 2001.

[31] C. Ozel, A. Inan and L. Ozler, "An Investigation on Manufacturing of the Straight Bevel Gear Using End Mill by CNC Milling Machine", *Journal of Manufacturing Science and Engineering,* vol. 127, pp. 503-511, 2005.

[32] C. Brecher, F. Klocke, T. Schroder and U. Rutjes, "Analysis and Simulation of Different Manufacturing Processes for Bevel Gear Cutting", *Journal of Advanced Mechanical Design, System and Manufacturing,* vol. 2, no. 1, pp. 165-172, 2008.

[33] Y. C. Tsai and W. Y. Hsu, "The study on the design of spiral bevel gear sets with circular-arc contact paths and tooth profiles", *Mechanism and Machine Theory,* vol. 43, pp. 1158-1174, 2008.

[34] L. Jing, "Tooth Surface Generation and Geometric Properties of Straight Noncircular Bevel Gears", *Journal of Mechanical Design,* vol. 134, pp. 084503-1-6, 2012.

[35] F. L. Litvin, Y. Zhang, M. Lundy and C. Heine, "Determination of Settings of a Tilted Head Cutter for Generation of Hypoid and Spiral Bevel Gears", *Journal of Mechanical Design,* vol. 110, pp. 495-500, 1988.

[36] T. J. Krenzer, "Computer aided corrective machine settings for manufacturing bevel and hypoid gear sets", in *Technical papers : Fall Technical Meeting*, Washington DC, 1984.

[37] C. Gosselin, "Corrective machine settings of spiral-bevel and hypoid gears with profile deviations", in *World Congress on Gearing and Power Transmission*, Paris, 1999.

[38] C. Gosselin, T. Nonaka, Y. Shiono, A. Kubo and T. Tatsuno, "Identification of the Machine Settings of Real Hypoid Gear Tooth Surfaces", *Journal of Mechanical Design,* vol. 120, pp. 429-440, 1998.

[39] C. J. Gosselin and L. Cloutier, "The Generating Space for Parabolic Motion Error Spiral Bevel Gears Cut by the Gleason Method", *Journal of Mechanical Design,* vol. 115, pp. 483-489, 1993.

[40] V. Simon, "Optimal Machine Tool Setting for Hypoid Gears Improving Load Distribution", *Journal of Mechanical Design,* vol. 123, pp. 577-582, 2001.

[41] V. Simon, "Advanced Manufacture of Spiral Bevel Gears on CNC Hypoid Generating Machine", *Journal of Mechanical Design,* vol. 132, pp. 031001-1-8, 2010.

[42] V. V. Simon, "Generation of Hypoid Gears on CNC Hypoid Generator", *Journal of Mechanical Design,* vol. 133, pp. 121003-1-9, 2011.

[43] V. Simon, "Machine-Tool Settings to Reduce the Sensitivity of Spiral Bevel Gears to Tooth Errors and Misalignments", *Journal of Mechanical Design,* vol. 130, pp. 082603-1-10, 2008.

[44] P. Y. Wang and Z. H. Fong, "Adjustability improvement of face-milling spiral bevel gears by modified radial motion (MRM) method", *Mechanism and Machine Theory,* vol.

2005, pp. 69-89, 2005.

[45] P. Y. Wang and Z. H. Fong, "Mathematical Model of Face-Milling Spiral Bevel Gear with Modified Radial Motion (MRM) Correction", *Mathematical and Computer Modelling,* vol. 41, pp. 1307-1323, 2005.

[46] P. Y. Wang and Z. H. Fong, "Fourth-Order Kinematic Synthesis for Face-Milling Spiral Bevel Gears With Modified Radial Motion (MRM) Correction", *Journal of Mechanical Design,* vol. 128, pp. 457-467, 2006.

[47] I. G. Perez, A. Fuentes and K. Hayasaka, "Analytical Determination of Basic Machine-Tool Settings for Generation of Spiral Bevel Gears From Blank Data", *Journal of Mechanical Design,* vol. 132, pp. 101002-1-11, 2010.

[48] A. Artoni, M. Kolivand and A. Kahraman, "An Ease-Off Based Optimization of the Loaded Transmission Error of Hypoid Gears", *Journal of Mechanical Design,* vol. 132, pp. 011010-1-9, 2010.

[49] C. Y. Lin, C. B. Tsay and Z. H. Fong, "Computer-aided manufacturing of spiral bevel and hypoid gears by applying optimization techniques", *Journal of Materials Processing Technology,* vol. 114, pp. 22-35, 2001.

[50] V. I. Medvedev and A. E. Volkov, "Synthesis of Spiral Bevel Gear Transmissions With a Small Shaft Angle", *Journal of Mechanical Design,* vol. 129, pp. 949-959, 2007.

[51] C. Gosselin, T. Guertin, D. Remond and Y. Jean, "Simulation and Expermental Measurement of the Transmission Error of Real Hypoid Gears Under Load", *Journal of Mechanical Design,* vol. 122, pp. 109-122, 2000.

[52] H. Stadtfeld, "The Ultimate Motion Graph", *Journal of Mechanical Design,* vol. 122, pp. 317-322, 2000.

[53] J. Achtmann and G. Bar, "Optimized Bearing Ellipse of Hypoid Gears", *Journal of Mechanical Design,* vol. 125, pp. 739-745, 2003.

[54] V. Simon, "Optimal Tooth Modifications in Hypoid Gears", *Journal of Mechanical Design,* vol. 127, pp. 646-655, 2005.

[55] V. V. Simon, "Influence of tooth modifications on tooth contact in face-hobbed spiral bevel gears", *Mechanism and Machine Theory,* vol. 46, pp. 1980-1998, 2011.

[56] Y. P. Shih and Z. H. Fong, "Flank Correction for Spiral Bevel and Hypoid Gears on a Six-Axis CNC Hypoid Generator", *Journal of Mechanical Design,* vol. 130, pp. 062604-1-11, 2008.

[57] Y. P. Shih and Z. H. Fong, "Flank Modification Methodology for Face-Hobbing Hypoid Gears Based on Ease-Off Topology", *Journal of Mechanical Design,* vol. 129, pp. 1294-1302, 2007.

[58] Q. Fan, "Enhanced Algorithms of Contact Simulation for Hypoid Gear Drives Produced by Face-Milling and Face-Hobbing Processes", *Journal of Mechanical Design,* vol. 129, pp. 31-37, 2007.

[59] Q. Fan, "Tooth Surface Error Correction for Face-Hobbed Hypoid Gears", *Journal of Mechanical Design,* vol. 132, pp. 011004-1-8, 2010.

[60] M. Gabiccini, A. Bracci and M. Guiggiani, "Robust Optimization of the Loaded Contact Pattern in Hypoid Gears With Uncertain Misalignments", *Journal of Mechanical Design,* vol. 132, pp. 041010-1-8, 2010.

[61] A. Artoni, M. Gabiccini and M. Guiggiani, "Nonlinear Identification of Machine Setting for Flank From Modifications in Hypoid Gears", *Journal of Mechanical Design,* vol. 130, pp. 112602-1-8, 2008.

108

[62] A. Artoni, A. Bracci, M. Gabiccini and M. Guiggiani, "Optimization of the Loaded Contact Pattern in Hypoid Gears by Automatic Topography Modification", *Journal of Mechanical Design,* vol. 131, pp. 011008-1-9, 2009.

[63] M. Kolivand and A. Kahraman, "An Ease-Off Based Method for Loaded Tooth Contact Analysis of Hypoid Gears Having Local and Global Surface Deviations", *Journal of Mechanical Design,* vol. 132, pp. 071004-1-8, 2010.

[64] M. Kolivand and A. Kahraman, "A Genaral Approach to Locate Instantaneous Contact Lines of Gears Using Surface of Roll Angle", *Journal of Mechanical Design,* vol. 133, pp. 014503-1-6, 2011.

[65] G. I. Sheveleva, A. E. Volkov and V. I. Medvedev, "Algorithms for analysis of meshing and contact of spiral bevel gears", *Mechanism and Machine Theory,* vol. 42, pp. 198-215, 2007.

[66] Y. Altintas, Manufacturing automation: metal Cutting mechanics, machine tool vibrations, and CNC design, Cambridge: Cambridge University press, 2000.

[67] S. Xie, "An accurate approach to modeling the genuine tooth surfaces of the face-milled spiral bevel and hypoid gears", Concordia University, Montreal, 2011.

[68] AGMA, "Design Manual for Bevel Gears", ANSI/AGMA, USA, 2005.

[69] P. R. Stephen, Dudley's handbook of practical gear design and manufacture, 2 ed., CRC, 2012.

[70] Gleason's, "Gleason's Work", Gear machine tool manufacturing, 2011. [Online]. Available: www.gleason.com.

[71] Klingelnberg, "Klingelnberg Works", Gear machine tool manufacturing , 2011. [Online]. Available: www.klingelnberg.com.

[72] Oerlikon, "Oerlikon Works", Gear machine tool manufacturer, 2011. [Online]. Available: www.oerlikon.com.

Curriculum Vitae

Surname: **Wasif**   Given Name: **Muhammad**

Education

Ph.D. Candidate   **2009-2012**
Department of Mechanical and Industrial Engineering, Concordia University, Montreal (QC) Canada.

M.Engg.   **2005-2007**
Department of Industrial and Manufacturing Engineering, NED University, Karachi, Pakistan.

B.E.   **2000-2003**
Department of Mechanical Engineering, NED University, Karachi, Pakistan.

Awards and Achievements

Achieved the Faculty development scholarship from NED University to pursue the Ph.D.   **2009-2012**
Passed the comprehensive examination with the exemption of oral examination   **2009**

Publications and Progress

- Wasif, M., Chen, Z.C., "Cutter radius and blade angle selection model for the high speed face milling of hypoid gear", *1st International Conference on Virtual Machining Process Technology*, Montreal, May-June, 2012.

- Wasif, M., Chen, Z.C., "Mathematical model of the pressure and spiral angles on hypoid gear teeth machined with industrial blade", *1st International Conference on Virtual Machining Process Technology*, Montreal, May-June, 2012.

- Chen, Z.C., Wasif, M., "An accurate approach to determine average cutter radius and blade pressure angle for the CNC face-Milling of hypoid gears," *Manuscript completed to submit to: Journal of Manufacturing Science and Engineering,* 2012.

- Chen, Z.C., Wasif, M., "A generic and theoretical approach to CNC programming and post-processing for multi-axis face-milling of hypoid gears," *Manuscript completed to submit to: Computer- Aided Design,* 2012.

Experience

Assistant Professor   **2006-todate**
Department of Industrial and Manufacturing Engineering, NED University of Engineering and Technology, Karachi, Pakistan.

- Taught the CAD course to the undergraduate students.

- Taught the mechanical engineering courses to the undergraduate students.

- Demonstrated the labs for the CNC lathe and the milling processes.

- Worked in the Product development center of the university to provide the CAD/CAM and reverse engineering services to the local industries.

Production Engineer   **2004-2005**
Worked in the assembly operations plant of the Hinopak motors limited, to control the flow of production.

Memberships and affiliations

ASME   **2009-todate**

PEC (Pakistan Engineering Council)   **2004-todate**

Skills

CAD/CAM

- CATIA R20.

- Pro E Wildfire 4.

- Autodesk AutoCAD (licensed trainer).

- Autodesk Inventor.